Comparative System Trades Between Structurally Connected and Separated Spacecraft Interferometers for the Terrestrial Planet Finder Mission

by

Robert L. Stephenson, Jr.

S.B., Aeronautics and Astronautics (1996)
Massachusetts Institute of Technology

Submitted to the Department of Aeronautics and Astronautics
in partial fulfillment of the requirements for the degree of

Master of Science in Aeronautics and Astronautics

at the

MASSACHUSETTS INSTITUTE OF TECHNOLOGY

May 1998

Author .....
Department of Aeronautics and Astronautics
22 May 1998

Certified by .....
Edward F. Crawley
MacVicar Faculty Fellow, Professor of Aeronautics and Astronautics
Thesis Supervisor

Certified by .....
David W. Miller
Assistant Professor of Aeronautics and Astronautics
Director, Space Systems Laboratory

Accepted by .....
Jaime Peraire
Associate Professor of Aeronautics and Astronautics
Chairman, Department Graduate Committee

Comparative System Trades Between Structurally Connected and Separated Spacecraft Interferometers for the Terrestrial Planet Finder Mission

by

Robert L. Stephenson, Jr.

Submitted to the Department of Aeronautics and Astronautics on
May 21, 1998, in partial fulfillment of the requirements for the
degree of Master of Science in Aeronautics and Astronautics

Abstract

The Terrestrial Planet Finder (TPF) is a space-based, infrared interferometer designed to directly detect extra-solar planets. TPF consists of four apertures which collect light and relay it to a single combiner bench to be interfered. A major design trade for the TPF is the choice between a structurally connected interferometer (SCI) and a separated spacecraft interferometer (SSI) architecture. Three metrics are applied to the architectural comparison in order to present an understanding of the trade-offs involved.

The primary metric is the wet mass for which reference designs are developed and the relevant mass drivers are examined. Additionally, the sensitivity of the wet mass values to different assumptions in the reference designs are discussed. The adaptability metric takes into account the flexibility of the system to changes in the functional requirements. Finally, the capability is measured by the level of performance provided by the two architectures in meeting four constraints: isolation, rate, integrity, and availability.

Additionally, the reference designs are validated against three industry contractor models for the Terrestrial Planet Finder in order to gain a more complete understanding of the uncertainties involved in the architectural comparison. The conclusion of this study is that a separated spacecraft interferometer is likely to be less massive than a structurally connected interferometer. On the other hand, the SSI is more sensitive to modifications in the functional requirements, while the capability considerations are split between the architectures. The indication, though, is that a separated spacecraft architecture merits serious attention as a possible design choice for the Terrestrial Planet Finder mission.

Thesis Supervisor: Edward F. Crawley, Sc.D
Title: Professor of Aeronautics and Astronautics, MacVicar Faculty Fellow

Acknowledgments

"For astronomy is not only pleasant, but also very useful to be known;
it cannot be denied that this art unfolds the admirable wisdom of God."

- John Calvin, *Commentaries on the Book of Genesis* (1554)

Through the two year duration of my graduate school struggles, I have been unbelievably blessed through the friendship and support of many people. I would like to acknowledge some of them here, although the list may be somewhat incomplete.

My thesis advisor, Professor Edward Crawley, has been a liberal source of technical knowledge and professional guidance in the course of my master's degree work. I am also deeply indebted to Professor David Miller who provided much direction and assistance in the essential presentation of the results and conclusions of this study as a whole. Loren Lemmerman, of the Jet Propulsion Lab, and Charles Beichman, of CalTech, acted as the technical monitors for this study and gave much appreciated input and advice concerning the TPF mission. I would also like to thank Ray Sedwick, of the MIT Space Systems Lab, for his assistance with orbital transfer mechanics and propellant analyses.

My family has been incredibly encouraging through all of my academic studies. Though my dad may not have understood the gist of my thesis, he still let me program the VCR and tinker with any other gadgets when I went home, just to prove that I was indeed being taught "how to be a rocket scientist," as he put it. And no one could have asked for a more supportive mother, someone who always reminded me that I was "much loved and prayed for" and "to just hang on." The

trust that my parents have placed in me is sometimes overwhelming, but their unconditional love is equally astounding. My brothers, Davy, Jason, and Tim, and my sister, Ashley, provided much needed humor and love whenever I spoke with them, too.

I managed to keep most of my sanity during the past two years because of my faithful and wonderful friend, Jodi Jenkins. Sunday night dinners, walking on the bridge, movies in the lecture hall, playing the organ in the chapel — I needed all of that for perspective. I would like to truly thank Roland Allen for his awesome friendship, his spiritual mentoring and brotherhood, and his amazing gift of hospitality. Monday nights with him and Brian Browning were a much needed escape over the past few months. I am also beholden to my virtual 'big sister,' Margaret Lo, who proved to me that an engineer could retain a deep appreciation for the arts, even while allowing me to dislike the ballet. She really put a great deal of effort in exercising the right half of my brain, and was indispensable in holding me accountable in my integrity.

Park Street Church in downtown Boston has played an essential role in my life as a graduate student. Being a member of that church family has given me much joy and an incredible sense of renewal each and every Sunday. I also have to say that the Park Street library is an excellent place for snoozing and letting your mind relax on sunny Sunday afternoons.

As an undergraduate and a graduate student at MIT, it has been my privilege to work with and to goof off with some great people. Corinne Ilvedson and Malinda Lutz have been great sources of encouragement and even better outlets for frustration release. The common experiences and trials that we have shared are certainly unique to MIT. My roommate this year, Tony Eng, put up with so many of my eccentricities, not to mention my endless playing of the many versions of "My Heart Will Go On."

The staff and students in the Space Systems Lab have been great help, as well. In particular,

SharonLeah Brown and Peggy Edwards really helped with those minor, yet still important, administrative details. And who could forget all the candy that Sharon gave out? Cyrus Jilla and Edmund Kong were great fun to work with, too.

This work was sponsored by the Space Systems Laboratory at the Massachusetts Institute of Technology with funding provided under the National Aeronautics and Space Administration grant JPL 960314. Additional support was given through a Graduate Student Fellowship from the National Science Foundation.

"This most beautiful system of the sun, planets, and the comets could only proceed from the counsel and dominion of an intelligent and powerful Being... This Being governs all things, not as the soul of the world, but as Lord over all; and on account of his dominion he is wont to be called Lord God."

- Isaac Newton, *Mathematical Principles of Natural Philosophy* (1687)

Table of Contents

List of Figures

List of Tables

Chapter 1

Introduction

1.1 Motivation

Astronomical and astrophysical research is increasingly concentrating on the question of the creation of the universe and the existence of life on other planets. The announcement that researchers had found potential evidence of an extra-solar planet orbiting the star 51 Pegasi, followed by several later announcements of planets being detected, brought that puzzle to the forefront of the public's attention in 1996. Drawing together scientists and engineers from a broad spectrum of disciplines, NASA began the Origins Program with the express purpose of answering some of the fundamental unknowns concerning the origins of the universe and the existence of life, namely:

- How do galaxies form?
- How do stars form?
- How do planetary systems form?
- Are there other life-sustaining planets around other stars?
- How did life begin on Earth?
- Is there other life out there?[1]

1. <URL:http://origins.stsci.edu/origins/under/understanding.html>. Accessed 28 April 1998.

These questions have prompted NASA to initiate several space-based astronomical missions within the Origins Program aimed at studying different spectral frequencies and stellar targets.

Astrophysical research can be performed through either direct or indirect detection. Direct detection of distant targets, where the target can actually be seen, requires large optical areas for collecting light and, in the case of a ground-based telescope, is very sensitive to degradation from both refraction and absorption by water and other molecules in the earth's atmosphere. Indirect observation depends on effects that the target has on other objects, such as gravitational lensing, orbital variations, and electromagnetic interactions, and provides data which is normally less accurate and more uncertain than direct evidence.

Space-based observatories can eliminate the atmospheric distortions from ground-based observations, but the inherent limitations on payload size imposed by launch vehicles restrict aperture diameters. However, rather than using a large, single-mirror telescope, astronomical missions are beginning to turn to multiple aperture interferometers. The advantage of interferometers lies in the fact that multiple mirrors separated by large baselines tend to act like a single mirror with an aperture diameter equal to the separation baseline. The angular resolution and precision of the instrument can be improved merely by increasing the baseline distance, provided the mirrors are positioned correctly.

Interferometers are ideal for the scientific objectives of the Origins Program because of their high angular resolution and small optics, and so several of the Origins missions involve space-based interferometers. The discrete nature of the optical architecture allows for various interferometer concepts, among them a structurally connected, monolithic architecture and a separated spacecraft architecture. A structurally connected interferometer (SCI) passively maintains the coarse collector positions by mounting them on a long truss assembly. A separated spacecraft

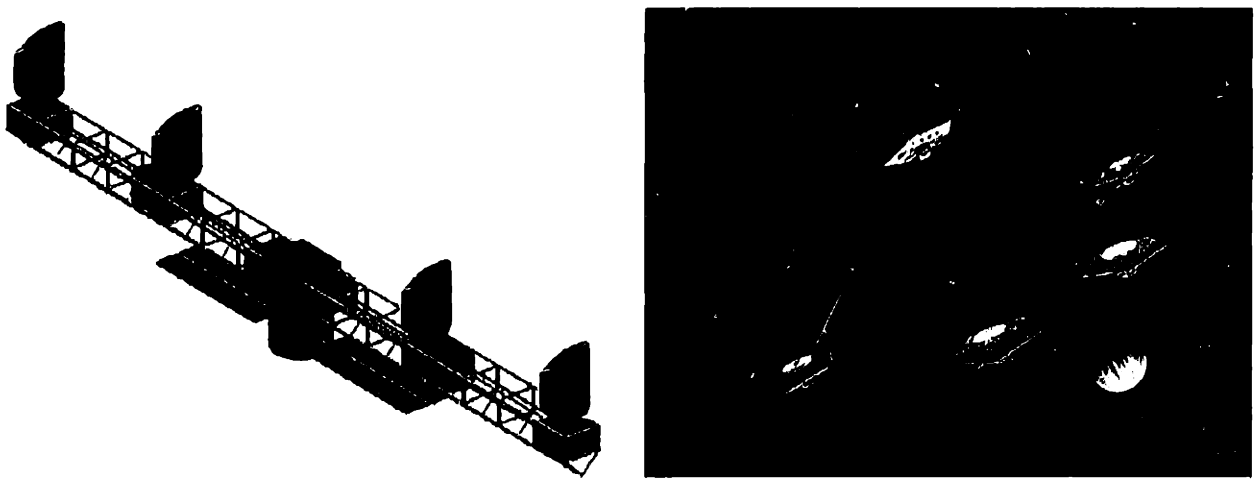

(a) (b)

Figure 1.1: Potential Terrestrial Planet Finder Architectures
a) Structurally Connected; b) Separated Spacecraft

interferometer (SSI) is composed of several individual spacecraft flying in formation and forming a virtually supported baseline.

The Terrestrial Planet Finder (TPF) is the capstone project for NASA's Origins Program and was proposed by a group put together by NASA charged with formulating a plan for the future Exploration of Neighboring Planetary Systems (ExNPS). As a reference design, the ExNPS report [7] offered a 75 m baseline Michelson interferometer using four collectors mounted on a truss, in a double Bracewell pair configuration. However, the ExNPS participants also recognized that a multiple spacecraft architecture might be more cost-efficient and better equipped for the TPF mission than a structurally connected architecture [ExNPS, 1996, p. 6-3]. Conceptual designs for both possible architectures from the Origins TPF library[1] are shown in Figure 1.1.

Because of this architectural question, the purpose of this study is to examine design issues and system trades between a structurally connected architecture and a separated spacecraft architecture, specifically with regard to the Terrestrial Planet Finder, and to determine which one more

1. <URL:http://origins.jpl.nasa.gov/missions/build.html>. Accessed 13 May 1998.

effectively achieves the scientific objectives of the mission.

1.2 Overview of the Terrestrial Planet Finder

In August of 1996, a team at the Jet Propulsion Laboratory released a study detailing a plan to search for and study extra-solar planets: *A Road Map for the Exploration of Neighboring Planetary Systems* [7]. The major recommendation to come out of the study was for the development of a large-scale, space-based, infrared interferometer. Such an instrument would provide greater clarity and performance than any ground-based telescope due to the lack of atmospheric distortion, and would allow the high angular resolution needed to distinguish Earth-like planets from their parent stars without the prohibitive size of a single-aperture telescope. The Terrestrial Planet Finder was born from the ExNPS report and represents the first generation in missions designed to directly detect extra-solar planets.

1.2.1 Mission Requirements

The fundamental objective of the ExNPS program is "the detection and characterization of terrestrial planets in the habitable zone around the nearest ~1,000 stars, or roughly to a minimum distance of ~13 pc" [ExNPS, 1996, p. 5-1]. The Terrestrial Planet Finder will focus on the direct detection of any Earth-like planets within the sphere of a 13 pc radius of space surrounding our Solar System. Once the light from the planet is isolated, it is spectrally spread to reveal absorption bands indicative of key planetary constituents necessary for life. To accomplish this objective, several requirements were listed in the ExNPS report which must be met by the Terrestrial Planet Finder design:

- The interferometer must be able to isolate a planet from its parent star, for any stellar system

out to the maximum distance of 13 pc from the Earth, which translates into a minimum angular resolution of approximately 0.038 arcsec for a planet orbiting at a radius of 0.5 AU In addition, the potential presence of an exo-zodiacal dust cloud requires a higher resolution, up to 0.01 arcsec for a cloud similar to that in our Solar System.

- The light from the parent star must be suppressed in order to detect the signal from the planet. The magnitude ratio between the intensities of the Sun and the Earth varies from roughly one billion to one in the visible spectrum to one million to one in the infrared. Therefore, the level of suppression provided by the interferometer must be at least 10^{-6}, with an additional order of magnitude to allow for intensity distribution patterns unlike those of the Sun and the Earth.

- The field-of-view must cover the habitable zone of the parent star, which extends from as close as 0.5 AU from a K2 class out to as far as 3.0 AU from an F0 class star, which sets the field of view to roughly 2 arcsec in diameter.

- Spectroscopic objectives are to be conducted in the 7-17 μm wavelength band (thermal infrared) of the spectrum since the magnitude of the electromagnetic intensity ratio is most favorable and molecular absorption bands for water, carbon dioxide, ozone, and methane are present in the this spectral band.

- In addition, the target goals are to image up to approximately 1000 stars during the nominal five year lifetime. The proposed operation profile begins with a general survey of nearly all the target stars with full spectroscopic images obtained later in the mission of any promising candidates, allowing the instrument to not only detect a terrestrial planet, but also to determine the viability of life on that planet based upon the detected absorption bands.

1.2.2 Interferometric Requirements

The scientific objectives of the mission translate into very clear instrument requirements necessary to carry out the program goals, such as:

- A spatial resolution of 0.038 arcsec implies an optical baseline of between 50 and 90 meters for resolving features in the infrared band of wavelengths of 7-17 μm.
- The suppression threshold of 10^{-6} dictates the optical configuration of the interferometer such that four collector mirrors are required, operating as a two superposed pairs.
- For the fringe detector to successfully measure the interference fringes, both the phasing and the pointing of the interferometer must be adequately controlled. The phasing condition is such that the interfering wavefronts must have equal phases to within λ/6000, or roughly 1.5 nm, while the pointing is such that the beam amplitudes in the beamsplitter must match to one part in 10^3.
- In order to synthesize the images, the signals from the planet must be modulated through the movement of the collector optics. While a structurally connected architecture can easily rotate, separated spacecraft must maneuver individually to provide the necessary coverage of the image plane.

1.2.3 Design Trade Space

Set to launch in 2010, TPF is still in the earliest stages of design and development. Several design trades remain which are crucial in continuing the program development.

- The most important question in the conceptual studies being done involves the architectural configuration of the instrument. At such a long baseline, a trade-off exists between connect-

ing the four collector mirrors using a structure and placing the mirrors on four independent, free-flying spacecraft.

- The orbit selection is still uncertain, as well. Both 1.0 AU and 5.2 AU orbit radii are being considered. The 1.0 AU orbit offers a close proximity to earth for launch and operation, but the local zodiacal noise as well as the thermal flux levels from the Sun are much higher, which makes placing TPF (which must operate at a temperature of approximately 30 K) in a 5.2 AU orbit more attractive.

- The actual layout and sizing of the mirrors is not yet determined. A 1-2--2-1 configuration, in which the numbers refer to the ratio of the mirror diameters, places the four collectors and the combiner at regular intervals. On the other hand, a 1-3-3-1 layout places equal lengths only between the collectors, with the combiner halfway between the inner pair. Each has its own advantages related to photon collection.

The primary objective in this study is to examine the trade between a structurally connected interferometer (SCI) architecture and a separated spacecraft interferometer (SSI) architecture. As a secondary consideration, the two architectures are examined in both orbits, 1.0 AU and 5.2 AU. The optical configuration is initially assumed to be a 1-3-3-1 array, with the alternative 1-2--2-1 configuration discussed in a later section.

1.3 Previous Work

Most of the component mass estimates used in this work are taken from other current interferometer designs. A review by the Jet Propulsion Laboratory (JPL) [15] covered the aspects of a stellar interferometer which became the Space Interferometry Mission (SIM), a proposed 10 m baseline,

Michelson interferometer using seven siderostats consisting of three collector pairs and a spare. SIM is due to be launched in early 2005. The New Millennium Interferometer (NMI) [21], which is a candidate for the third mission in the Deep Space initiative of the New Millennium program, is a separated spacecraft array technology demonstration flight, scheduled for launch in 2001. Other sources of information were the Multiple Spacecraft Interferometric Constellation (MUSIC) [23] and the Next Generation Space Telescope (NGST) [31] proposals. MUSIC is an ambitious separated spacecraft interferometer using sixteen collector elements put forward by JPL, while NGST is a monolithic telescope seeking to expand on the scope of the Hubble Space Telescope. The European Space Agency has also selected an Infrared Space Interferometer as a candidate mission for their Horizons 2000 program, with the proposed Darwin project [19]. Darwin is a two-dimensional, five aperture separated spacecraft design with the collectors in a hexagonal configuration. The hexagon formation is 50-100 m in diameter, and the instrument will be placed in a 5.2 AU orbit.

However, nearly all of these interferometer concepts and projects have made an *a priori* assumption concerning the architecture, whether structurally connected or multiple spacecraft. Surka [32] conducted a general study of the two architectures and developed a method for determining the more optimal one, based on several variables in the design and the operating environment. The primary focus of his work was calculating the baseline at which an SCI became more mass efficient than an SSI as a function of the mission lifetime. The primary result was that for a nominal 15-yr mission in a 1.0 AU orbit, a separated spacecraft architecture became less massive than a structurally connected architecture only for baselines greater than 400 m. However, the interferometer configuration assumed by Surka, a simple, single collector pair, and the component mass estimates and operational parameters used in his study are different for the Terrestrial Planet

Finder mission, and thus his conclusion does not necessarily imply that TPF should be a structurally connected architecture. Nonetheless, his analysis provided an important beginning framework for this study.

The technology needed for optical nulling has been the subject of much study in recent years, as well. In a series of papers prepared during the ExNPS study, different aspects of the Planet Finder mission were examined. The first paper, by Woolf [35], focused on the science behind the nulling and presented an optical configuration with four collectors in a double Bracewell pairing. Also, the study included larger arrays consisting of eight or more collectors and compared the advantages of full, interspersed arrays against paired arrays where each pair is staggered by a $\lambda/4$ phase spacing. The second publication by Woolf and Angel [36] was a comprehensive overview of techniques for the direct detection of planets beyond the solar system. The focal plane instrumentation and affects of slight errors in the signal on the central null were the subject of the third paper in the series, by Woolf, Angel, and Burge [37]. The fourth [38] was a cursory look at the engineering aspects of the Planet Finder mission, such as mirror sizes, propulsion and power requirements, and architecture design. Much of the optical design in the current study draws from this series of papers.

1.4 Principles of Stellar Interferometry

An understanding of the theory behind an interferometer used for astrophysical observations is useful for an operational comparison of potential architectures. One of the first proposals for direct detection of planets through nulling interferometry was by Bracewell [8], in 1978. A detailed review of the history of optical interferometry, as well as an explanation of interferometric principles, is given by Shao and Colavita [29].

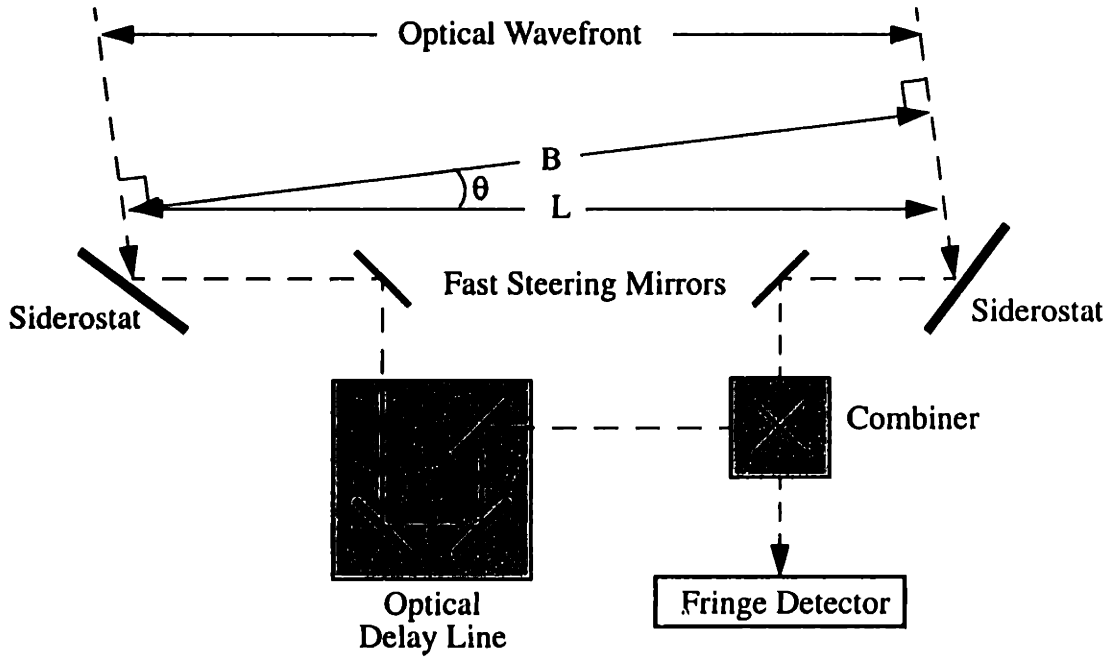

Figure 1.2: A Stellar Michelson Interferometer

In order to obtain the increasingly higher resolution needed for astrophysical observation using a monolithic telescope, the aperture size of the observing mirror has to likewise grow because of the relation

$$\Theta_{filled} = 1.22\frac{\lambda}{D} \tag{1.1}$$

where Θ_{filled} is the angular resolution of the filled aperture telescope, λ is the wavelength of the light, and D is the aperture diameter. Beyond a certain point, the large diameter mirror becomes prohibitive in both size and cost. Fortunately, by taking advantage of the interference patterns of light, an interferometer with small diameter apertures can provide the same level of performance, in terms of the angular resolution, as a single, large-diameter mirror, as given by

$$\Theta_{fringes} = \frac{\lambda}{B} \tag{1.2}$$

where $\Theta_{fringes}$ is the resolution, as defined by the fringe spacing, and B is the effective baseline.

An interferometer functions by combining the light from two mirrors in such a way that the two waves interfere with each other, creating fringe patterns which reveal information about the source of the light.

The Terrestrial Planet Finder is a type of pupil plane interferometer, commonly called a Michelson interferometer, in which the signals from the apertures are overlapped in the pupil plane. The basic elements of a Michelson interferometer are shown in Figure 1.2. Two apertures, separated by the distance, L, collect the incoming light using small mirrors, or siderostats, and redirect it to an optical combiner. The angular separation of the point source from the median angle of the interferometer is given by the angle, θ, with the effective baseline, B, being the projection of the separation baseline on the plane normal to the incident radiation. Within the combiner, the light is passed through a series of steering mirrors, optical delay lines, and beamsplitters, and then interfered to create fringe patterns on a detector. The actual position of the signal source can be determined by deconvolving the signal and reconstructing the image through an inverse Fourier transform.

In order to reach the high angular resolution, the wavefronts of the two incoming beams of light must have a phase difference of less than a fraction of a wavelength, $\lambda/6000$ for TPF, where λ is the wavelength of the light being observed. Optical delay lines (ODL) are responsible for correcting optical path length differences (OPD) up to a centimeter in magnitude so that the two wavetrains coincide.

1.4.1 Nulling Interferometry

Direct detection of a planet requires the emitted light from the planet to be isolated from the light from its parent star. The ratio between the intensities of the star and the planet is a function of the

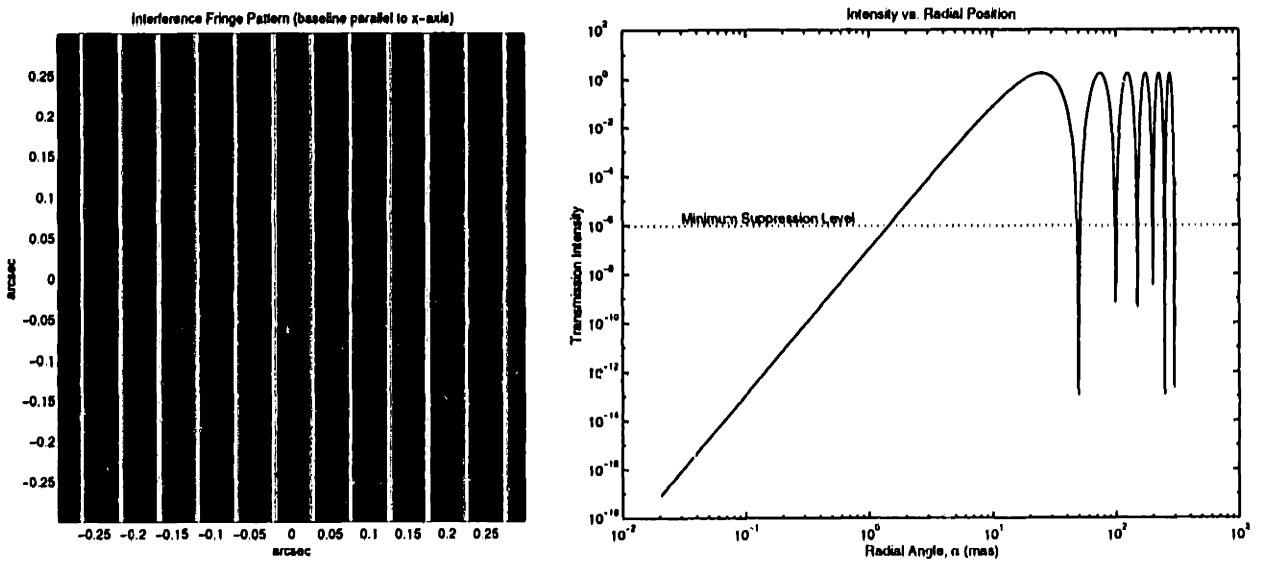

(a) (b)

Figure 1.3: Fringe Pattern From a Four-Element Bracewell Interferometer
a) Transmission Field; b) Radial Transmission Magnitude

wavelength and varies from over one billion to one to nearly one million to one over the electromagnetic spectrum for a sun-like star and an earth-like planet. The infrared band of the spectrum is more favorable to detection than visible light with intensity ratios on the order of 10^6 to one. The concept of a nulling interferometer, which effectively blocks the light around the central line of sight in order to suppress the parent star, was initially advanced by Bracewell in 1978 [8]. Fundamentally, the light from one arm of the interferometer is given a phase delay of π radians, which causes the light from an on-axis source to deconstructively interfere and disappear from the detector. Any off-axis source, such as a planet, produces signals which constructively interfere and appear as a signal modulated by the rotation of the interferometer.

A simple, two-element Bracewell pair does not provide a central null with adequate width or depth for the Planet Finder mission. In the infrared band, a suppression level of at least 10^{-6} is required to make the light from the star and the planet of the same magnitude, while 10^{-7} would provide a clearer signal. The level of light suppression from a single Bracewell nulling pair is

effectively only 10^{-3} over a narrow central band. As a modification to the original Bracewell interferometer, Angel [1] suggested increasing the number of collectors to four, incorporating two pairs of Bracewell elements to deepen the central null. Later, varying the diameter and spacing of the collector pairs was used by Angel and Woolf [2] to induce a broader null. A four element Bracewell design with equal spacing between collectors and a diameter ratio of one to three between the outer and inner pairs produces the fringe pattern shown in Figure 1.3. The minimum suppression level is taken to be 10^{-6} such that the planet has an intensity greater than or equal to the parent star. The graphic on the left is the transmitted intensity field of the interferometer, with the baseline parallel to the horizontal axis of the figure, where the white bands represent the constructive fringes. The graph on the right is a logarithmic plot of the transmitted intensity from the center to the edge of the field-of-view. The central null, as delimited by a 10^{-6} transmission intensity threshold, is roughly four milliarcseconds wide and several intensity peaks are within one arcsecond of the origin, which is the habitable zone for many of the intended stellar targets.

The operation of the interferometer is not unlike holding a picture of a solar system behind a picket fence with the star behind the central dark fringe (Figure 1.3a) and rotating the fence about an axis through the central fringe; the light from a planet will alternately be blocked and transmitted as the bands (pickets) pass in front of it, producing a signal like that shown in Figure 1.4. The wide peaks are where the planet is located inside (between pickets) and is moving parallel to a transmission band, while the narrow peaks are the result of the planet passing perpendicular to the transmission fringes. Measurements are taken at several wavelengths in the infrared spectrum and an image of the target system is reconstructed in a process similar to those used in radio astronomy. The actual equations involved are discussed in Chapter 3 when the signals are optimized for spacecraft propellant usage.

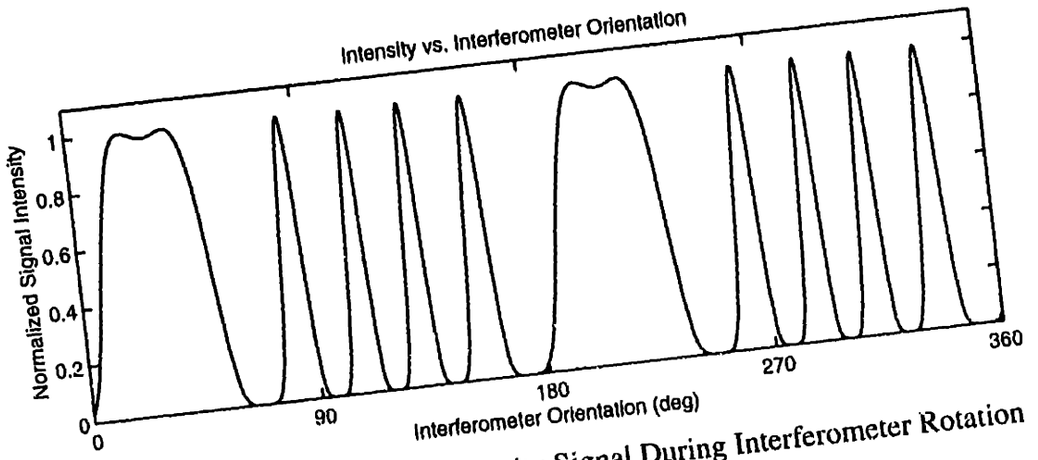

Figure 1.4: Simulated Planet Intensity Signal During Interferometer Rotation

1.5 Study Objectives

The primary objective of this study is to both qualitatively and quantitatively compare two potential architectures for the Terrestrial Planet Finder, a structurally connected interferometer and a separated spacecraft interferometer. Following a general analytic framework for comparing distributed satellite systems proposed by Shaw *et al* [30], three metrics are defined and applied in the comparison. The first metric in the approach taken by Shaw is the cost per performance. However, due to the infancy of the TPF program, any estimates of the program cost at this point would be highly uncertain. Since the cost of most space programs scales as the launched mass, the primary metric in this study is the total system *wet mass*, made up of the estimated dry mass of the interferometer plus the total propellant required for the duration of the mission, excluding the launch vehicle and orbital insertion phase. Also, the performance of the two architectures is assumed to be equal since they will be meeting the same scientific requirements.

The second metric is the *adaptability* of the architecture, which is a measure of the sensitivity of the design to changes in the functional requirements. Judging the flexibility of the design in accommodating growth and modifications in the functional requirements is an important consid-

Table 1.1: Application of Comparison Metrics

Metric	Definition	TPF Application
Cost Per Function	Cost to provide common level of performance among systems	Total mass of system architecture, including optics and propellant
Adaptability	Sensitivity of the design to modifications in the functional requirements	Sensitivity of the design to modifications in the functional requirements
Capability	Ability and efficiency of the system at performing its design role	Ability and efficiency of the system at performing its design role
Resolution	Angular resolution of the interferometer in isolating the planet	Acquiring and isolating the planet signal from the parent star
Rate	Time to detect and disseminate information	Mean time to construct an accurate image of the target system
Integrity	Error control and noise rejection of the system	Image sensitivity to zodiacal noise and environmental disturbances
Availability	Reliability and probability of being operational during lifetime	Failure compensation modes for combiner or collector failure

eration in evaluating the two architectures. Cost overruns, program delays, and even outright cancellation can result from poor adaptability.

Thirdly, the ability and the efficiency of the system at performing its design role over the mission lifetime is captured in the *capability metric.* As Shaw defines it, the capability is a measure of how well the system meets four types of constraints: isolation, rate, integrity, and availability. The *isolation* corresponds to the angular resolution of the interferometer as it impacts the isolation of the planet apart from the parent star. The *rate* performance is a measure of the imaging time and target detection of the instrument. The error control and noise rejection of the system is the *integrity* constraint, while the *availability* gauges how the first three constraints vary over the lifetime of the mission due to component degradation or failure. In this study, the rate constraint of the

interferometer is taken to be solely dependent on the optical hardware and thus, no distinguishing factors exist between the two architectures.

These three metrics, wet mass, adaptability, and capability, define the analysis coverage given in Table 1.1. Also, since the values used in the wet mass comparison are only early estimates, an attempt is made to characterize the uncertainties in the models through a comparison with other current industry studies.

In summary, the primary objectives of this study are:

(i) to reduce a general distributed satellite systems analysis framework to a more specific level by relating three specific metrics, the wet mass, adaptability, and capability, to the Terrestrial Planet Finder mission concept,

(ii) to apply those metrics to a comparison of structurally connected and separated spacecraft interferometers in order to judge the relative merits of each architecture,

(iii) to validate that comparison by including preliminary designs from industry contractors and gauging the variation in mass estimates and operational profiles,

(iv) to provide a general presentation of the issues in selecting an architecture for the Terrestrial Planet Finder as a guideline for future, more detailed research.

1.6 Approach and Outline

The primary metric in this study is the *wet mass* of the system, which is introduced in Chapter 2. Reference designs are built up from system components whose masses are estimated from other current and proposed space-based astronomy missions. Both the structurally connected interferometer (SCI) and the separated spacecraft interferometer (SSI) are assumed to be composed of similar components; the components which exist in one architecture, but not the other, form the

basis for the actual architectural comparison.

Several key assumptions were made in this study in order to simplify the mass comparison. The most important one is in the modeling of the system components. The breakdown of the subsystems is a very simple one, and many have been grouped together as one component. The assumption is that errors in the components masses are somewhat averaged out in the final total, which is verified later in the comparisons with contractor models. Secondly, the assumption is made that a fair comparison of the cost of the architectures can be simplified to the wet mass comparison without performing an explicit analysis of the projected cost. This assumption is a typical one in the aerospace industry for decisions made early in the design process.

Chapter 3 examines the actual assumptions made in the development of the two reference designs by considering possible modifications to several of the reference components. Since the deployment mechanism is the largest mass component in the reference SCI design, its design is crucial to the wet mass comparison. Correspondingly, potential improvements in the propulsion system for the separated spacecraft are examined, as well. The chapter concludes by discussing the possible optimization of the trajectories followed by the collector spacecraft and an analysis of the ramifications on the image quality.

The *adaptability metric* is presented in Chapter 4. Possible modifications in the functional requirements such as the optical configuration, separation baseline, mission duration, imaging process, and mission objectives are studied to determine their effects on the architectural comparison.

Chapter 5 covers the *capability metric* and is broken down into four areas which examine the constraints given above, the resolution, rate, integrity, and availability. Except for the rate requirement, the other three have different impacts on the two architectures which are each considered in

turn.

In Chapter 6, three initial contractor models obtained from TRW, Inc., Ball Aerospace & Technologies Corp., and Lockheed Martin Corp. are used to validate the final mass estimates and reference designs used in the comparison. The mass budgets from their designs are consolidated into the same subsystem components as the reference designs so that a direct system comparison can be made. Also, although all three companies focused on a structurally connected architecture, the assumptions made in their designs can be used to extrapolate other possible SSI designs. This comparison establishes an estimate of the uncertainty in the designs as well as an indication of whether or not this uncertainty is large enough to impact the selection between the two architectures.

Finally, Chapter 7 concludes with a summary of each of the three metrics and the areas in which the two architectures excel. The relative merits of each architecture are presented and a final conclusion is made. In the end, the objective is to present a more complete discussion of the trade-offs between a structurally connected architecture and a separated spacecraft architecture with regard to the Terrestrial Planet Finder mission.

Chapter 2

Wet Mass Comparison

Based on the requirements drawn from the ExNPS report [7] and presented in Chapter 1, reference designs for both the structurally connected (SCI) and the separated spacecraft (SSI) architectures for the Terrestrial Planet Finder (TPF) are developed in this chapter. Components of these designs are drawn from several other astronomy missions and form the foundation for the primary comparison in this study, that of the wet mass. The wet mass is defined to encompass the mass of the telescope over its operational lifetime. Therefore, the maneuvering propellant required by the separated spacecraft for rotating the fringe pattern on the sky is included in the mass estimate, while the launch vehicle shrouding mass and orbital transfer propellant, tanks, and thrusters are not. Altogether, four complete mass estimates are made, an SCI and an SSI in both a 1.0 AU and a 5.2 AU orbit.

This chapter begins with a rationalization for choosing such a standard for comparison and properly defines it. Section 2.2 introduces the reference designs for each architecture, beginning with the functional requirements for the Terrestrial Planet Finder and the assumptions made concerning its operational profile. Then, each of the components included in the reference designs are presented along with their mass estimates. Finally, Section 2.3 presents the total system masses

for both orbits and highlights the mass drivers of each architecture. The differences in wet mass are then summarized, along with potential implications on the architectural selection.

2.1 Metric Definition

The primary metric in this comparative study is taken to be the total mass of the interferometer once placed into its final orbit. The rationale behind this choice of definition lies in the fact that for most space payloads, the cost scales proportionally with the total mass put into orbit. Accordingly, the cost metric for this comparison of interferometer architectures is defined as the total wet mass required to perform the functional requirements of the program, including, but not limited to, structural mass, guidance, navigation, and control elements, optical instruments, and propellant. This wet mass is the sum of the dry mass, which depends on the actual architectural design, and the propellant mass, which depends on the operational profile of the mission. However, neither launch nor orbital transfer elements are included. Both architectures provide the same level of performance, as dictated by NASA, of imaging the requisite number of star systems during the mission lifetime.

One potential drawback to using a strict mass metric is identified by Surka [32] as being the correlation between spacecraft complexity and its cost. Separated spacecraft interferometers have not yet been flown, and the cost of building and testing new control hardware and instrumentation may not conform to the accepted mass-to-cost relationship. For example, increasing the truss mass may cost substantially less than improving the formation flying capabilities of the free-flyers, though at a similar mass penalty. However, adding mass for the increased complexity of an SSI is an insubstantial solution not explored in this study.

2.2 Initial Reference Designs

Using the requirements placed on the Terrestrial Planet Finder, assumptions are made which allow for a preliminary estimate of the mass of the system components which make up each architecture. Certain of the components are invariant over architecture and orbit, while other components require actual design. The mass estimates are based on other current and future astronomical missions. The Space Interferometry Mission (SIM) [15] [34] is well along in its design phase and has current mass estimates available. The New Millennium Interferometer (NMI), a candidate design for DS-3 [21], is a separated spacecraft interferometer currently under review by NASA. Other sources of information were the Multiple Spacecraft Interferometric Constellation (MUSIC) [23] and the Next Generation Space Telescope (NGST) [31] proposals.

2.2.1 Assumptions

An assumption inherent in the approach is that the designs may be broken down into components which are independently designed. The total configuration can then be constructed using these components as building blocks. While this approach may not be entirely realistic, it provides a framework which serves to highlight the issues which drive the total system mass and simplifies the modifications required for different orbital radii and optical configurations. By recognizing that certain system components are likely to be similar in both architectures, the final discussion can concentrate on the components which are unique between them.

Other assumptions are made concerning the functional design of each instrument. First, for the structurally connected interferometer, the truss is assumed to be deployed using a threaded canister design currently in use by AEC-Able Engineering [12]. Two deployment canisters are needed, one for each half of the boom assembly. In the case of the separated spacecraft interfer-

Table 2.1: Reference Design Assumptions

Parameter	Value
Separation Baseline	75 m
Propulsion System	Pulsed Plasma Thrusters (I_{sp} = 1000 sec)
Deployment Mechanism	Two Threaded Canisters
Optical Configuration	1-3-3-1
Primary Mirror Diameter	6.0 m (1.0 AU) 1.5 m (5.2 AU)
Rotation Period	2 hr
Mission Lifetime	5 yr

ometer architecture, the propulsion system assumed in the design is a pulsed plasma thruster (PPT), which provides a high specific impulse with a fine degree of thrust control and accuracy. High levels of thrust are not needed and the use of teflon as a propellant is very mass efficient.

Also, some assumptions are made about the scientific operation of the interferometer. The size of the optics is dictated by the orbit and various models of the local zodiacal cloud. The values used initially in this study are taken from the first reports by members of the ExNPS team [6]. The inner mirror diameter is assumed to be 6.0 m for an interferometer in a 1.0 AU orbit and 1.5 m for a 5.2 AU orbit. The mirrors are in a 1-3-3-1 configuration, meaning the ratio of the diameters of the inner pair to the outer pair is three to one. Therefore, the smaller, outer mirrors have 2.0 m diameters at 1.0 AU and 0.5 m diameters at 5.2 AU. The rotation rate allowed by the imaging equipment is still uncertain and so certain inferences are made, based on other characteristics of the mission, resulting in the assumption of a two hour rotation period. The lifetime of the mission is also an assumption subject to future modification with a value used in this study of five years. The assumptions are all summarized in Table 2.1.

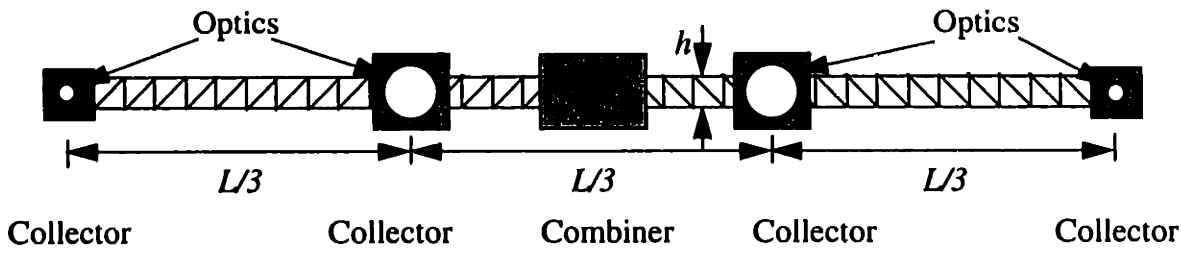

Figure 2.1: Reference Structurally Connected Interferometer Model

2.2.2 Global SCI Architecture

Six major components are included in the design for the structurally connected interferometer, shown in Figure 2.1. The largest component is the truss assembly itself on which all the subsystems are mounted. Two separate truss sections are assumed, one for each side of the interferometer. In the center of the spacecraft are the optical combiner and the main spacecraft bus, which contains the propulsion, power, communications, and thermal subsystems. Four collector components are spaced along the truss and contain the hardware needed to direct the mirrors and reflect the light to the combiner. The actual optical systems which collect the light are housed within these collectors and correspond to the primary mirrors. The final component of the SCI design is the deployment mechanism containing the canisters needed to deploy the truss in its final orbit. One canister is added for each side of the boom assembly. The breakdown is listed in Table 2.2.

Table 2.2: SCI Component Listing

Component	Quantity
Optical Combiner	1
Collector	4
Optical System	4
Spacecraft Bus	1
Truss Assembly	2
Deployment Canisters	2

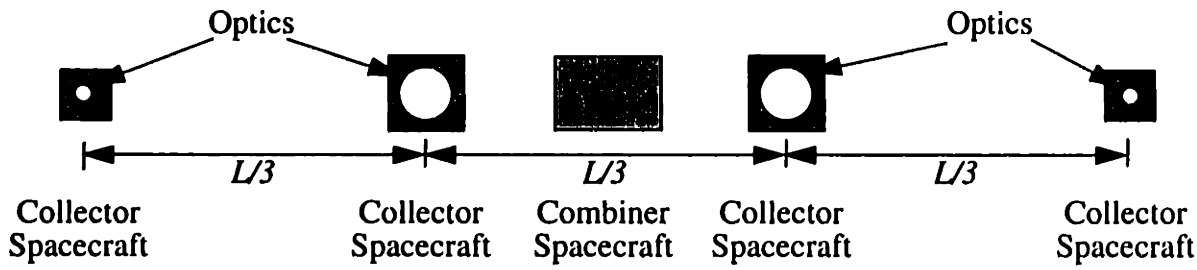

Figure 2.2: Reference Separated Spacecraft Interferometer Model

The SCI design rotates freely in space using momentum wheels to control the torque on the spacecraft, providing the maneuvering needed for image synthesis. While propellant will be needed for periodically desaturating the momentum wheels and re-orienting the telescope, the amount of mass required has been found to be small relative to the other components and is ignored in the SCI mass calculation.

2.2.3 Global SSI Architecture

The separated spacecraft design uses similar components, but requires five independently free flying spacecraft, as shown in Figure 2.2. Accordingly, the SSI requires five spacecraft buses. In this study, because the separated spacecraft buses must contain propulsion, power, communication, and thermal systems just as the SCI bus does, each of the SSI buses are assumed to be equal in mass to the SCI bus. In addition, one combiner and four collectors are needed, with corresponding optical subsystems. A large portion of the SSI wet mass lies in the propellant mass needed for maneuvering the four collector spacecraft around the combiner. For simplicity, the total propellant mass for the entire constellation is considered to be one component, rather than separately listing the mass for each spacecraft. Only the propellant needed for maneuvering is calculated in this study; slewing to reorient the line-of-sight of the instrument was found to be negligible relative to the maneuvering. The component list is shown in Table 2.3.

Table 2.3: SSI Component Listing

Component	Quantity
Optical Combiner	1
Collector	4
Optical Subsystem	4
Spacecraft Bus	5
Maneuvering Propellant	1

2.2.4 System Components

Taken together, all of the components listed above comprise every subsystem and function of the interferometer. Under the assumption that each can be independently designed, the component masses are estimated or calculated as explained in the following sections.

Optical Combiner - The combiner component of the interferometer lies in the center of the linear configuration and combines the light from each collecting mirror. The Terrestrial Planet Finder has two pairs of Bracewell interferometers which are independently combined and then the outputs of the two pairs are themselves combined. The path taken by the light rays is shown in Figure 2.3. The optical delay lines contain mirrors which shift in order to fractionally delay the light, thereby maintaining the wavefront coherence. All three beam combiners sit in the center of the interferometer configuration, along with the optical delay lines. Also, the combiner contains the fringe detector and the other instruments used for planet detection. The total mass estimated for the combiner module is the same for both the SCI and the SSI architectures and is assumed to be 150 kg, equal to the DS-3 design [21].

Collector - The collector module is composed of the hardware necessary for reflecting the collected starlight in towards the combiner. The instruments are also responsible for keeping the collecting optics locked in position once the target star is located. Again based on the system

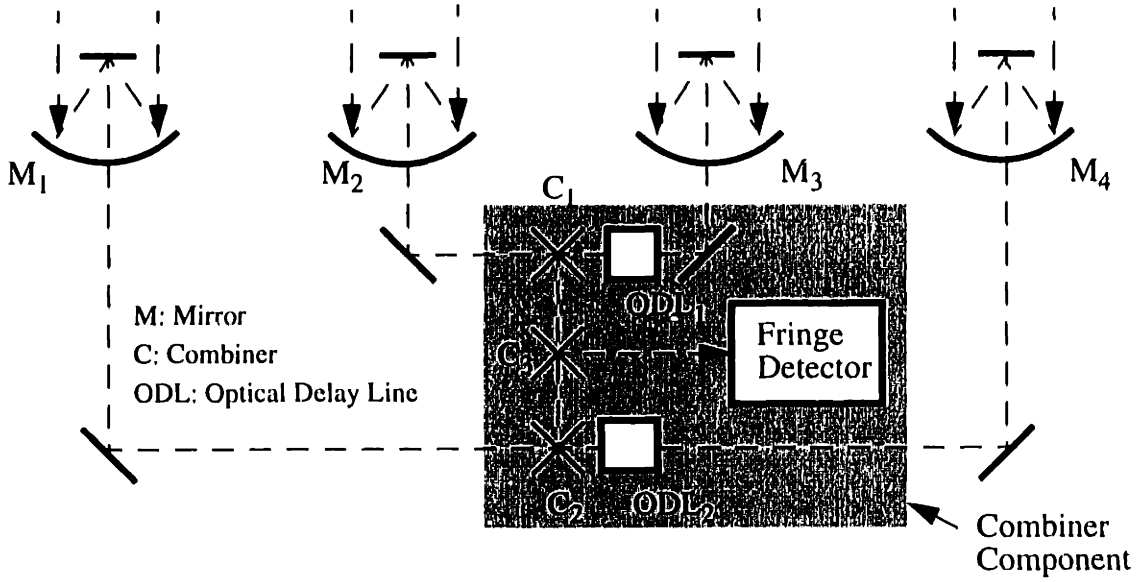

Figure 2.3: Schematic of a Four-Collector Bracewell Interferometer

breakdown for DS-3, the collector mass is estimated to be 25 kg in both architectures.

Optical System - The actual mirrors used to collect the light from the star system are a separate component because their mass can be calculated using current estimates for optical areal densities. The latest designs for the Next Generation Space Telescope [9] call for a mirror design with a mass of approximately 750 kg for a diameter of 8 m, which implies an areal density of about 15 kg/m^2. The optical requirements for TPF dictate inner mirror diameters of 6 m and 1.5 m for the 1.0 AU and 5.2 AU orbits, respectively. The current configuration for TPF also calls for a 1-3-3-1 array in which the outer mirrors would have a diameter one-third of the inner ones. Using an optical areal density, ρ_{optics}, of 15 kg/m^2, the optical system masses can be calculated as

$$m_{optics} = \rho_{optics}\pi R^2 \tag{2.1}$$

where R is the mirror radius. The values used in this study are shown in Table 2.4. The mass of the optics is assumed to be independent of the interferometer architecture.

Spacecraft Bus - The bus of the spacecraft is largely a generic component responsible for the

Table 2.4: Calculation of the Optical System Mass

Parameter	1.0 AU Orbit		5.2 AU Orbit	
	Inner Pair	Outer Pair	Inner pair	Outer Pair
Diameter	6.0 m	2.0 m	1.5 m	0.5 m
Mirror Mass	425 kg	47 kg	26.5 kg	3 kg
Quantity	2	2	2	2
Total Optics Mass		**944 kg**		**59 kg**

non-optical operations of the interferometer. It handles all communications, either inter-spacecraft or earth downlink, and includes the necessary antennas and transceivers. It is also charged with maintaining the global position of the spacecraft relative to its orbit or to other spacecraft, for which thrusters and propellant storage units are included. In addition, the power system needed for the operation of the pulsed plasma thrusters is included in the spacecraft bus. All these systems are summarily grouped into the spacecraft bus component. Based on present designs for DS-3 and SIM, the mass of the spacecraft bus is estimated to be 100 kg. The spacecraft bus does not include any propellant.

Truss Assembly - The truss is the primary component of the structurally connected interferometer architecture. It connects the four collectors with the combiner and provides rigidity for the spacecraft. The truss also allows the SCI to passively maintain the fixed relative positions of the mirrors while rotating by carrying the constant centripetal load.

The truss is assumed to be composed of cubic bays, each with four longerons, four diagonal struts, and a square batten frame. For the most part, the analysis of the truss design and mass calculation follows that of Surka [32].The three variables which completely describe the truss are its

length, L, its aspect ratio, AR, and its areal density, υ, defined as

$$AR = \frac{L}{h} \tag{2.2}$$

$$\upsilon = \frac{A}{h^2} \tag{2.3}$$

where h is the truss height, equal to its width, and A is the cross-sectional area. Both the aspect ratio and the areal density are non-dimensional quantities.

In the original work by Surka, the aspect ratio and the areal density were artificially limited to set boundaries for the study, with a range for the aspect ratio of 1-1000 and of 0.001-1 for the areal density. The only practical restraint placed on the truss design was the thickness of the truss struts. Not surprisingly, the minimum mass design always drove the aspect ratio to its maximum and the areal density near to its minimum. However, in this study, the aspect ratio is limited to a value of 100 which is more characteristic of current truss models, examples of which are shown in Table 2.5. The Structural Assembly Demonstration Experiment (SADE) was an experiment designed to demonstrate the on-orbit assembly and deployment of a space structure from the Space Shuttle [26]. The Middeck 0-gravity Dynamics Experiment (MODE) was a project by the MIT Space Systems Lab which studied the structural dynamics of a deployable truss in micro-gravity [5]. The Interferometric Stellar Imaging System is a JPL proposal for which MIT submitted a design [24]. Two other trusses which provided estimates for the aspect ratios were the second Interferometry Program Experiment (IPEX) and the Shuttle Radio Topography Mission (SRTM) [27], both of which use AEC-Able Engineering deployable trusses. The parameter values for the final two trusses were given by AEC-Able Engineering [12] as justification for the deployment mechanism empirical mass formula.

Table 2.5: Current Truss Model Parameters

Truss Model	Length	Height	Cross-Sectional Area	Aspect Ratio	Areal Density
SADE	978 cm	140 cm	22.6 cm^2	7	0.0012
MODE	183 cm	20 cm	0.775 cm^2	9	0.0018
ISIS	25 m	30 cm	7.0 cm^2	83	0.0078
IPEX-II	30 m	30.5 cm	1.34 cm^2	98	0.0015
SRTM	60 m	77 cm	--	78	--
SCI Model	75 m	75 cm	5.6 cm^2	100	0.001

The total mass of the truss can be calculated by expressing the mass per bay in terms of the three parameters above and then multiplying the result by the number of bays. The truss bay cross-section layout is shown in Figure 2.4. Each bay has four struts in the frame, four longitudinal struts, four diagonal struts, plus a diagonal through the center which gives

$$m_{bay} = (8 + 5\sqrt{2})\rho L_s A_s \tag{2.4}$$

where m_{bay} is the mass of the truss bay, ρ is the material density, and L_s and A_s are the length and cross-sectional area of the individual struts. The strut length is defined by the aspect ratio.

$$L_s = \frac{L}{AR} \tag{2.5}$$

Although Surka further defined and calculated the strut area, the strut thickness, and the wall thickness, the small areal density implies a solid strut cross-section and so the value of the strut cross-sectional area can simply be expressed as a fraction of the total cross-sectional area.

$$A_s = \frac{1}{(4 + 4\sqrt{2})} A \tag{2.6}$$

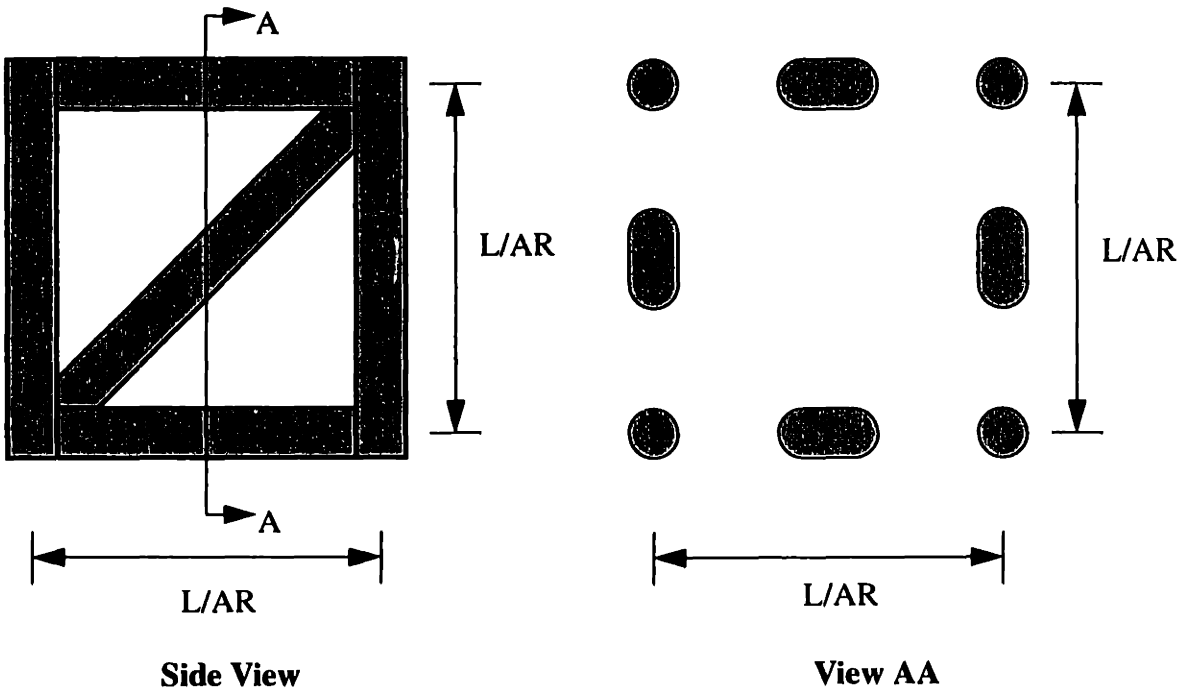

Figure 2.4: Truss Bay Cross-Section

Combining these formulas with Equations 2.2 and 2.3 provides a simplification of the mass per unit bay as

$$m_{bay} = \frac{(8+5\sqrt{2})}{(4+4\sqrt{2})}\rho\upsilon\frac{L^2}{AR} \tag{2.7}$$

Because the bays are cubic, the number of bays is merely the length divided by the aspect ratio which gives the final mass of the truss as

$$m_{truss} = f\rho\upsilon\frac{L^3}{AR^2} \tag{2.8}$$

where f is the volumetric constant, equal to approximately 1.56 for a rectangular truss such as the one shown, and ρ is the material density. In addition, the area moment of inertia is needed for the performance analysis in Appendix A and is calculated using the radius of gyration of the truss, r_g,

Table 2.6: Calculation of the Total Truss Mass

Parameter	Value
Material Density	1744 kg/m^2
Areal Density	0.001
Section Length	37.5 m
Section Aspect Ratio	50
Section Mass	57.4 kg
Quantity	2
Total Truss Mass	**114.8 kg**

which is assumed to be equal to half of its width, giving

$$I = \frac{A}{2} r_g^2 = \frac{\upsilon}{8}\left(\frac{L}{AR}\right)^8 \tag{2.9}$$

The material density was one of the trades examined in the original work. Graphite/epoxy, with a density of 1744 kg/m^3, was clearly the best material choice for space trusses and is assumed to be the material used in constructing TPF. The boom is assumed to be divided into two 37.5 m long sections, one for each side of the instrument. Table 2.6 lists the parameters which lead to the calculation of the total mass of the metered truss and gives the result of 115 kg.

Deployment Mechanism - Because the interferometer must fit within a reasonable volume in order to be launched, the SCI does not extend the booms to their full length until the final orbital position is reached. Current designs offer a variety of techniques for the deployment mechanism, but the 75 m length of the truss makes most of them prohibitively massive or complex.

AEC-Able Engineering utilizes a technique for their truss designs which extends the boom through the use of a threaded canister. Based on information obtained from AEC-Able [12], an empirical formula was used to calculate the mass of the deployment mechanism. For each section

Table 2.7: Calculation of the Deployment Mechanism Mass

Parameter	Value
Section Length	37.5 m
Section Aspect Ratio	50
Section Mass	499 kg
Quantity	2
Total Deployment Mass	**998 kg**

of a metered truss, the estimated mass for its deployment was calculated as

$$m_{deploy} = 490\left[\left(1.3\frac{l}{AR}\right)^2 + \left(\frac{l}{554}\right)\right] \tag{2.10}$$

where l is the length of each boom and AR is its aspect ratio. This formula is based on the design experience of AEC-Able and fits well to current truss designs, primarily the Shuttle Radar Topography Mission (SRTM) [27], which uses a 60 m truss developed from the truss design to be used on the International Space Station.

The assumption was made that one truss section would deploy on either side of the combiner. The outer collectors are permanently fixed to the ends of their respective trusses and the inner collectors grasp their respective intermediate bays as they deploy. Accordingly, the total configuration contains two deployment canisters, with each section length equal to half of the total baseline. Table 2.7 summarizes the deployment mechanism mass parameters. The potential necessity of having four deployment canisters because of the complexity of the grasping function, as well as other possible deployment techniques, is discussed in Chapter 3.

Propellant - The total propellant mass estimate for the separated spacecraft interferometer includes propellant for the four collector spacecraft to maneuver about the combiner. The propellant needed for repointing maneuvers was calculated to be negligible relative to the amount

required for rotation, since the collector spacecraft continuously maneuver to modulate the signal from the star. The non-stop thrusting requires a significant amount of propellant to be carried onboard the collector spacecraft. The thrusting needed for orbital transfer is ignored.

Assuming that each spacecraft constantly fires its thrusters as it moves in a circular rotation about the combiner spacecraft, the amount of ΔV per spacecraft required for one full rotation is the centripetal acceleration multiplied by the rotation period,

$$\Delta V_{i,\,rot} = \omega^2 R_i T_{rot} \tag{2.11}$$

where ω is the angular velocity, R_i is the distance from the combiner spacecraft, and T_{rot} is the rotation period. Simplifying by the definition of the rotation rate gives

$$\Delta V_{i,\,rot} = \frac{4\pi^2 R_i}{T_{rot}} \tag{2.12}$$

The total ΔV required over the mission lifetime per spacecraft is then

$$\Delta V_{i,\,life} = \frac{4\pi^2 R_i}{T_{rot}^2} T_{life} \tag{2.13}$$

where T_{life} represents the total lifetime.

Once the velocity requirement is calculated, the propellent mass ratio can be found using a modified form of the rocket equation,

$$\frac{m_{prop}}{m_{dry}} = \left[\exp\left(\frac{\Delta V_{life}}{I_{sp} g}\right) - 1\right] \tag{2.14}$$

where m_{prop} and m_{dry} represent the propellent and dry mass of the spacecraft, respectively, I_{sp} the

Table 2.8: Calculation of the Total Propellant Mass

Parameter	1.0 AU Orbit		5.2 AU Orbit	
	Inner Pair	**Outer Pair**	**Inner Pair**	**Outer Pair**
Rotation Time	2 hr	2 hr	2 hr	2 hr
Rotation Radius	12.5 m	37.5 m	12.5 m	37.5 m
Specific Impulse	1000 s	1000 s	1000 s	1000 s
Mission Lifetime	5 yr	5 yr	5 yr	5 yr
Lifetime ΔV	1.5 km/s	4.5 km/s	1.5 km/s	4.5 km/s
Dry Mass	550 kg	172 kg	151.5 kg	128 kg
Propellant Mass	91 kg	100 kg	25 kg	74.5 kg
Quantity	2	2	2	2
Total Propellant Mass		**382 kg**		**199 kg**

specific impulse of the micro-propulsion system, and g the gravitational constant at the earth's surface. The propellant mass is found by using the total dry mass of each spacecraft to calculate its propellant mass and then summing the four values. The values used for the propellant calculation are shown in Table 2.8 for both the inner and the outer pair of spacecraft and for both orbits.

The rotation time of the interferometer can be inferred from several factors. First, as pointed out by Woolf [37], approximately 1000 separate data points must be taken in order to accurately measure the fringe of a target planet. With an integration time per point of four seconds, the instrument must not rotate faster than once every 67 minutes. As a lower limit, Woolf suggests that the decision of whether or not to make further analysis of the target system should be made within several hours. The initial assumption made in this study is a rotation rate of once every two hours, which is the value advanced by the Jet Propulsion Laboratory for current TPF studies.

The choice of propellant follows from the analysis done originally by Surka. Because the required thrust levels are not high, a fuel with a high specific impulse is desired. Pulsed plasma

thrusters provide a specific impulse of roughly 1000 sec and their low power requirements make them ideal for deep space missions. In addition, a PPT system can deliver small discrete impulse bits which makes the precision thrusting for optical alignment possible [25]. A pulsed plasma thruster is capable of thrust up to a maximum of several millinewtons. A bank of PPTs can be used if higher thrust values are required for maneuvering. Also, PPTs are simple propulsion systems, not needing tanks, pressurization, or cryogenic storage.

2.3 Conclusions

As stated in the introduction, a modified cost comparison can be made by comparing the total wet mass of each of the architectures. For most space applications, the financial cost of the missions scales with the launched mass. Since the two architectures are assumed to have the same performance, the final cost per function metric simplifies to a comparison of the total wet mass. Because the optical subsystem and propellant components have different values for the two possible orbits, two different comparisons must be made.

The wet mass comparison can be reduced by noting that the block elements which are invariant over architecture can be effectively cancelled between the designs, leaving only the unique components to form the real comparison. For these modules for Planet Finder, the basic comparison is between the truss and deployment mechanism for the SCI and the propellant mass plus the added spacecraft buses for the SSI. When the propellant mass is significantly less than the estimated mass for the truss and deployment canisters, the SSI is the more mass-efficient architecture. Conversely, if the propellant requirement grows to the point that the sum of its mass and the mass of the buses surpasses the truss and deployment mass, the SCI becomes the more optimal design. As an example, since the truss and deployment masses of the SCI are independent of mission life-

Table 2.9: Architectural Wet Mass Summary For 1.0 AU Orbit

Component	Structurally Connected Interferometer		Separated Spacecraft Interferometer	
	Quantity	Total Mass	Quantity	Total Mass
Optical Combiner	1	150 kg	1	150 kg
Collector	4	100 kg	4	100 kg
Optical System	4	944 kg	4	944 kg
Spacecraft Bus	1	100 kg	5	500 kg
Truss Assembly	1	115 kg	--	--
Deployment Mechanism	2	998 kg	--	--
Propellant	--	--	1	382 kg
Total Wet Mass	**--**	**2407 kg**	**--**	**2076 kg**

time, longer mission lifetimes will require more propellant for the SSI, eventually making the SCI the more mass efficient architectural design.

2.3.1 Wet Mass Results For 1.0 AU Orbit Radius

The breakdown and calculation of the wet mass for interferometers in a 1.0 AU solar orbit is shown in Table 2.9. In this case, the mass of the truss and the deployment mechanism is over twice as massive as the spacecraft buses and the propellant for five years of operation, and so the separated spacecraft configuration is more mass efficient and can meet the operational requirements with a smaller wet mass. The deployment mechanism is clearly the mass driver for the SCI design, accounting for nearly 42% of the total. This extreme ratio indicates that a new, more mass efficient technique for extending the truss could drastically reduce the deployment mass, but the deployment mass must be reduced by a third in order to make the reference SCI design competitive. Other options for the deployment mechanism, other than the threaded canister design, are discussed in Chapter 3. Also, the empirical formula used in this study is based on present truss

Table 2.10: Architectural Wet Mass Summary For 5.2 AU Orbit

Component	Structurally Connected Interferometer		Separated Spacecraft Interferometer	
	Quantity	Total Mass	Quantity	Total Mass
Optical Combiner	1	150 kg	1	150 kg
Collector	4	100 kg	4	100 kg
Optical System	4	59 kg	4	59 kg
Spacecraft Bus	1	100 kg	5	500 kg
Truss Assembly	1	115 kg	--	--
Deployment Mechanism	2	998 kg	--	--
Propellant	--	--	1	199 kg
Total Wet Mass	**--**	**1522 kg**	**--**	**1008 kg**

design masses which are likely to fall within the next few years.

Each of the outer two spacecraft in the SSI configuration must carry roughly 100 kg of propellant, with the inner pair requiring slightly less, 90 kg. The total propellant mass is just over 18% of the total SSI wet mass, with the optical subsystem making up just under half of the total mass, at 45%. For this reference case, the separated spacecraft architecture is just over 330 kg, or 16%, less massive than the structurally connected architecture.

2.3.2 Wet Mass Results For 5.2 AU Orbit Radius

At an orbit further from the sun, the optical subsystems are smaller due to the lower level of background noise and zodiacal interference. The decrease in spacecraft dry mass lowers the propellent requirement as well. The total breakdown is shown in Table 2.10.

The mass of the SCI falls by about 885 kg for the larger orbit because of the smaller optical subsystem masses. The truss and deployment mechanism remain the same, with the relative mass

percentage of the deployment canisters rising to 65.6%, which is extremely high. In order for the wet mass of the structurally connected design to be comparable to the SSI, the deployment mass must be on the order of 500 kg, or about half of its present estimate.

The separated spacecraft design becomes even more mass efficient in this case because of the reduced dry mass. The spacecraft bus make up about half of the total mass, which, bearing in mind the inclusive definition of the component, is realistic for present designs. The propellant mass at a 5.2 AU orbit makes up about 20% of the total wet mass of the SSI. On the whole, for the reference designs in a 5.2 AU orbit, the structurally connected interferometer architecture mass is over 500 kg higher than the separated spacecraft interferometer architecture mass, a difference of over 50%.

2.3.3 Summary

The separated spacecraft architecture is more mass efficient than the structurally connected architecture for these reference designs, with a wet mass that is 86% and 66% of the comparable SCI mass for the 1.0 AU and the 5.2 AU orbits, respectively. The major factor in the disparity of the system masses is the large size of the model of the deployment mechanism. Using a threaded canister design implies a large truss housing and so the mass of the deployment system may be overly inflated due to the size of the Terrestrial Planet Finder boom. Therefore, using different methods for extending the truss is one of the factors examined in the next chapter which focuses on variations in the assumptions made in the reference model designs.

The wet mass comparison is practically a trade-off between the truss and deployment mechanism on the part of the SCI and the propellant and spacecraft bus on the part of the SSI. Other than these components, the two architectures are roughly equal, since the same collectors, combiner,

and hardware are used. The results of this study disagree slightly with the conclusion of Surka's work which is attributable to the fact that Surka neglected to include a deployment mechanism and allowed a much more fragile truss design.

The decision concerning the orbital radius of the Terrestrial Planet Finder mission is still uncertain, but the profile of the Galileo mission to Jupiter can offer some information. Galileo used the Inertial Upper Stage (IUS)[1] booster, built by the Boeing Company, to provide the roughly 4 km/s of velocity corrections needed for a gravity assist trajectory profile which carried the Galileo spacecraft to Venus, to Earth twice, and then on to Jupiter. The wet mass of the IUS is roughly 14,740 kg, with a propulsion system which uses solid propellant. The IUS has also been used for several other space missions, notably Magellan and Ulysses. The IUS provides over 200,000 N of thrust which should be sufficient for the TPF spacecraft. Therefore, in some sense, the wet mass values given in this chapter are for the payloads to be inserted in either the 1.0 AU or the 5.2 AU orbit, and the orbital transfer to 5.2 AU can be achieved by the IUS booster at no penalty to the TPF design.

---

1. STS-73 Press Kit, NASA. <URL:http://shuttle.nasa.gov/sts-73/shutref/carriers.html>. Accessed 20 May 1998

Chapter 3

Design Sensitivities

Many assumptions were made in Chapter 2 in order to allow reference designs to be developed. However, many of these assumptions were not based upon hard and fast requirements. As a first example, two truss deployment canisters were chosen for the SCI reference design. Instead, four may be needed if problems arise in attaching the inner collector bays to the truss as it deploys. Or, a different technique may be used altogether, instead of threaded canisters, to deploy the truss, such as hinged trusses or inflatable booms. Second, pulsed plasma thrusters (PPTs) were selected for maneuvering the collector spacecraft in the SSI design. Other types of propulsion could be used in the place of PPTs, such as cold gas or Xenon-ion thrusters. Third, instead of maneuvering the SSI collector spacecraft along the circumference of a circle, the operational profile may have them maneuver along the sides of a closed polygon (e.g., a square) in order to possibly save fuel or to lessen the disturbances associated with the maneuver burns. In any case, this chapter explores the sensitivity of the wet mass to variations in some of the component technologies which comprise the TPF reference designs. High sensitivities will identify those technologies whose further development will be most instrumental in reducing the wet mass, and therefore the cost, of the TPF mission.

The first section discusses the truss deployment mechanism and how potential modifications could affect the architectural comparison. Section 3.2 examines other, more efficient propulsion systems, with the final section examining the trajectories followed by the collector spacecraft and the resulting propellant usage.

3.1 Truss Deployment Mechanism

The most massive component in the reference structurally connected interferometer design is the deployment mechanism needed to extend the truss, which accounts for over half the total wet mass for the 5.2 AU orbit design. The estimated mass is calculated using an empirical formula obtained from AEC-Able Engineering [12] which is extrapolated from current truss designs and technologies. The truss uses a threaded screw canister to deploy the boom, with a canister mass based primarily on the width and height of the truss. In the deployment canister mass equation,

$$m_{deploy} = 490\left[\left(1.3\frac{l}{AR}\right)^2 + \left(\frac{l}{554}\right)\right] \tag{3.1}$$

where l represents the length of the truss section and AR the section aspect ratio, the width of the truss is included as (l/AR). The coefficients in the equation imply that 99% of the mass is dependent on the width, with the length of the truss section barely affecting the deployment mass.

Because of this large dependence on the width, the natural consideration in examining the design sensitivity to the truss size is to calculate the truss width which causes the total wet masses to be equal. Assuming a constant truss areal density of 0.001, as defined in the previous chapter, increasing the aspect ratio of the truss decreases its mass as well as the mass of the deployment mechanism. The SCI mass is equal to the SSI mass for an aspect ratio of 114.4 in a 1.0 AU orbit, which is a very small increase from the assumed value of 100. Therefore, the architectural mass

comparison, and primarily the deployment mechanism mass, is extremely sensitive to the characteristics of the truss design.

A problem, however, with using two deployment canisters, as the reference SCI design does, is that the inner collector bays must latch on to the truss as it deploys. Furthermore, the truss will have to extend through the inner collector bay. If further research indicates that such a system introduces insurmountable problems in collector stability and positioning, four deployment canisters may be required. Four truss sections would be deployed, with a collector bay mounted at the tip of each section. The outer boom sections would be attached to the ends of the inner boom sections.

Because of the absence of a significant mass dependence on the actual length of the truss section being deployed, using four deployment canisters would effectively double the mass of the deployment mechanism, to nearly 2000 kg. In the reference SCI design, a deployment mechanism of 2000 kg would represent nearly 80% of the total wet mass of an interferometer in a 5.2 AU orbit. Such a large, disproportionate component mass might be a prohibitive penalty in selecting a structurally connected architecture for the Terrestrial Planet Finder.

On the other hand, the mass of the deployment mechanism may be reduced by avoiding large deployment canisters. A TPF concept proposed by Lockheed Martin, which is presented in Chapter 6, uses hinged truss sections which unfold once the spacecraft is in orbit. A 'finesse' truss concept using guy wires and sub-booms was suggested by TRW and is also included in Chapter 6. The ExNPS Road Map [7] mentioned inflatable trusses as being advantageous because of their high packaging efficiency. The launch of the Shuttle Radar Topography Mission (SRTM) [27] in May of 2000 will demonstrate a 60 m truss deployed from the space shuttle bay and will provide more experience with large truss deployment technologies. In any event, the mass comparison

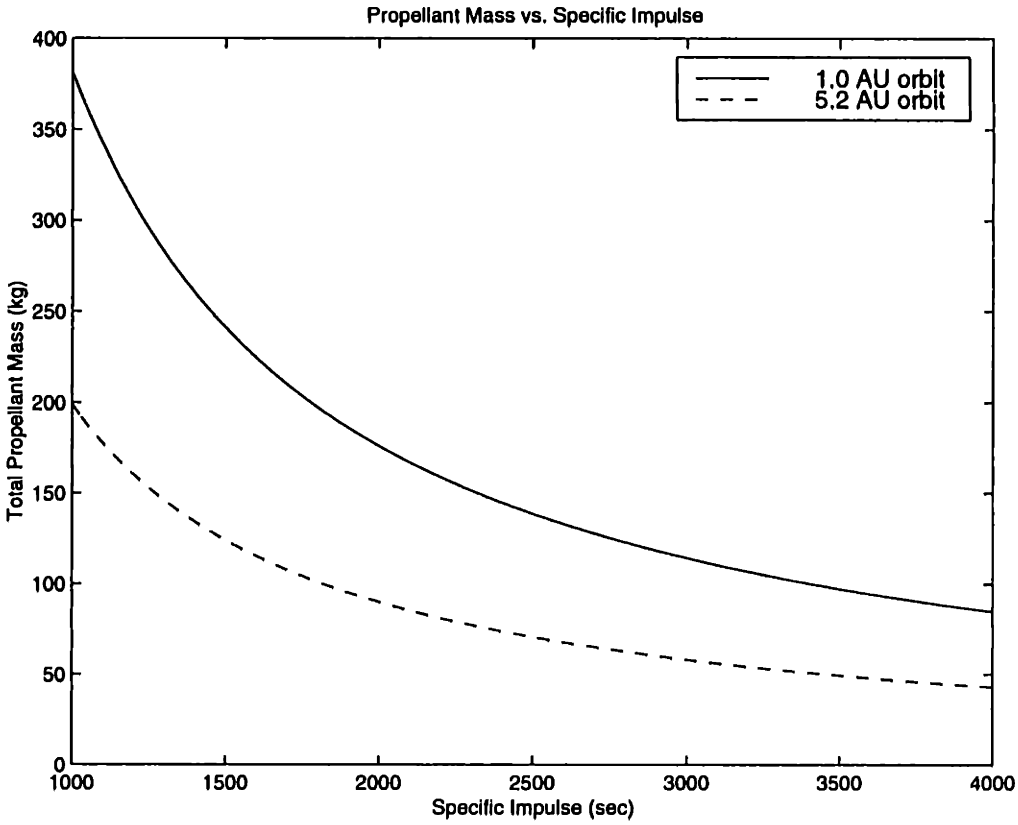

Figure 3.1: Propellant Mass vs. Propellant Specific Impulse

between the two architectures is very dependent on the truss deployment system, so further research on the viabilities of deployment technologies is critical for accurate mass comparisons.

3.2 Propulsion System

The specific impulse of 1000 sec assumed in the calculations for the propellant mass is actually on the low end of the range for pulsed plasma thrusters. Recent development of pulsed plasma thrusters for orbit corrections on small satellites has obtained specific impulses of over 1400 sec [18] [25]. Increasing the specific impulse has the direct effect of decreasing the amount of teflon needed to operate the interferometer over its lifetime. Figure 3.1 shows the propellant mass decreasing as the specific impulse improves, with an I_{sp} of 3000 sec lowering the propellant mass to 115 kg in a 1.0 AU orbit and 58 kg in a 5.2 AU orbit from the reference values of 382 kg and

199 kg obtained using an I_{sp} of 1000 sec.

Alternatively, instead of a PPT system, xenon-ion propulsion might be considered for TPF. Ion propulsion provides a much higher specific impulse, with values reaching 20,000 sec. The major drawback in using ion propulsion, though, is the massive amount of power needed to operate the thruster, 400 W for xenon propellant. In effect, an ion thruster would trade propellant mass for power system mass. Increasing the specific impulse would decrease the propellant needed at the cost of requiring a bigger power supply.

The wet mass of a separated spacecraft interferometer is very sensitive to a more efficient propulsion system, as measured by the specific impulse and the thrust-to-weight ratio of the entire propulsion and power subsystem. An additional mass savings of perhaps 250 kg could be realized using more efficient PPTs, which would widen the mass difference between the two architectures even further.

3.3 Collector Spacecraft Maneuvering Profiles

The normal assumption about the maneuver paths which the collector spacecraft follow in a separated configuration is that they are circular, which follows from the pure rotation of a truss. However, circular movement requires a constant thrust to provide the centripetal acceleration. Alternatively, the spacecraft may instead fire its thrusters and then drift for a bit before thrusting again. The resulting path becomes a polygon. Optimizing the profile indicates that the fewer legs in the polygon, the less velocity change is required. Because the linear configuration must remain symmetric about the central combiner spacecraft, polygons with an odd number of sides are eliminated from consideration, making a square the optimal path.

Each spacecraft moves in a straight line, thrusting only at the four corners. The optical base-

line of the interferometer lengthens and contracts as the formation moves along the square. In order to justify modifying the maneuver profile to a square, the quality of the reconstructed image must be equal to or better than the quality of an image taken following a circular path. Furthermore, this image quality is not strictly defined as the resolution of the interferometer; more accurately, the image quality is a measure of the level of planet detectability produced by the interferometer. The verification of the image quality is discussed later in this section.

As derived in the previous chapter in the analysis of the propellant usage, the total velocity change for a circular rotation path is given by

$$\Delta V_{i,\,life} = \frac{4\pi^2 R_i}{T_{rot}^2} T_{life} \tag{3.2}$$

where $\Delta V_{i,life}$ is velocity change for the i^{th} spacecraft, R_i is the distance from the combiner, and T_{rot} and T_{life} are the rotation period and mission lifetime, respectively. The rotation period is assumed to be two hours, with a mission lifetime of five years.

For a square maneuvering profile, the average velocity of each spacecraft is the perimeter divided by the period,

$$V_i = \frac{4a_i}{T_{rot}} \tag{3.3}$$

where a_i is the length of the side of the square path followed by the i^{th} spacecraft. At each corner, a relatively quick velocity change is affected so that the direction of the velocity vector shifts by 90°. The magnitude of the vector change, assuming the thrust is directed 135° from the original

flight path, is then

$$\Delta V_i = \sqrt{2} \cdot \frac{4a_i}{T_{rot}} \tag{3.4}$$

giving a total ΔV per complete circuit of

$$\Delta V_i = 4\sqrt{2} \cdot \frac{4a_i}{T_{rot}} \tag{3.5}$$

The total ΔV over the mission lifetime is then the product of the circuit velocity change and the number of completed circuits made during the lifetime, or

$$\Delta V_{i,\,life} = 4\sqrt{2} \cdot \frac{4a_i}{T_{rot}^2} T_{life} \tag{3.6}$$

Therefore, the ratio of the velocity expenditure for a square profile to a circular profile is given by

$$\frac{\Delta V_{square}}{\Delta V_{circle}} = \frac{4\sqrt{2}a_i}{\pi^2 R_i} = 0.573\frac{a_i}{R_i} \tag{3.7}$$

Since the resolution of the interferometer is linearly dependent on the baseline, the natural selection for the perimeter value is one which keeps the time-averaged baseline constant. The time-averaged baseline can be found by integrating the baseline around one complete circuit and dividing by the rotation period. Because of symmetry, the integration can be reduced to one-eighth of the complete path, such that the time-averaged baseline, $\overline{B}$, is given by

$$\overline{B} = \frac{1}{T_{rot}/8} \int_0^{T_{rot}/8} 2\left[\left(\frac{a}{2}\right)^2 + \left(\frac{4a}{T_{rot}}t\right)^2\right]^{\frac{1}{2}} dt \tag{3.8}$$

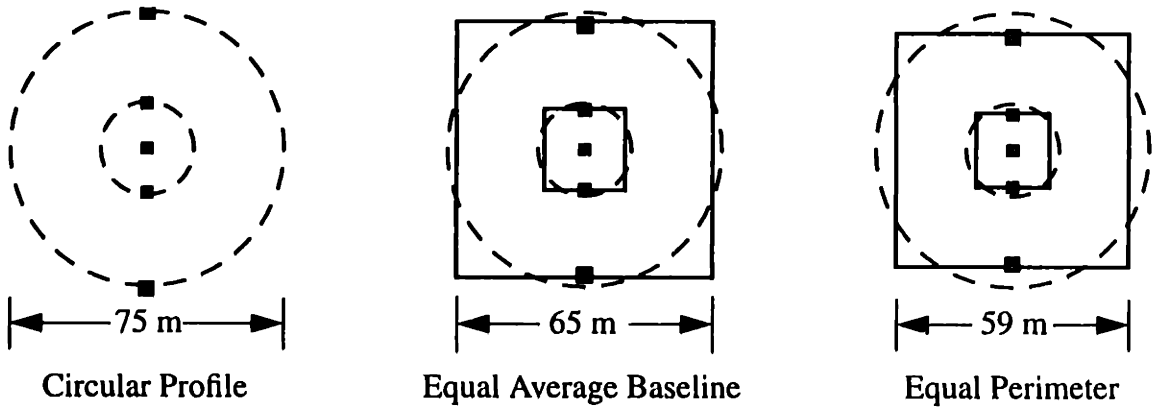

Figure 3.2: Different Maneuver Profile Trajectory Paths

where the time, t, is the variable of integration. Substituting variables by the relations

$$x = \frac{4a}{T_{rot}}t;\ dx = \frac{4a}{T_{rot}}dt;\ a' = \frac{a}{2} \tag{3.9}$$

results in the equation

$$\bar{B} = \frac{4}{a'}\int_0^{a'} \sqrt{a'^2 + x^2}\,dx \tag{3.10}$$

Performing the integration gives the final time-averaged baseline as

$$\bar{B} = \sqrt{2}a' + a'\ln[(1+\sqrt{2})a'] - a'\ln(a') = 2.296a' = 1.148a \tag{3.11}$$

Setting the time-averaged baseline of the square equal to the time-averaged baseline of the circle, which is merely the 75 m diameter, gives a side length, a, of 65.3 m. Therefore, the velocity ratio given in Equation 3.7 equals 0.998, indicating that a square which has the same time-averaged separation baseline as the original circle does not provide any propellant mass savings.

The next profile considered has a perimeter equal to the original circle's circumference, mean-

Table 3.1: Maneuver Profile Characteristics

Parameter		Circular Profile	Equal Avg. Baseline	Equal Perimeter
Average Outer Spacecraft Velocity		3.3 cm/s	3.6 cm/s	3.3 cm/s
Average Inner Spacecraft Velocity		1.1 cm/s	1.2 cm/s	1.1 cm/s
Total ΔV Requirement		12 km/s	12 km/s	10.8 km/s
Percent Velocity Change		N/A	0%	-10%
Total Propellant Mass	(1.0 AU) (5.2 AU)	382 kg 199 kg	382 kg 199 kg	338 kg 176 kg
Percent Propellant Mass Change	(1.0 AU) (5.2 AU)	N/A	0%	-11.5% -11.8%

ing the side length is given by

$$a = \frac{2\pi R}{4} \tag{3.12}$$

which gives an outer side length, a, of 58.9 m, resulting in a time-averaged separation baseline of 67.6 m. Relative to the circular path, this profile decreases the ΔV requirement by 10%, which translates to a propellant mass savings of over 11%. The three profiles are graphically shown in Figure 3.2, with the velocity characteristics and resulting propellant masses for the three profiles summarized in Table 3.1.

3.3.1 Thrust Constraint

The caveat to any decrease in ΔV, and subsequently the mass, is that a higher level of thrust is required to turn the corner in a sufficiently short amount of time. Assuming an optimal thrust angle of 135° off the velocity vector, the required thruster force, F_{thrust}, is

$$F_{thrust} = \frac{m\Delta V_c}{\tau} \tag{3.13}$$

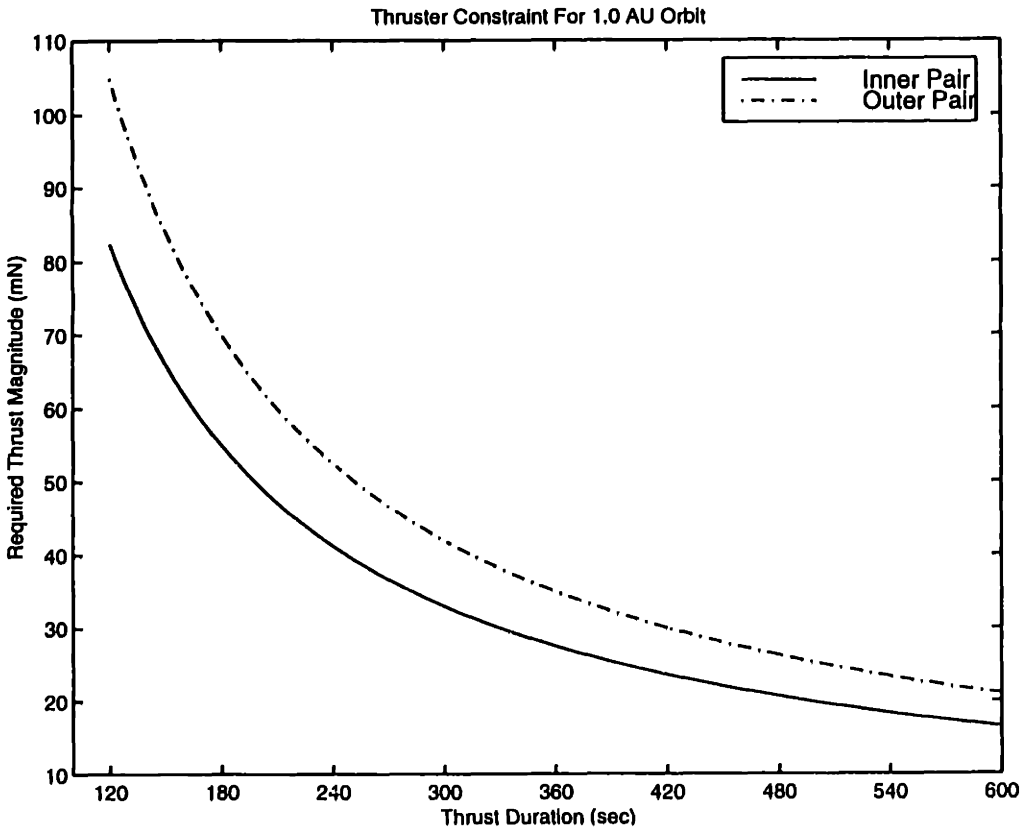

Figure 3.3: Thrust Level Requirement For Equal Perimeter Profile (1.0 AU Orbit)

where m is the spacecraft mass, ΔV_c is the velocity change at one corner, and τ is the time to turn the corner. For a five minute thruster duty cycle, the required thrust of the outer spacecraft in the equal perimeter profile for a 1.0 AU orbit, which has an initial wet mass of 272 kg, is 42 mN. Doubling the cornering time to ten minutes lowers the thrust requirement to 21 mN. The thrust level as a function of the time required to turn the corner, for the dry masses of the 1.0 AU SSI, is plotted in Figure 3.3. The corresponding thruster level required in a circular profile to maintain the centripetal acceleration of the outer collector spacecraft is roughly 7.9 mN.

The maximum thrust from a pulsed plasma thruster is on the order of several millinewtons, so a bank of several PPTs would be needed in order to implement either square maneuver profile, while perhaps only a pair for a circular path. This additional requirement would impact the spacecraft bus mass because of the additional solar array and battery optimization necessary, so a more

detailed mass analysis would be required in order to determine any actual mass savings to be gained from square maneuvering profiles.

3.3.2 Verification of Detection Sensitivity

As noted previously, the mass savings realized through a non-circular maneuver profile are only practical if they do not degrade the ability of the interferometer to detect a planet. The resolution of an interferometer, as measured by the spacing of the interference fringes, is given by the relation

$$\Theta_{fringes} = \frac{\lambda}{B} \tag{3.14}$$

where $\Theta_{fringes}$ is the fringe spacing, λ is the wavelength of the light, and B is the baseline normal to the incoming wavefront. Therefore, a profile which results in a smaller average baseline reduces the average resolution of the interferometer. However, the resolution alone does not constitute the planet detectability of the instrument; the actual isolation of the planet apart from the parent star and the exo-zodiacal noise may be more dependent on the position of the planet. Therefore, in order to gauge the effect of non-circular trajectories on the actual performance of the interferometer, the actual reconstructed images of a reference stellar system made by spacecraft following each of the three maneuver profiles must be compared.

Following the cross-correlation algorithm developed by Angel and Woolf [2], the transmitted intensities using the three maneuver profiles can be predicted and the reference images can be reconstructed and compared. For a single, two-element interferometer, the amplitude of the signal from a point source is the sine of the normalized angle,

$$a = \sin(\phi) \tag{3.15}$$

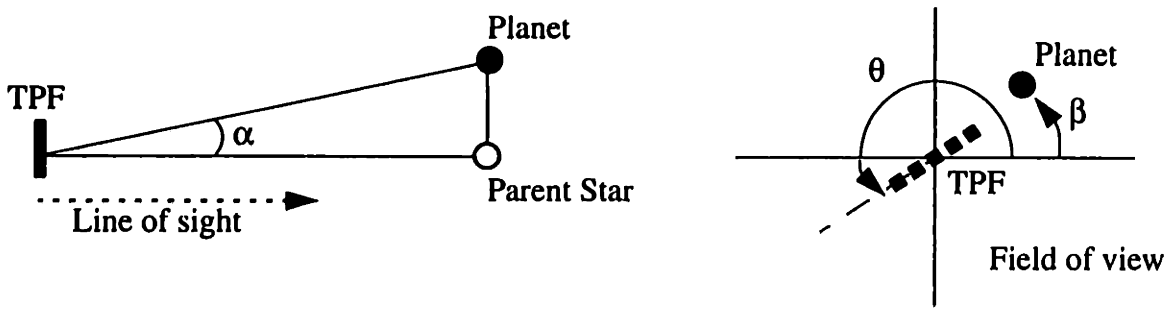

Figure 3.4: Representation of the Reference Star System

which depends on the position of the source and the relative orientation of the interferometer, and is given by

$$\phi = \left(\frac{2\pi}{\lambda}\alpha s\right)\cos(\beta - \theta) \tag{3.16}$$

where λ is the wavelength of the light, α is the angular separation of the planet from the parent star in the median plane of the interferometer, s is the separation baseline between the two collector apertures, β is the clock angle of the planet, and θ is the rotational position of the interferometer, as shown in Figure 3.4. The lobed nature of a single aperture beam profile is neglected.

Since the Terrestrial Planet Finder uses two Bracewell interferometer pairs, their outputs are superposed. The two pairs, of spacings s and $3s$ in the 1-3-3-1 array, have a 180° phase difference so that the outputs are out of phase at the center and cancel each other to high order. The difference in their amplitudes is sampled as

$$a = \sin(\phi) - \frac{1}{3}\sin(3\phi) = \frac{4}{3}\sin^3(\phi) \tag{3.17}$$

where a is the amplitude and ϕ is the normalized angle, defined in Equation 3.16. The three-to-one ratio in signal amplitudes is such that the two functions and their derivatives sum to zero around the origin, thus providing the central null that is key to the operation of the interferometer. The

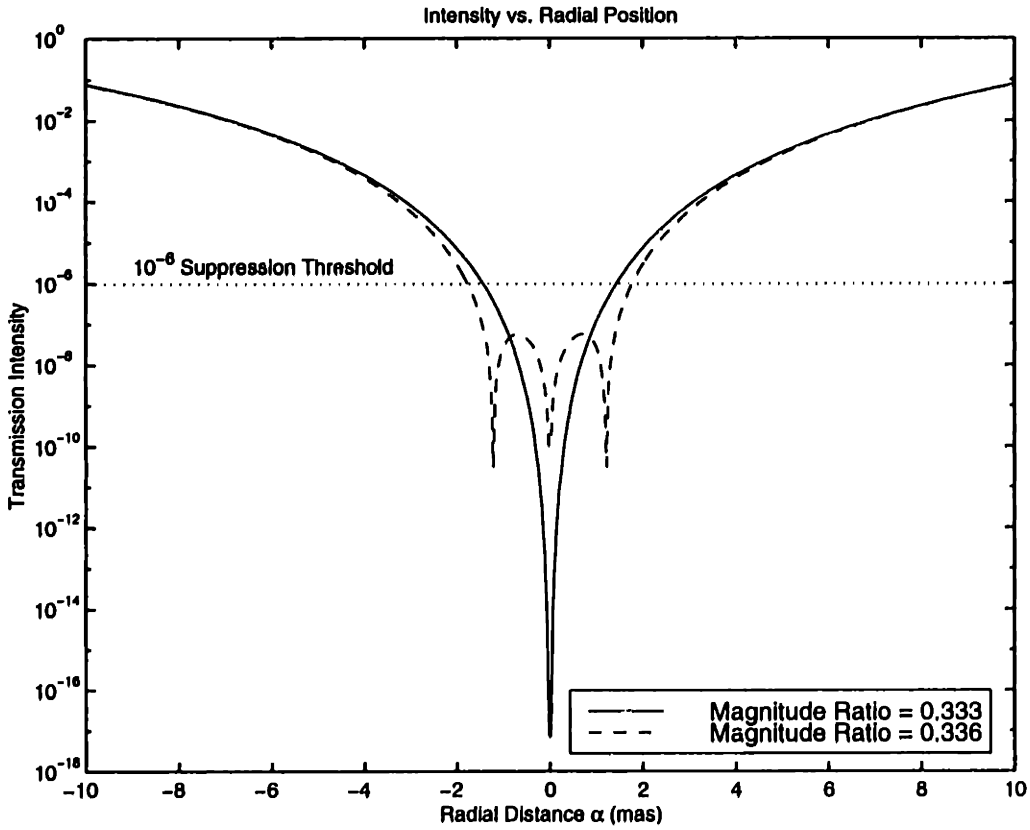

Figure 3.5: Transmission Intensity of Proposed Four-Element Interferometer

intensity of the signal is the square of the amplitude

$$T(\alpha, \beta, \lambda, \theta) = a^2 = \frac{16}{9}\sin^6(\phi) \tag{3.18}$$

and is shown in Figure 3.5 over the narrow range near the line-of-sight. Changing the amplitude ratio between the inner and outer pairs to 0.336, rather than 0.333, broadens the central null further by adding a triple peak to the amplitude curve, which is also shown in the intensity plot, as a dashed line.

Using Equation 3.18, the intensity transmission plots of the three maneuver profiles can be compared by using a reference star system which is a twin to the Earth-Sun system. A representation of the reference star, with the planet at an orientation of 30°, is shown in Figure 3.4. A planet 1.0 AU from a target star 10 pc from the Earth subtends an angle of 0.1 arcseconds. Using a wave-

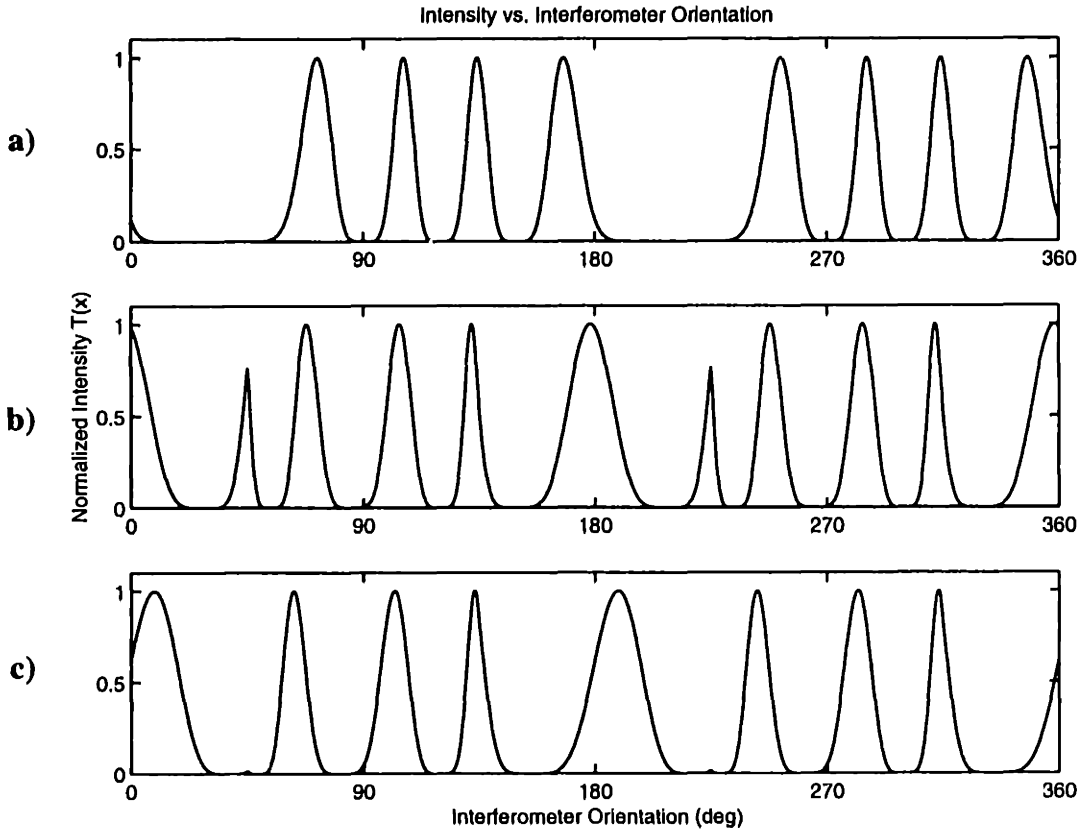

Figure 3.6: Transmission Intensity vs. Interferometer Orientation For Each Profile
a) Circular Profile; b) Equal Avg. Baseline Profile; c) Equal Perimeter Profile

length of 12 nm, roughly in the center of the thermal infrared band, the normalized intensity of the reference planet for the three trajectories through one full rotation of the interferometer is shown in Figure 3.6.

Discontinuities exist at orientations of 45° and (45 + n90)° in Figures 3.6b and 3.6c because of the transition points where the baseline stops increasing and begins decreasing at the corner of the square. The primary dip in the top graph is wide because the planet's orbital radius places it directly between two fringe peaks for this particular wavelength and baseline. The fact that the profile with an equal average baseline has a much larger maximum separation baseline is reflected in the two additional intensity peaks in the middle plot.

To reconstruct the image, an inverse Fourier transform is performed using signals measured

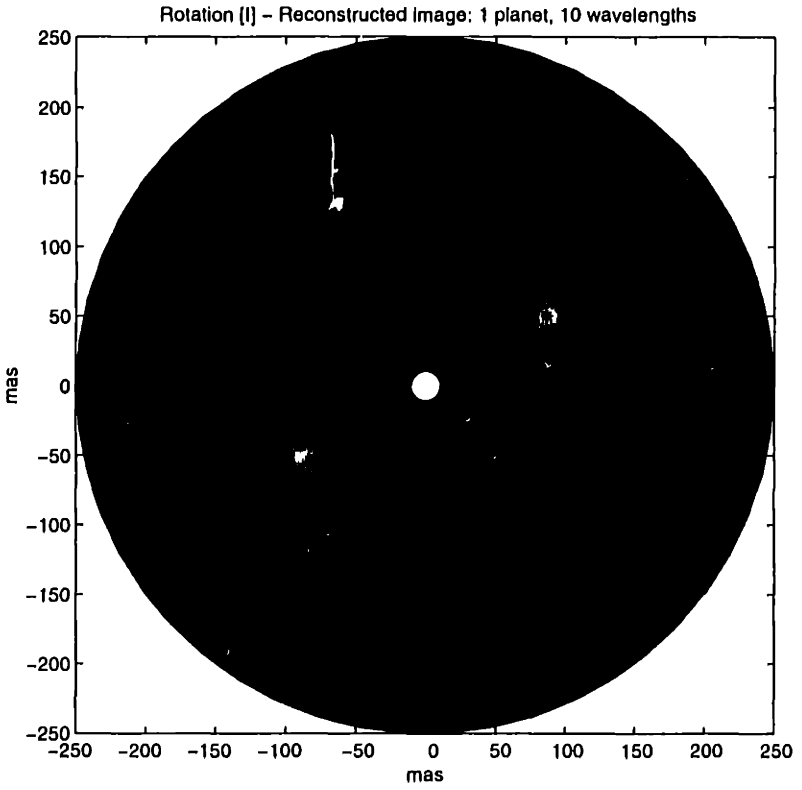

Figure 3.7: Reconstructed Image of Reference Star Using Circular Maneuver Profile

over a range of wavelengths.

$$I(\alpha, \beta) = \sum_{\lambda} \sum_{\theta} D(\lambda, \theta) T(\alpha, \beta, \lambda, \theta) \tag{3.19}$$

where $I(\alpha, \beta)$ is the intensity at the polar point (α, β), D is the measured signal strength, and T is the interferometer transmission. The summation over wavelength is equivalent to summing the signals over variations in the baseline. Because of the linearity of the interferometer, the image is symmetric through the center, with any planets appearing twice.

Using those transmission functions and the reference solar system, a simulated data signal was generated. Photon counts were taken at two degree intervals through a full rotation of the interferometer, with no assumed errors in pointing or wavelength. The result from reconstructing the images is shown in Figures 3.7-3.8. The dark asterisk in the three plots is the actual reference

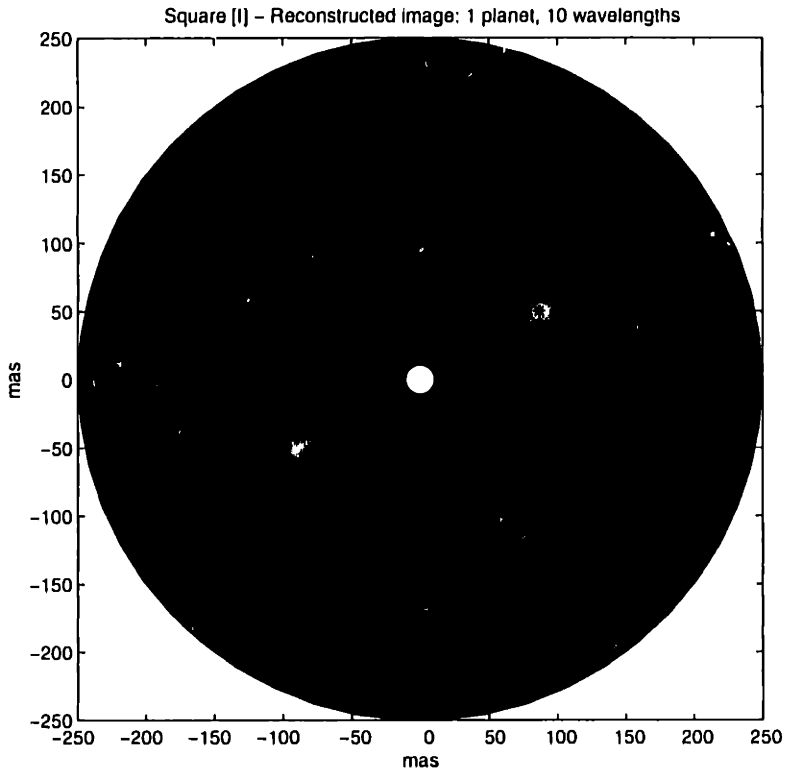

Figure 3.8: Reconstructed Image of Reference Star Using Equal Average Baseline Profile

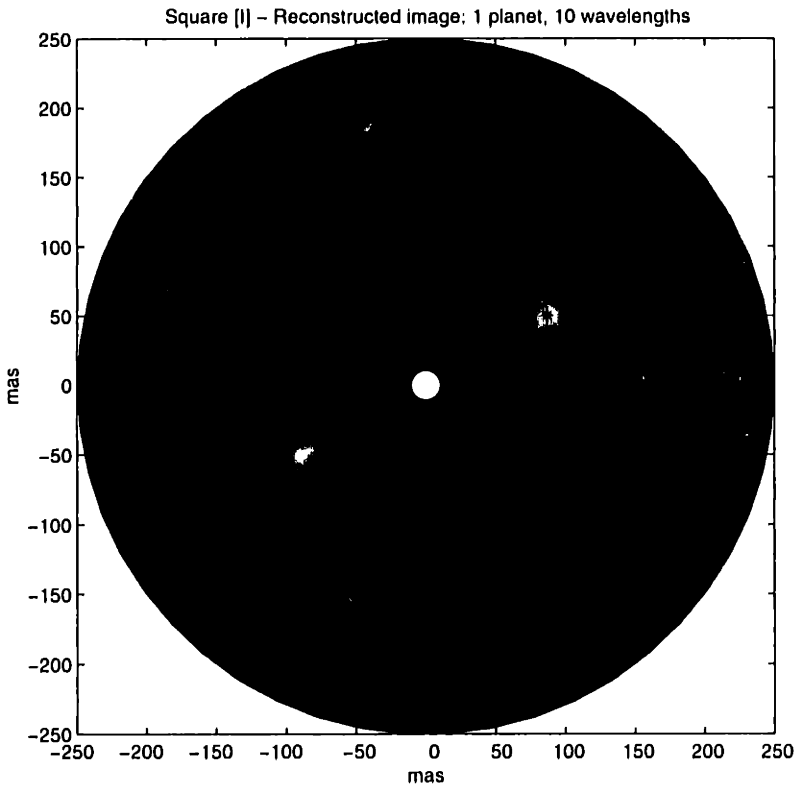

Figure 3.9: Reconstructed Image of Reference Star Using Equal Perimeter Profile

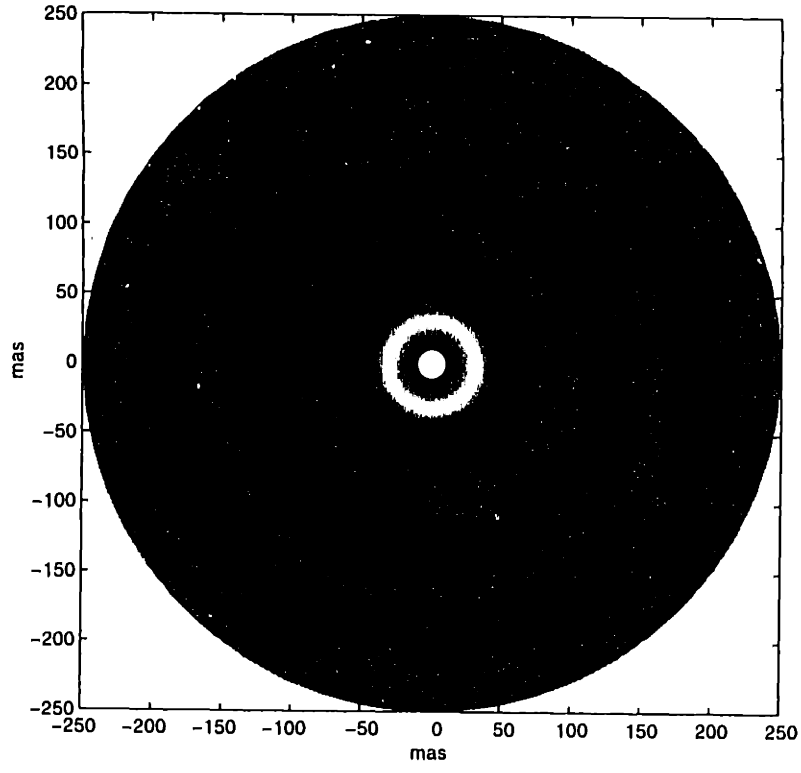

Figure 3.10: Full Field of View Integration Using Circular Maneuver Profile

planet position. The quality of these reconstructed images seem to be nearly equivalent and the relative magnitudes of the reconstructed point source to the background error is roughly equal.

Not only is the actual magnitude of the detected planet a concern, but the sensitivity of the interferometer for actually detecting a planet, regardless of its position in the field of view, is also critical in determining the image quality. In addition, the possibility of seeing multiple planets in a solar system exists, and so the three maneuver profiles must all have a relatively smooth detection levels in the focal plane. One way to examine this issue is to remove the dependence on the planet position by merely integrating the transmission function over the entire field of view, which is, in effect, imaging a bright sky of equal intensity everywhere. The full integration field patterns are shown in Figures 3.10-3.11.

The radial symmetry of the circular profile is exhibited in the first plot, Figure 3.10. The high-

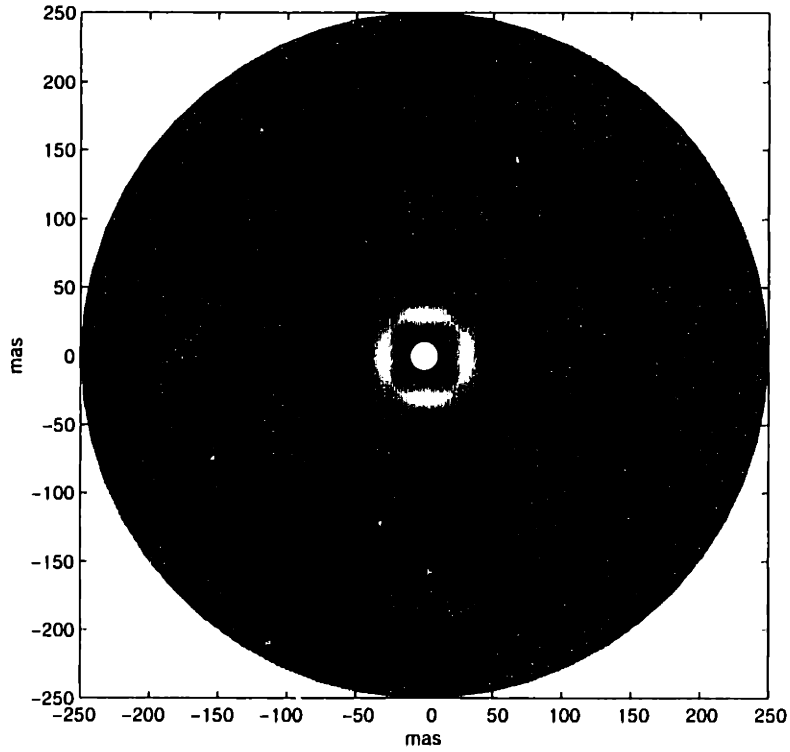

Figure 3.11: Full Field of View Integration Using Equal Average Baseline Profile

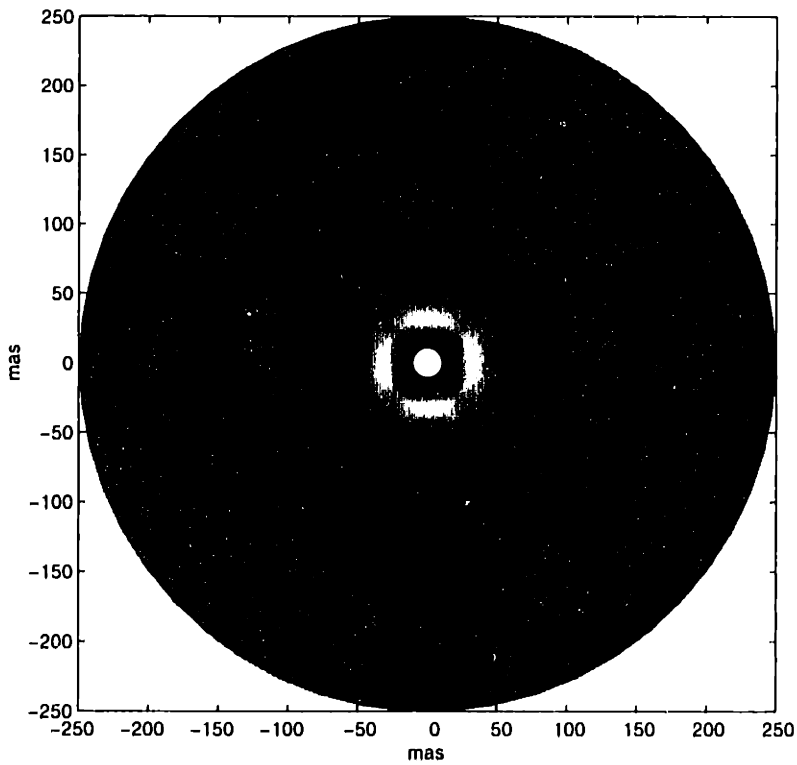

Figure 3.12: Full Field of View Integration Using Equal Perimeter Profile

est level of sensitivity in the field is at an angular separation of approximately 70 mas with a second broad band centered at 100 mas. In the next two plots, Figures 3.12 and 3.11, the variable baseline of the square maneuver paths causes the sensitivity to be axially symmetric rather than radially symmetric. In both plots, the square path is aligned with the axes such that the shortest baselines, which come at the midpoint of the side of the square, lie on the x- and the y-axis. More variation in the level of the measured intensity is seen along the axes as well. Dark patches indicate troughs where a planet might 'hide,' to some degree, and be less visible above the background noise of the instrument.

A more qualitative analysis of the sensitivity of the interferometer to the planet position is made by again using the simulated signal from the reference planet and then moving the planet and measuring the resulting variation in the reconstructed signal. This sensitivity of the signal to variation in the planet angular position is shown in Figure 3.13. For clarity, only the circular and the equal perimeter profiles are shown, since the larger square has a similar variation as the smaller. The planet is moved circumferentially, maintaining an radial position of 100 mas, equal to an orbit radius of 1.0 AU at 10 pc.

The reconstructed images are laid out on a 50 x 50 polar grid and when the planet is placed on or near a grid node, the measured signal is stronger than when the planet is between grid points. As a result, the circular maneuver profile has a high frequency minor variation equal to the incremental grid spacing. The intensity pattern of the equal perimeter profile shows the same high frequency pattern, but also the result of the changing baseline. At the corners of the square, the baseline is just over 83 m so the sensitivity of the interferometer is higher than for the 75 m constant baseline of the circular profile. But, moving 45 degrees further decreases the baseline to 59 m and the sensitivity reflects that drop.

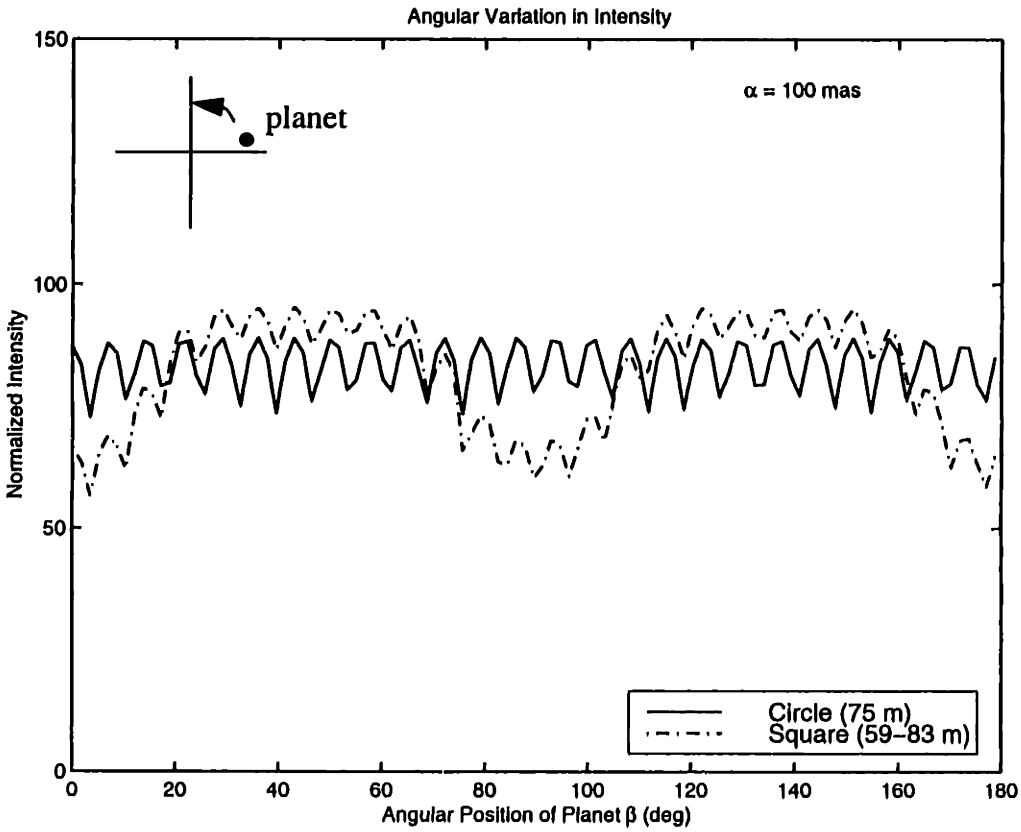

Figure 3.13: Angular Variation of Simulated Planet Intensity

The radial variation is important as well because the Terrestrial Planet Finder will be imaging solar systems at a distance between 4 and 13 pc from the earth and so the radial position of any detected planets is likely to be anywhere in the field of view. Using an angular position placing the planet on the x-axis, the simulated planet position is varied from 0.5 AU to the limit of TPF's field of view at 2.5 AU, equalling a radial angle as seen from the earth of between 50 and 250 mas. The resulting variation in detected intensity is shown in Figure 3.14, again with only the circular and equal perimeter profiles shown. As before, the high frequency modulation in the signal is due to the grid spacing of the reconstructed image. The nominal rotational path of the interferometer produces a graph which is relatively flat, with a normalized intensity mean of 123 and a standard deviation of 8.4. The square path has a normalized mean almost exactly equal to the circular profile, but the standard deviation is much higher at 19.1. The equal perimeter's sensitivity peaks

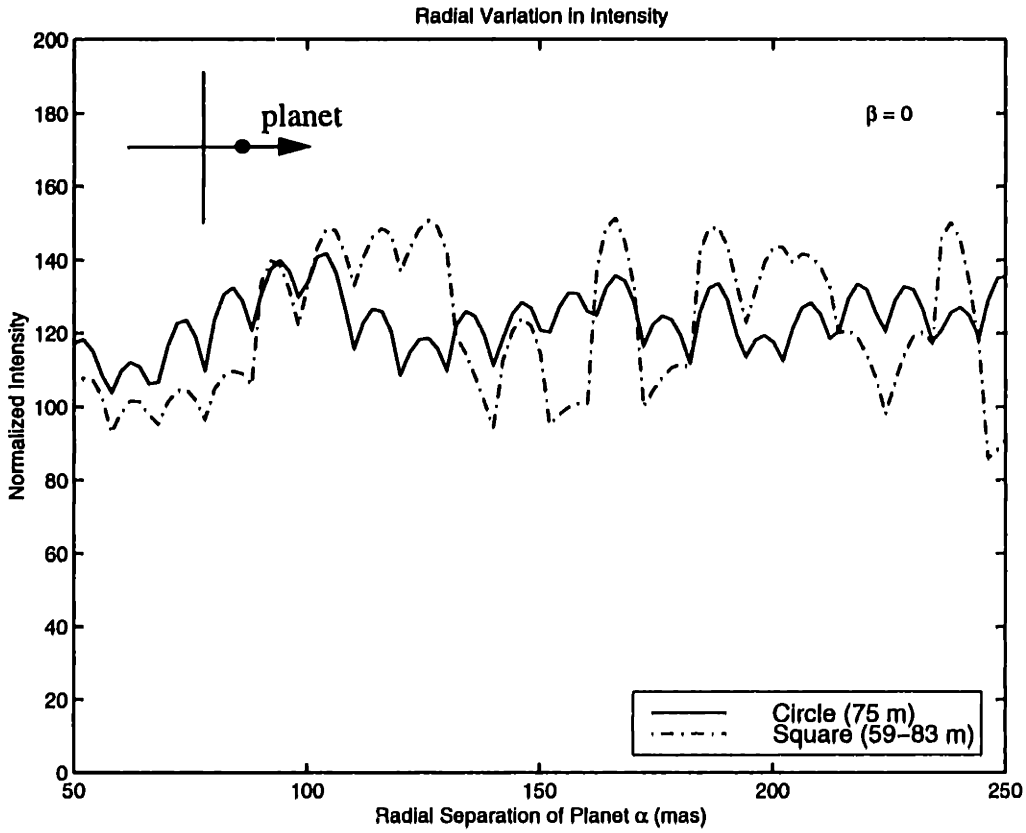

Figure 3.14: Radial Variation of Simulated Planet Intensity

much higher at a radial separation of about 120 mas, but has a deep valley in the 150 mas range. To place the intensity plot in context, the square profile has a greater sensitivity threshold for detecting Earth in our own solar system, but a lower chance of detecting Mars.

These analyses indicate that while non-circular trajectories provide some level of mass savings, some potential degradation in the optical sensitivity of the interferometer does exist. The square profiles have one additional advantage, though; while the collectors are gathering photons and performing optical measurements, the thrusters are not firing, which removes one potential disturbance source from the environment. In addition, constant thrusting by the spacecraft in a circular trajectory may form a particulate cloud from the thruster plume which could interfere with the incoming starlight. More simulation and experimentation is certainly needed to more adequately judge the relative merits between potential flight paths.

Chapter 4

Adaptability Comparison

As defined in Chapter 1, the *adaptability metric* is the sensitivity of the wet mass to changes in the functional requirements of the Terrestrial Planet Finder (TPF) mission. During development, every mission is subject to requirements growth and modifications which often lead to cost overruns, schedule slips, or outright cancellation. If the cost per function of a mission (the wet mass in this study) is only modestly sensitive to functional modifications, it will stand a better chance at accommodating these changes.

These changes in the functional requirements can take two forms, homogeneous and heterogeneous. Homogeneous changes are those which basically call for more of the same function which the mission is already designed to provide. Examples include improving the optical integrity, changing the separation baseline, extending the life of the mission, or observing more exo-solar planetary systems. Heterogeneous changes are those which introduce a new functional requirement to the existing mission requirements. This broadening of the mission objectives sometimes occurs in order to garner more advocacy for the mission across a scientific or funding community, or to allow the mission to also act as a technology or scientific precursor to other, follow-on missions. For the Space Interferometry Mission (SIM) [15], the added requirement that it act as a pre-

cursor for TPF by demonstrating white light nulling was a critical element in its selection for mission start as well as a performance driver for SIM's design. An example of a heterogeneous modification for TPF would be the addition of synthetic aperture imaging where the collectors are constantly repositioned to a variety of different separation and angular baselines in order to fill the image plane (Fourier plane) and thereby reconstruct the image of some celestial object. Such synthetic imaging could broaden TPF's appeal across the scientific community. While this study does not quantitatively combine the adaptability and wet mass metrics in order to reveal the optimum TPF architecture, the adaptability metric is presented in order to indicate some of the implications of, and possibilities for, requirements growth in the TPF mission.

The first section discusses implications of modifying the requirements for the optical configuration to reflect new knowledge of the intended stellar targets for TPF. Modifying the separation baseline is considered in Section 4.2. Then, general extensions in the mission lifetime or in the target acquisition schedule are examined in Section 4.3. Following that, the effects of changing the imaging or rotation time of the interferometer are studied. The final discussion, Section 4.5, introduces the heterogeneous expansion of the mission objectives to include synthetic imaging.

4.1 Optical Configuration

While the initial proposed interferometer configuration in the ExNPS report consisted of four equal diameter apertures, equally spaced from each other and from the combiner, a recent study by Angel and Woolf [2] pointed out that having different size apertures for the inner and outer pairs increases the efficiency of the photon collection and minimizes photon leakage, while placing more fringe peaks within the habitable zone of most stellar targets. The optical configuration included in the reference designs in Chapter 2 follows the 1-3-3-1 array proposed by Angel and

Woolf, in which the numbers refer to the ratios between the mirror diameters and the dashes indicate an equal distance between each collector. One other possibility is a 1-2--2-1 configuration, which provides a similar level of sensitivity and central nulling, but with more total collecting area. TPF precursor missions will be gathering data on the exo-zodiacal clouds in the target stellar systems, and further analysis may determine that a 1-2--2-1 configuration would improve planet detectability, which represents a modification in the functional requirement for optical imaging.

Aside from the different mirror sizes, the two arrays primarily differ in their optical path lengths. A 1-3-3-1 linear array has equal distances between each collector, which implies that the baseline of the inner pair is one-third of the baseline of the outer pair. In contrast, a 1-2--2-1 array equally spaces all five elements, including the combiner, along the same 75 m length, making the inner baseline half of the outer. One potential problem with such a layout is the coarse equalization of the path length. While a 1-3-3-1 array can reflect the inner light twice to make the length equal to the outer pair path, a 1-2--2-1 would have to have reflecting mechanisms situated between the inner collectors and the combiner.

The reference designs can be modified to reflect this second, 1-2--2-1, optical configuration array in order to gauge the adaptability of the designs. The most obvious effect that such a modification has on the cost metric is in the mass of the collector optics. The diameter of the inner apertures was assumed to be 6.0 m, in a 1.0 AU orbit, and 1.5 m, for a 5.2 AU orbit. These values provide equal signal-to-noise ratios for the two orbits, the value of which is dependent on the local zodiacal noise. In the 1-3-3-1 and 1-2--2-1 configurations, the primary mirror sizes apply to the larger, inner pair and so the inner pairs are the same size. In the modified 1-2--2-1 design, the outer pair is larger and consequently, is more massive than those in the 1-3-3-1 design. Assuming the same 15 kg/m^2 optical areal density, the new optical subsystem masses are shown in Table 4.1

Table 4.1: Modified Optical System Mass For 1.0 AU Orbit

Variable	1-3-3-1		1-2--2-1	
	Inner Pair	**Outer Pair**	**Inner Pair**	**Outer Pair**
Diameter	6.0 m	2.0 m	6.0 m	3.0 m
Mirror Mass	425 kg	47 kg	425 kg	106 kg
Quantity	2	2	2	2
Total Optics Mass		**944 m**		**1062 kg**

Table 4.2: Modified Optical System Mass For 5.2 AU Orbit

Variable	1-3-3-1		1-2--2-1	
	Inner Pair	**Outer Pair**	**Inner Pair**	**Outer Pair**
Diameter	1.5 m	0.5 m	1.5 m	0.75 m
Mirror Mass	26.5 kg	3 kg	26.5 kg	6.6 kg
Quantity	2	2	2	2
Total Optics Mass		**59 kg**		**66.2 kg**

for a 1.0 AU orbit and Table 4.2 for a 5.2 AU orbit. A 1-2--2-1 configuration represents an mass increase of 12% in the optics for both orbits. However, both the structurally connected interferometer (SCI) and the separated spacecraft interferometer (SSI) suffer from the mass increase equally, leaving the mass difference the same.

The real contrast occurs in the mass of the propellant, a variable which only affects the SSI model. An increase in the total dry mass of each spacecraft implies that more thrusting, and therefore more fuel, is needed to maneuver. In addition, the inner collector spacecraft in a 1-2--2-1 array are positioned farther from the central combiner and so must maintain a higher velocity. Tables 4.3 and 4.4 show the propellant mass estimates for a separated spacecraft array in a 1-2--2-1 optical configuration, relative to the original 1-3-3-1 array. The same propellant assumptions are

Table 4.3: Modified Propellant Mass For 1.0 AU Orbit

Variable	1-3-3-1		1-2--2-1	
	Inner Pair	**Outer Pair**	**Inner Pair**	**Outer Pair**
Lifetime ΔV	1.5 km/s	4.5 km/s	2.25 km/s	4.5 km/s
Dry Mass	550 kg	172 kg	550 kg	231 kg
Propellant Mass	91 kg	100 kg	142 kg	135 kg
Quantity	2	2	2	2
Total Propellant Mass		**382 kg**		**554 kg**

Table 4.4: Modified Propellant Mass For 5.2 AU Orbit

Variable	1-3-3-1		1-2--2-1	
	Inner Pair	**Outer Pair**	**Inner Pair**	**Outer Pair**
Lifetime ΔV	2.25 km/s	4.5 km/s	2.25 km/s	4.5 km/s
Dry Mass	151.5 kg	128 kg	151.5 kg	131.6 kg
Propellant Mass	25 kg	74.5 kg	39 kg	77 kg
Quantity	2	2	2	2
Total Propellant Mass		**199 kg**		**232 kg**

made as before, using pulsed plasma thrusters. The larger radial distance increases the lifetime ΔV requirement by 750 m/s, from 1.5 km/s to 2.25 km/s, for the inboard pair. In a near-Earth orbit, changing the optical configuration to a 1-2--2-1 array increases the propellant requirement by about 45%, to 554 kg. For a 5.2 AU orbit, the change in mass is about 16.5%, increasing the total to 232 kg. Particularly for the 1.0 AU orbit where the 1-2--2-1 array requires 172 kg more propellant, modifying the optical configuration could be a significant factor in the wet mass comparison, the totals for which are shown in Tables 4.5 and 4.6 with the recalculated optical system and propellant masses.

Table 4.5: Modified Total Wet Mass For 1.0 AU Orbit

Component	1-3-3-1		1-2--2-1	
	SCI	SSI	SCI	SSI
Optical System	944 kg	944 kg	1062 kg	1062 kg
Propellant	--	382 kg	--	554 kg
Other Components	1463 kg	750 kg	1463 kg	750 kg
Total Wet Mass	**2407 kg**	**2076 kg**	**2525 kg**	**2366 kg**

Table 4.6: Modified Total Wet Mass For 5.2 AU Orbit

Component	1-3-3-1		1-2--2-1	
	SCI	SSI	SCI	SSI
Optical System	59 kg	59 kg	66 kg	66 kg
Propellant	--	199 kg	--	232 kg
Other Components	1463 kg	750 kg	1463 kg	750 kg
Total Wet Mass	**1522 kg**	**1008 kg**	**1529 kg**	**1048 kg**

4.2 Separation Baseline

The assumption made in Chapter 2 for the separation baseline was 75 m, which is the nominal value put forth by the Jet Propulsion Laboratory for the Terrestrial Planet Finder. However, the baseline is a functional requirement which could be modified at a later date, and so the adaptability of the two architectures to a different separation distance should be considered.

First, in the case of the structurally connected interferometer, the mass of both the truss and the deployment mechanism will change. Assuming that the truss aspect ratio remains equal to 100 and the truss areal density to 0.001, the total mass can then be calculated. For the separated spacecraft interferometer, the propellant mass will change slightly when the baseline changes because of the dependence on the velocity needed to maneuver. Plots of both the SCI and the SSI wet

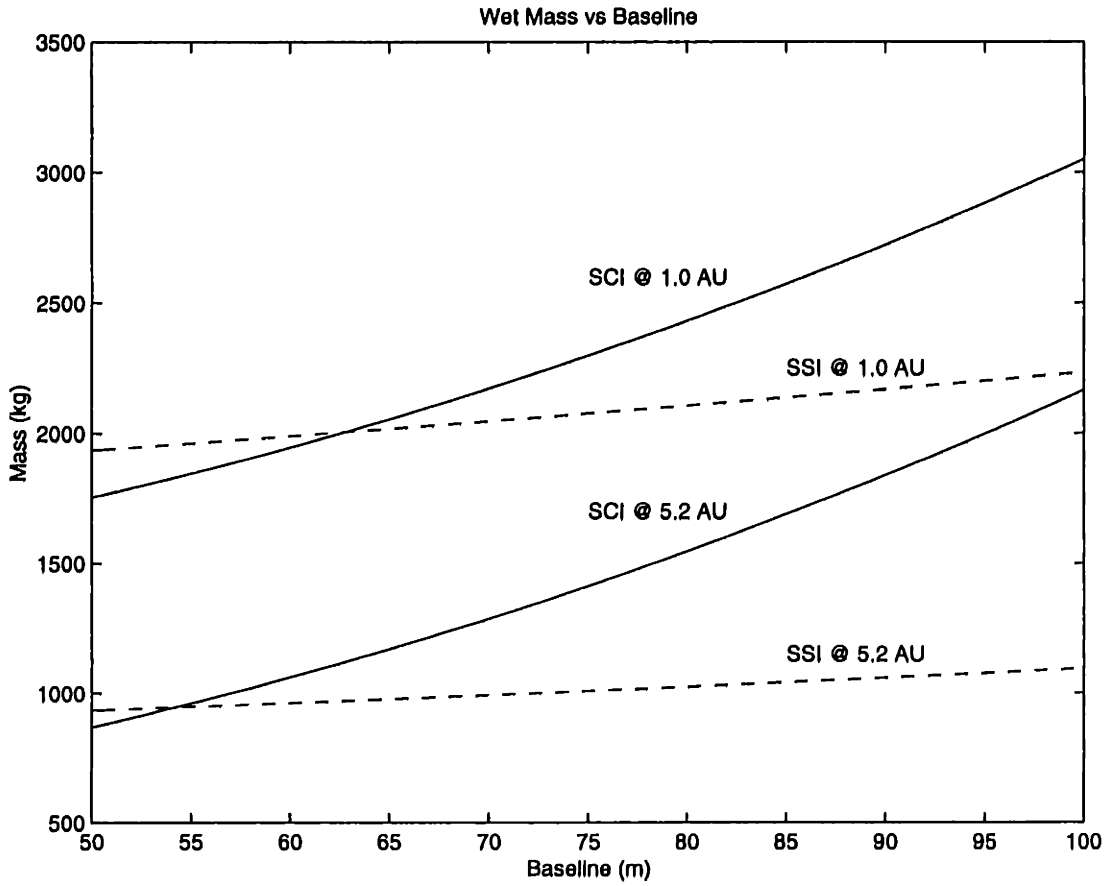

Figure 4.1: Architectural Wet Masses vs. Separation Baseline

masses as functions of the baseline in both orbit possibilities are given in Figure 4.1.

If the baseline for TPF were reduced to roughly 60 m, the SCI would then have a lower wet mass than the SSI in a 1.0 AU orbit. The crossover baseline at which the two architectures have equal masses is slightly lower for the 5.2 AU orbit, at just under 55 m.

4.3 Extended Operations

The original ExNPS report set the goal of the Origins Program as a study of the closest 1000 stars which lie in the spherical volume within approximately 13 pc of the Earth. The suggested observation profile begins with a broadband search of 100 to 200 stellar objects in the first year, followed by spectroscopic studies of any promising candidates. Recent information available on the

Terrestrial Planet Finder program places its observation goal as being several hundred star systems within five years of operation. An extension of the operational coverage could take two forms, either a protraction of the lifetime of the instrument or an increase in the number of stellar targets or revisits. In either case, the rotation period is assumed to remain constant at two hours.

The mission duration primarily affects the propellant requirement of the SSI. Once the propellant onboard each independent spacecraft is exhausted, the interferometer is essentially dead and unable to perform any science. On the other hand, because a structurally connected interferometer maintains its coarse collector positions and orientation passively through rotation, only momentum wheels and a minor amount of propellant are needed to keep it operational. Adding propellant to a spacecraft for a longer operational duration means that even more propellant is needed to push the added mass, which is reflected in the exponential nature of the rocket equation. As shown previously in Equations 2.13 and 2.14, repeated below, the amount of velocity change is linearly dependent on the mission lifetime, and the propellant mass is exponentially dependent on the velocity change.

$$\Delta V_{life} = \frac{4\pi^2 R}{T_{rot}^2} T_{life} \tag{4.1}$$

$$\frac{m_{prop}}{m_{dry}} = \left[\exp\left(\frac{\Delta V_{life}}{I_{sp} g} \right) - 1 \right] \tag{4.2}$$

Using the dry mass values from Chapter 2, the wet mass of each system architecture as a function of the operational lifetime of the interferometer can be calculated. The results are shown in Figure 4.2, in which the mass of the reference designs are plotted as a function of the mission lifetime. The SCI mass is assumed to be constant over lifetime because of the absence of a depen-

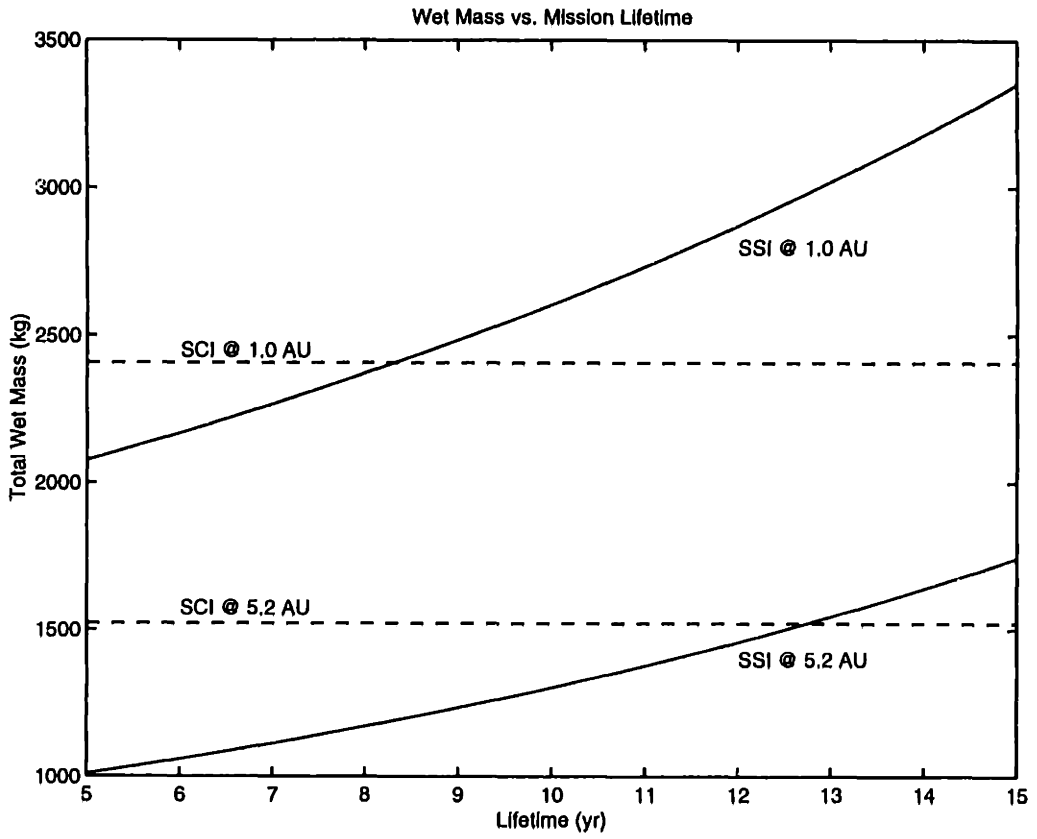

Figure 4.2: Total Wet Mass vs. Mission Lifetime

dence on propellant. On the other hand, the SSI mass increases exponentially because of the increasing propellant mass. For longer mission lifetimes, the SCI becomes more mass efficient. The crossover point lies at about eight years for the 1.0 AU orbit and just short of 13 years for the 5.2 AU orbit. Furthermore, adding propellant requires bigger fuel storage units and structural support, so the mission duration at which the wet masses become equal is actually slightly less than that shown in the plot.

In any event, in terms of the adaptability of the architecture to extending the mission requirements, the structurally connected architecture is much better. For the separated spacecraft interferometer, a longer lifetime and more stellar targets both require a large addition of propellant, which causes the SSI system mass to increase rapidly, surpassing the structurally connected interferometer's wet mass.

4.4 Imaging Time

One of the primary variables in the functional requirements for the Terrestrial Planet Finder is the time required to complete one image. The total imaging time is tied to the rotational period of the interferometer through the signal-to-noise ratio (SNR) generated from the photon collection. If more time is required to process each measurement while the instrument is rotating, the period must be lengthened, which may decrease the number of targets properly imaged per year. On the other hand, if a high SNR is being obtained, fewer measurements are required, and the interferometer might be rotated faster, so as to allow for more targets in a given amount of time. Because the propellant requirement is related to the square of the rotation period for the SSI, relatively small fluctuations in the period drastically change the predicted propellant mass.

Following Equation 2.13, reproduced below, the propellant mass as a function of the rotation period can be calculated.

$$\Delta V_{life} = \frac{4\pi^2 R}{T_{rot}^2} T_{life} \tag{4.3}$$

The fastest rotation rate, which can be inferred from the likely requirement to have 1000 data points of four seconds each per rotation, is roughly just over one rotation per hour. And, in order to perform an initial scan on every stellar system within the target volume within the proposed five year lifetime, a decision on making further analysis of the target should be made within several hours, making any rotation period longer than five hours or so unlikely [37]. The range is probably centered around the reference assumption of a two nour rotation period.

The propellant mass sensitivity to the rotation period is shown in Figure 4.3. Decreasing the period by 25%, from 2 hr to 1.5 hr, would increase the SSI propellant mass by 396 kg, or 104%, at

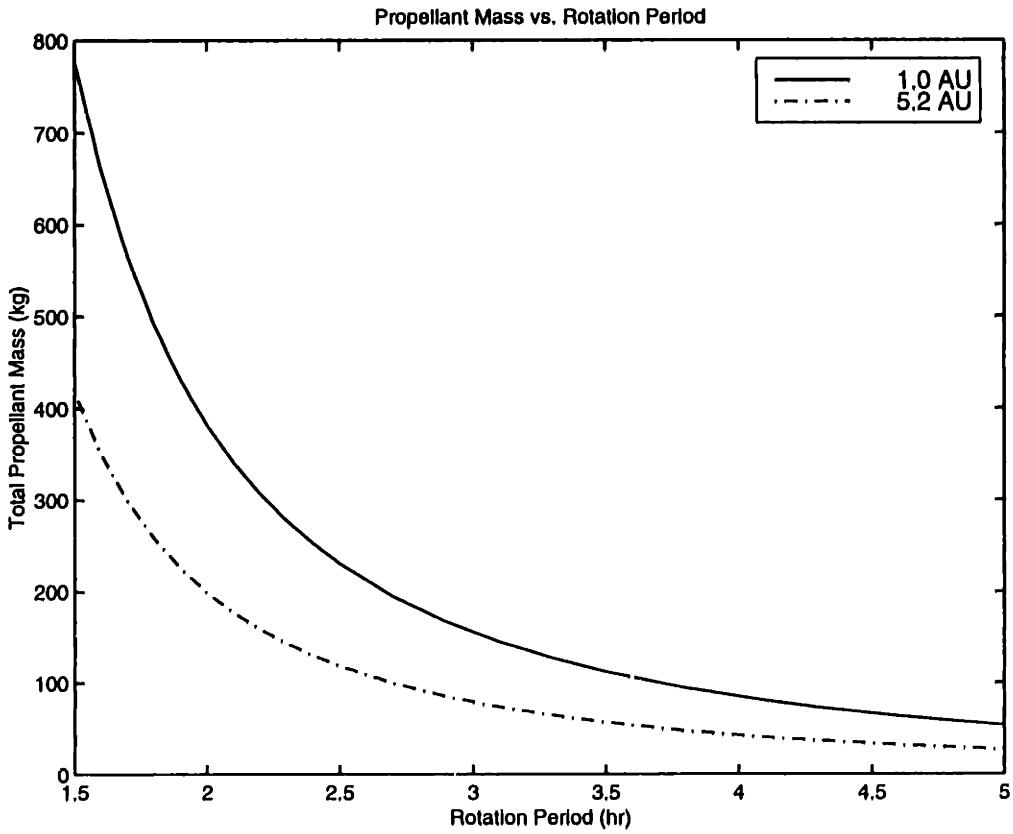

Figure 4.3: Propellant Mass vs. Rotation Period

a 1.0 AU orbit and 219 kg, or 110%, at a 5.2 AU orbit. Alternatively, increasing the period to 2.5 hr lowers the propellant mass to 231 kg and 119 kg for the 1.0 AU and 5.2 AU orbits respectively, representing a 40% reduction. Clearly, the rotation period is a critical factor in the separated spacecraft propellant mass and indicates a high sensitivity to modifications in this functional requirement.

The structurally connected interferometer architecture, on the other hand, would require slightly more propellant to get up to speed if a faster rotation were desired, but the relative increase in propellant is negligible in this case. However, a larger reaction wheel is more likely to be used instead in order to accommodate the higher angular momentum. The reaction wheels would require momentum dumping more often, but that is a relatively minor concern and does not significantly impact the estimated mass of the SCI design. Therefore, the adaptability of the archi-

tectures to modifications in the imaging time is primarily relevant for the separated spacecraft interferometer.

4.5 Synthetic Imaging

Expanding the scope of the scientific operation of the Terrestrial Planet Finder is a heterogeneous modification to the functional requirements which broadens the support of the program across the scientific and funding community. Specifically for TPF, the potential exists for a more encompassing scientific study of the target solar systems, as well as other celestial objects, through synthetic imaging, which is the process of constructing a two-dimensional map of the brightness across the field-of-view through varying the separation vector of the collectors in both magnitude and direction. The separated spacecraft architecture could provide this synthetic imaging because of its capacity to freely move the apertures to form new baseline vectors.

With the positions of the two collector apertures given by (X_1, Y_2) and (X_1, Y_2), the separation vector is simply

$$\underline{B} = (X_1 - X_2, Y_1 - Y_2) \tag{4.4}$$

The complex intensity, $V(u, v)$, as measured by the interferometer as it moves through different baselines, is normally given in the Fourier plane where the separation vector is transformed by the relation

$$(u, v) = \left(\frac{X_1 - X_2}{\lambda}, \frac{Y_1 - Y_2}{\lambda}\right) \tag{4.5}$$

In order to produce an image of the entire plane, the complex intensity must be known for a certain number of points in an $n \times m$ array which covers the (u, v) plane. Then, the brightness map of

the sky, $\Gamma(\theta_x, \theta_y)$, is given through a reverse Fourier transform as

$$\Gamma(\theta_x, \theta_y) = \iint V(u, v) e^{-2\pi j(u\theta_x + v\theta_y)} du dv \tag{4.6}$$

where θ_x and θ_y are the angular coordinates in the field-of-view. Equation 4.6 becomes a summation instead of an integral in this case because discrete points in the Fourier plane are sampled. Therefore, the separation vector between the two collectors must be varied in both magnitude and direction in order to provide more data points. In doing so, a two-dimensional map of the image brightness is constructed.

Obviously, the fidelity of the image is contingent upon the number of points included in the Fourier plane mapping. More measurements lead to a higher resolution in the reproduced image. The four collector spacecraft of the Terrestrial Planet Finder would be able to simultaneously provide more baselines than a single collector pair. Optimizing the path taken by the collector spacecraft would minimize the fuel expenditure while gaining the most number of unique Fourier points. This subject has been treated with regard to the Deep Space 3 interferometer by Kong and Miller[17].

The high angular resolution offered by the collector optics would allow synthetic imaging of a wide range of stellar targets, including proto-planetary disks, exo-zodiacal clouds, or even the surfaces of objects within the Solar System itself. By adding the instruments needed to perform synthetic imaging to the collectors in the separated spacecraft architecture, the scope of the Terrestrial Planet Finder could be expanded to include more areas of astrophysical study, which has the important side effect of increasing the level of support in the scientific community, a factor which is always important for a program as large and expensive as the Terrestrial Planet Finder is likely to be.

Table 4.7: Adaptability Summary

Adaptability Issue	Structurally Connected Interferometer	Separated Spacecraft Interferometer
Optical Configuration	*Aside from increased mirror masses, very minor torque increase*	Aside from increased mirror masses, more propellant needed
Separation Baseline	Large mass dependence on separation baseline	*Minor mass dependence on separation baseline*
Extended Operations	*Minor increase in fuel mass needed for longer lifetime or more targets*	Requires much more fuel to extend lifetime or to add more stellar targets
Imaging Time	*Minor mass dependence on rotation period*	Major mass dependence on rotation period
Synthetic Imaging	Fixed baseline for taking optical measurements	*Able to perform synthetic imaging with more coverage of Fourier plane*

4.6 Summary

This chapter introduced the concept of the adaptability of a spacecraft architecture as a measure of the sensitivity of its design to modifications in the functional requirements of the mission. Much of the adaptability analysis is summarized in Table 4.7, which includes functional modifications in the optical system and the separation baseline, as well as in the operational procedures of the interferometer. Italics indicate the more favorable trends between the two architectures for each issue.

The functional requirements which dictate the optical configuration of the instrument might be changed because of new information concerning the exo-zodiacal clouds of the intended targets. A 1-2--2-1 mirror array was shown to increase the dry mass of both the SCI and the SSI and additionally, to increase the propellant mass for the separated spacecraft interferometer by 172 kg and 33 kg for the 1.0 AU and 5.2 AU orbits, respectively.

The mass of the structurally connected interferometer has a high sensitivity to changes in the separation baseline because the mass of the truth is dependent on the cube of the truss length. If the width of the truss is kept constant, the mass of the deployment mechanism is only slightly affected. The mass of the separated spacecraft interferometer has a small dependence on the separation baseline due to the expansion of the array and the additional propellant required to rotate in the same amount of time. The crossover baseline at which the mass of the reference SCI equals the mass of the reference SSI is about 60 m for the 1.0 AU orbit and 55 m for the 5.2 AU orbit.

Modifications in the operational profile were also examined for their influence on the architectural selection. Operational parameters such as the mission lifetime, the breadth of the stellar target catalog, and the time periods needed for imaging and rotation were examined to gauge their relative effects on the masses of the two interferometer architectures. A separated spacecraft interferometer was found to be more sensitive to these changes because of its dependence on propellant mass for operation. Synthetic imaging was included as a potential function offered by the separated spacecraft interferometer which could broaden the operational profile of the Terrestrial Planet Finder and significantly increase the scope of the scientific coverage offered. Altogether, the primary conclusion is that the separated spacecraft interferometer is highly sensitive to most functional modifications because of the additional propellant required, but at the same time, the potential for synthetic imaging by the SSI is a important consideration in the architectural comparison.

Chapter 5

Capability Comparison

The third metric used in this study is the *capability metric,* which assesses both the ability and the efficiency of a system at performing its design role over the duration of the mission. Because distributed systems operate on a different principle than normal monolithic spacecraft, namely that of the coordination of operations among a constellation of independent spacecraft, a typical cost, or mass, comparison fails to take into account the additional capabilities offered by a separated spacecraft architecture. Therefore, an examination of the level of performance which can be achieved by both a structurally connected interferometer (SCI) and a separated spacecraft interferometer (SSI) is valuable in comparing the architectures.

The capability offered by the system is measured relative to the four constraints identified in Chapter 1: isolation, rate, integrity, and availability. The first, *isolation*, is merely the resolution of the instrument. The primary operation of the interferometer requires the planet to be resolved apart from its parent star which implies a certain level of resolution and image processing accuracy from the collector and the combiner optics. The level of resolution offered by the two architectures is quite similar because of the scientific requirements, but the manner in which the resolution can be adjusted is conditional on the configuration. The *rate* requirement dictates the

time needed to image a solar system as well as the total number of images taken over the mission lifetime. Since this constraint is a function of the optical systems, the rate does not distinguish between the architectures. The *integrity* of the system represents the level of error rejection offered by the architecture. In interferometry, the primary source of error in the measurement is the differential path length (DPL) control between the two legs in the interferometer, since any inaccuracy in the DPL significantly affects the optical performance. The two architectures use different technologies to control the DPL matching to the required precision. (A cursory examination of some possible disturbances and the structural control of the truss is given in Appendix A.) Finally, the *availability* of the spacecraft in maintaining its required isolation, rate, and integrity over its mission lifetime depends upon the levels of reliability and failure compensation provided by the system. The structurally connected interferometer (SCI) and the separated spacecraft interferometer (SSI) designs are affected differently by the failure modes of the architecture and their ability to adapt to failure is an important component of the capability metric.

This chapter provides a detailed look at these constraints and how they differentiate between the two architectures. Resolution (isolation) issues are examined in the first section, with a detailed look at the dependence of the planet isolation on the characteristics of the central null. A brief mention of the rate requirement is made in the next section. Section 5.3 follows with a discussion of the disturbance rejection which maintains the system integrity. The final section deals with the availability of each architecture, with the focus on system reliability and failure compensation modes, and includes a brief mention of some propellant contamination issues. The chapter concludes with a summary of the capability comparison and the insights gained in the architectural study.

5.1 Resolution

The primary function of the Terrestrial Planet Finder is the direct detection of extra-solar planets, so its resolution must be fine enough to accurately isolate a planet orbiting as close as 0.5 AU from its parent star, which is the habitable zone for a K2 class star, at a maximum distance of 13 pc from the earth, which corresponds to an angular separation of 38 mas. Adequate capability in the spatial resolution also must exist to separate the planet from any exo-zodiacal noise. Consequently, the minimum performance requirement put forth by the ExNPS group is on the order of 10 mas. Other resolution requirements for the interferometer are a minimum light suppression of the central star of one part in one million, insensitivity to asymmetries in the zodiacal cloud, and the ability to resolve multiple objects orbiting the target star.

The resolution constraint, though, must be met by both architectures, and therefore, there is not much contrast in the resolution performance. Neither architecture will be selected for the Terrestrial Planet Finder mission unless the minimum resolution is met. However, another aspect of the resolution is the width and maintenance of the central null which provides the light suppression of the parent star to better than one part in one million.

The primary factor in setting the width of this central null is the optical baseline. A structurally connected architecture can vary its effective baseline by tilting the boom away from the plane normal to the line-of-sight to the parent star, thereby projecting a shorter baseline. If the array is still rotated about its maximum moment-of-inertia, the collector optics must slew in a coning motion and the optical delay lines must have a much larger stroke. If the array were rotated about the line-of-sight to the star instead, articulated or multiple reaction wheels would be needed and the complication of precession would be introduced by the rotation about a non-principal axis. Therefore, for baseline tuning, the separated spacecraft interferometer is favored since the optical

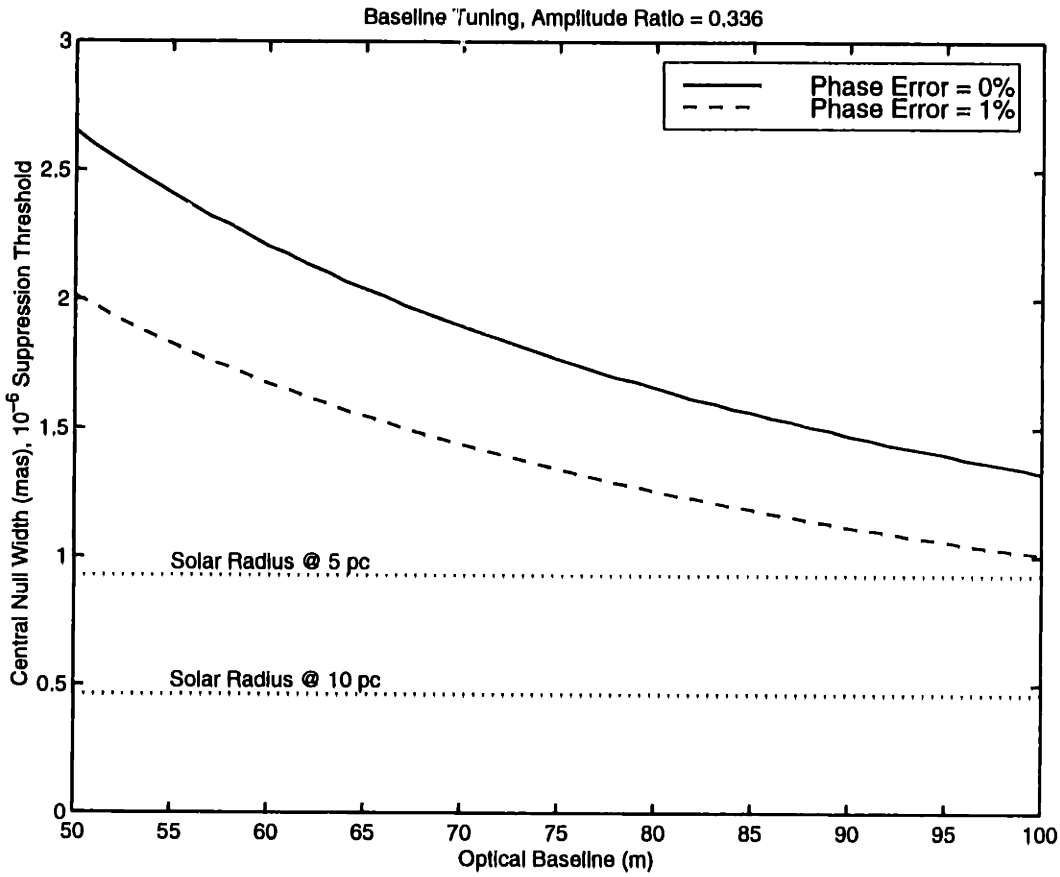

Figure 5.1: Central Null Width vs. Optical Baseline

baseline can easily be adjusted by maneuvering the collector spacecraft nearer or farther from the combiner.

This added capability might be useful, for example, if the interferometer were to move from imaging a K2 star at 13 pc to an F2 star at 5 pc, where the apparent size of the star is much larger. Increasing the baseline places more peaks in the fringe pattern closer to the null which increases the sensitivity of the detector to planets closer to the parent star, but it also decreases the width of the nulled area in the center. Decreasing the baseline improves the signal-to-noise ratio for some wavelengths, depending on the exo-zodiacal cloud. Figure 5.1 shows the relation of the width of the central null, measured by a maximum suppression threshold of 10^{-6} and a mirror diameter ratio of 0.336, to the optical baseline. The dotted lines represent the radius of the sun, not includ-

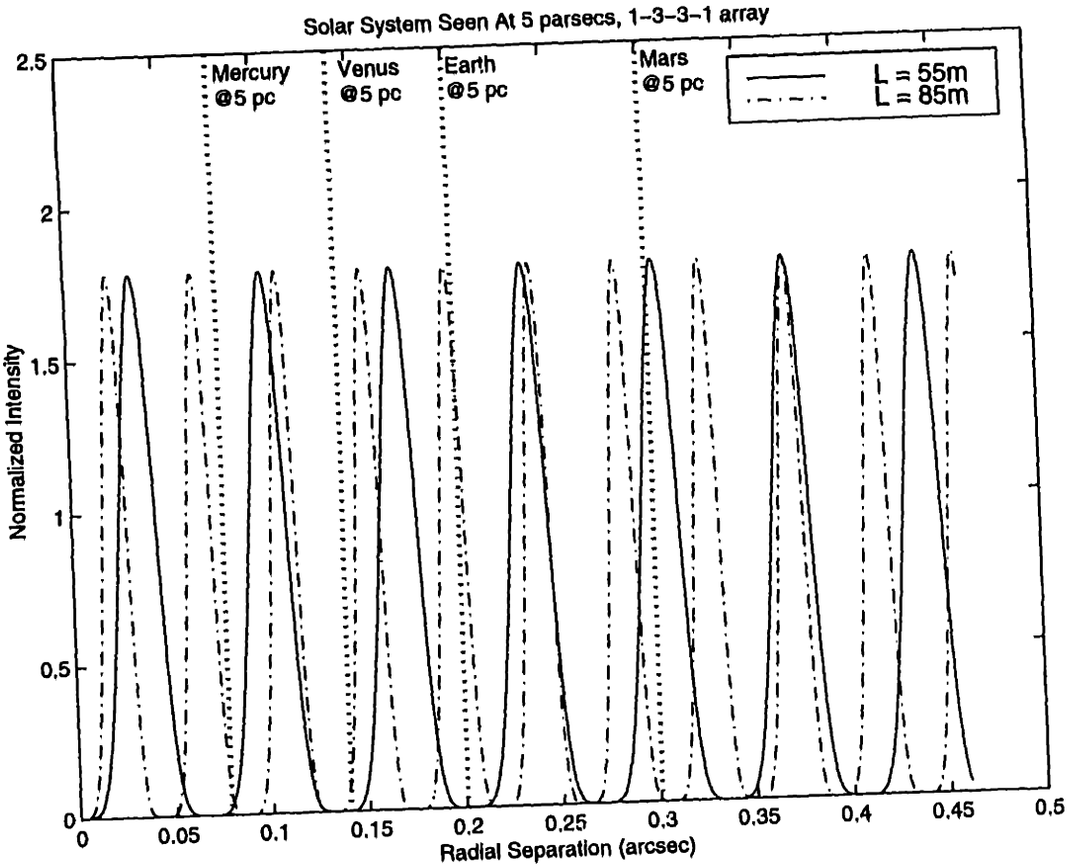

Figure 5.2: Intensity Pattern For Two Optical Baselines

ing the corona, as seen from a distance of 5 and 10 pc, showing that the null width is sufficiently wide to suppress the starlight even for baselines greater than 100 m. However, the dashed line is the width of the null with a 1% phase error which shows that imperfect suppression due to small errors in pointing or phase matching sets a likely maximum of 100 m or so for the baseline, past which length, the larger stars begin to show photon leakage around the null.

In Figure 5.2, the intensity patterns for both a 55 m and an 85 m optical baseline are shown. To give some measure of possible planet positions, the first four planets in the solar system are shown, as seen from 5 pc. The longer baseline has five fringe peaks within a 1.0 AU orbit of a star five parsecs from the Earth, and seven fringe peaks within 1.5 AU, while the shorter baseline only has three and five, respectively, which demonstrates that longer baselines provide higher resolu-

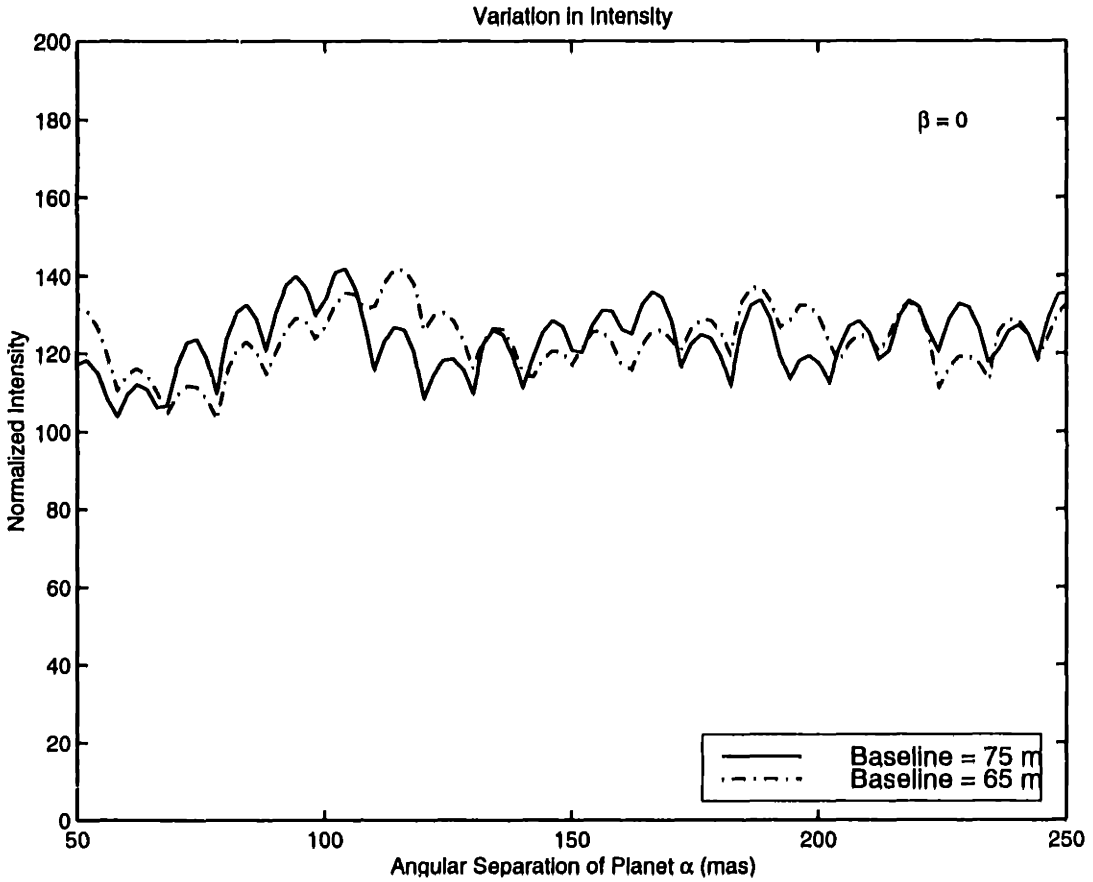

Figure 5.3: Variation of Radial Planet Intensity For Two Baselines

tion and sensitivity for detecting planets.

However, the planet intensity may also depend on the actual position of the fringe peaks and whether or not they directly pass over the planet, which could be adjusted with variable baselines,. Figure 5.3 is a representation of the calculated intensity of a reference planet as a function of the angular position of the planet from the parent star. The plot is calculated in the same way as the intensity plots in the last section in Chapter 3 with the high frequency variations due to the grid spacing of the reconstructed image. Two baselines, 65 m and 75 m, are used, and the conclusion is that for certain radial positions, a smaller baseline actually pinpoints the reference planet more accurately. So, having the ability to fine-tune the optical baseline to maximize the resolution for the target stellar system is a great advantage for the separated spacecraft architecture.

5.2 Rate

The program objectives for the Terrestrial Planet Finder require the instrument to image over 500 stellar systems within the five-year operating lifetime. In addition, some spectroscopic analysis is expected, which lengthens the amount of time needed for each target. This imaging time is largely a function of the exo-zodiacal noise seen by the interferometer and its rotational period because of their influence on the signal-to-noise quality of the image. The period currently being used in the TPF program is one rotation every two hours, which is the value used in this study. On the whole, however, the imaging time and thus, the rate constraint of the interferometer, is set by the optical system itself and therefore, the rate is not a distinguishing factor in the architectural selection.

5.3 Integrity

The error control in the optics determines the integrity of the system. While filled aperture telescopes align themselves internally and rely on mirror surface precision, interferometers must use dynamic structural elements to control and maintain the optical differential pathlength (DPL). The coarse control of the interferometer restricts the collector displacements to a range which can be absorbed by the fine control elements. These elements, which have internal adjustable reflecting surfaces, are called optical delay lines (ODL) and are placed in one of the interferometer legs to control the precise optical phasing. Small displacements in the collector positions introduce pathlength errors which are counteracted by the ODLs, which typically have stroke lengths on the order of tens of centimeters.

A structurally connected interferometer relies on the structural rigidity of the truss, along with any active structural control, to provide the coarse control of the path length difference between the collector elements. Disturbances, originating either from onboard instruments or from the

external environment, can propagate along the truss and resonate in intensity. These disturbances must be either isolated from the optical subsystems or damped using active control.

Possible sources of error include gravitational gradients, solar pressure, thruster misalignment, optical delay line actuations, and reaction wheels. The external disturbances are several orders of magnitude lower than the internal ones, especially in a 5.2 AU orbit. Furthermore, the external disturbances are at much lower frequencies where the optical control is very effective. Optical delay line reaction torques were one of the biggest disturbances in the original study by Surka [32], with the model of a 2 cm stroke providing a central torque on the order of 2.8 mNm. The thrusters for the SCI will likely be placed on the ends of the boom in order to provide the highest level of torque control on the spacecraft. A cursory examination of three possible disturbances is included in Appendix A, which shows that a thrust level of several millinewtons is sufficient to counteract the modeled disturbances. On the whole, the disturbance environment is relatively benign, but because of the highly sensitive optical measurements being performed, the structural control is critical.

For the separated spacecraft interferometer, the baseline support is virtual and the separation is maintained by each spacecraft rather than by an intervening structure. However, the SSI will likely use similar technology for control feedback as does a monolithic spacecraft [34]. For the New Millennium Interferometer (DS-3), the propulsion system provides coarse level control down to 0.01 m along any axis and 0.3 milliradians relative orientation. Beyond that, the optical delay line can absorb the DPL error to reduce it to the requisite 10 nm level.

On the one hand, a structurally connected interferometer must use structural isolation and perhaps active control to restrict the collector displacements to a level controllable by the optical delay lines. Structural control is a mature technology and although the large truss implies a very

flexible structure, maintaining the DPL precision is merely an extension of current technology. On the other hand, formation flying to less than a centimeter of relative position error has not yet been demonstrated in space and represents a major technical hurdle for the separated spacecraft interferometer to overcome. In this case, the integrity requirement seems to favor the structurally connected interferometer.

5.4 Availability

The reliability of the system as an operational whole is a major factor in the capability metric. The availability is a measure of the reliability in that it is defined as "the probability that the interferometer is fully operational and able to meet the functional requirements placed upon it at any given instant in time during its lifetime" [30]. Beyond the reliability, the level of compensation in the event of operational failure is important for recovering some measure of availability in the system and represents a critical distinction between the two architectures. Furthermore, a separated spacecraft interferometer has to account for a higher likelihood of optical quality degradation due to propellant contamination.

5.4.1 Failure Compensation

The structurally connected interferometer architecture is relatively fixed in its system reliability. In the event of a single point failure in a critical subsystem such as the combiner, the interferometer becomes useless and unable to perform its mission at all, reducing its effective availability to zero. Or, if only a collector or its controlling hardware malfunctions, the instrument could operate in a crippled state as a single Bracewell pair at a fixed baseline. To regain full availability, the entire instrument would have to be replaced.

On the other hand, a separated spacecraft interferometer offers several solutions for failure compensation. At the very least, the system can operate as a single Bracewell interferometer pair, just as the SCI can, but with the added advantage of being able to vary the baseline. Furthermore, the SSI could still perform synthetic imaging, which was discussed in Chapter 4 as part of the adaptability metric. This baseline tuning is mentioned in the previous section on resolution and gives the SSI a lower failure compensation cost, which is the amount of operational coverage lost due to component failure. More of the operational objectives can be accomplished following a collector failure by a separated spacecraft array than for a fixed baseline, structurally connected architecture.

Another consideration in determining the availability of the SSI architecture is the potential for fully replacing a malfunctioning spacecraft. If a collector spacecraft or even the combiner spacecraft becomes unable to function properly, a substitute can be built and launched, thereby restoring the interferometer to full operational status. However, such a scenario is only realistic for the 1.0 AU orbit because of the short flight time to the orbital position. For a 5.2 AU interferometer, the better solution would be to launch the replacement spacecraft along with the five requisite ones. But, doing so would require choosing which spacecraft type to include, whether a combiner, a large collector, or a small collector. This failure compensation mode of replacing the malfunctioning spacecraft is unique to the SSI architecture and represents, in and of itself, a major advantage for the SSI. While the additional cost and mass for the replacement spacecraft would have to be considered relative to the increased reliability of the system, the extra security it would provide is considerable.

Another possibility for elevating the system reliability of a separated spacecraft interferometer is to use modular and multifunctional spacecraft (MAMS/C), a solution studied by Jilla and

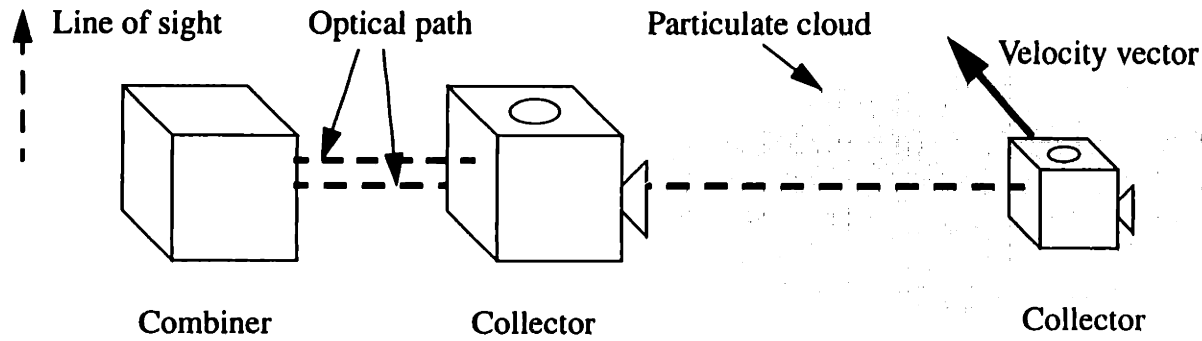

Figure 5.4: Thruster Plume Impingement on Outer Spacecraft

Miller [16]. Each independent spacecraft is identical and capable of acting either as a collector or a combiner. In the event of a failure in one component, two of the spacecraft can switch positions in the array and exchange their operational modes, thereby maintaining the maximum level of availability. The system reliability is greatly increased since no single point failure exists in the optical path, and the required reliability of each individual spacecraft could be lowered while still providing the same level of system availability as the SCI design. The amount of additional mass needed to add this functionality to the architecture is likely to be lower than simply including an additional spacecraft.

5.4.2 Propellant Contamination

For a separated spacecraft interferometer, the potential danger exists of having the optical performance degraded by thruster plumes from either the spacecraft's own thrusters or those of the other spacecraft. The centripetal acceleration vector for both a circular and a non-circular maneuver profile places the outer spacecraft directly in line with the thruster plumes of the inner pair. The plume impingement pattern of the inner spacecraft expands to envelope the outer collector spacecraft, causing cross-contamination, as in Figure 5.4. The plume may even introduce a net force on the outer spacecraft due to the particulate impacts. As a constant problem, the propellant contam-

inant can build up on the outside of the mirrors, forming deposits which degrade the optical performance.

Furthermore, the expelled propellant particulates form a cloud around the spacecraft and can impede the photon collection from the target star system as well as the reflected signal from the collector to the combiner. The cloud of expelled hot gas is a source of infrared emissions which could interfere with the interferometer's operation. Though the cloud may not be very dense, the size of the particulates is on the order of the wavelength of the incoming infrared light, causing scattering problems. Also, since TPF is likely to be cryogenically cooled, there is a higher chance that thick layers of molecular and water contamination may build up on the optical surfaces [10].

The pulsed plasma thrusters may also introduce electromagnetic impulses because of the capacitive discharges in the propulsion system. The shielding between the thrusters and the collector hardware must contain the by-products of the PPT operation. More information on propellant contamination and the plume flows involved can be found in Dettleff [13]. In summary, the propellant contamination issues can be categorized as:

- Deposits formed on optics from propulsion exhaust products
- Plume impingement forces on other spacecraft
- Local gas cloud
- Infrared emission from hot gaseous exhaust
- Electromagnetic impulses due to PPT capacitive discharge

Potential solutions to propellant contamination include thrusting only when no data is being collected, which is possible with the square flight paths discussed earlier, or by pointing the thrusters slightly away from the other spacecraft so as to thrust in a slightly non-optimal direction. The issue, however, is that the separated spacecraft architecture must overcome the problem of

contamination in order to maintain the same level of availability as a structurally connected interferometer. The level of optical backscattering is a topic for further research which could affect the performance of an SSI. The integrity of the instrument is affected, as well, making optical degradation due to the propulsion system a defining point of comparison in the capability metric.

5.5 Summary

The *capability metric* provided a basis for comparing the ability and efficiency of a system through an examination of four constraints and their application to each of the two architectures. The isolation, or *resolution*, of the instrument is dependent on the baseline and the optical nulling of the target star, which was discussed in Section 5.1. The ability of the SSI to tune the baseline in order to maximize the resolution was presented as an important architectural advantage. The *rate* constraint was found to be equally met between the two architectures and so no distinguishing factors existed. The *integrity* of the interferometer is dependent on the differential path length (DPL) between the optics being kept to a certain level of accuracy, which is maintained in different ways. The SCI relies on the structural damping and any active control to keep the DPL errors to a level manageable by the optical delay line, while the SSI requires formation flying to maintain the separation baseline. Structural control is a mature technology and extending its range further, to nanometer levels, is certainly feasible. However, precise formation flying has yet to be demonstrated on a large scale.

The *availability* of the system was another component of the capability metric. The two architectures were shown to provide different levels of compensation in the event of a failure in a collector element. The structurally connected interferometer would only be able to operate at a fixed baseline, with the sole remaining optical pair. A limited amount of astrophysical interferometry

Table 5.1: Capability Summary

Capability Issue	Structurally Connected Interferometer	Separated Spacecraft Interferometer
Resolution	Fixed baseline restricts central null characteristics	*Baseline tuning can adjust null to optimize planet detection*
Rate	Imaging time and rotation period dictated by optics	Imaging time and rotation period dictated by optics
Integrity	Structure must damp disturbances to less than centimeter magnitude. High bandwidth optical control may be needed.	Formation flying to requisite precision level requires more study and research
Availability	Limited options for component failure; full instrument replacement required to return to full availability. *Less critical potential of propellant contamination*	*Lower failure compensation costs with crippled instrument; on-orbit element replacement also possible.* Optics subject to propellant contamination.

would be possible in such a crippled state. While a separated spacecraft interferometer would also be limited to a single pair, the baseline could be varied to increase its performance. Additionally, synthetic imaging, as discussed in the adaptability metric, could still be performed. Replacing a failed collector in orbit was also introduced as a possibility for a separated spacecraft architecture, an important potential capability for an interferometer in a 1.0 AU orbit. As another consideration in the system availability, the separated spacecraft interferometer is subject to propellant contamination of the mirrors and the optical paths, as determined in the last section of the chapter.

Table 5.1 contains a summary of the capability issues examined in this study with the favorable trends between the architectures italicized. On the whole, the qualitative availability of the two architectures is somewhat mixed. The added capacity of separated spacecraft for baseline tuning is certainly a considerable advantage, but the complexities of formation flying should not be overlooked. Also, while an SSI architecture may have a higher system reliability, the potential for propellant contamination must be examined further.

Chapter 6

Model Validation

Much of the analysis of the wet mass metric in this study is based on mass estimates extrapolated from other interferometer designs and is therefore somewhat uncertain. The sensitivity of the wet mass comparison result to variations in the component masses can be characterized to some extent by validating the reference designs against other proposals for the Terrestrial Planet Finder (TPF). This chapter contains an overview of three other TPF models made during industry studies conducted in parallel with this one. The final concept reports given by the TRW, Ball Aerospace, and Lockheed Martin were used to extract candidate mass estimates for the components in the TPF designs. These estimates are then compared with the values used in Chapter 2 to determine their validity. When the contractors did not provide designs for a separated spacecraft architecture, appropriate extrapolations were made from the structurally connected mass estimates.

The purpose of this comparison between the reference architectural designs in this study and the contractor designs is to gauge the variability and possible range of mass estimates in designing TPF, and then to determine if that variability is significant enough to impact the fundamental conclusion concerning the architecture. The level of confidence in the end result of this study can be determined from the sensitivity of the architectural conclusions to the design variations found. If

the conclusion is found to depend strongly on the component mass estimates, then a more in-depth analysis of the component technologies is needed to select the better architecture for TPF.

In this chapter, each contractor model is presented with the mass budgets provided by the contractor. Then, the budgets are examined and the listings are consolidated into the same components used in the reference designs. The last portion of each contractor section attempts to make an architectural comparison using the components designed by the contractor. The chapter concludes by drawing together the observations made from each contractor model and summarizing the mass estimates and the assumptions made in each design.

6.1 Review of Reference Designs

The wet mass results for the reference designs from Chapter 2 are listed for reference in Table 6.1. The results indicated that the reference separated spacecraft interferometer was less massive than the reference structurally connected interferometer for both orbits considered in this study.

Table 6.1: Summary of Wet Mass Results From Reference Designs

	Structurally Connected Interferometer	**Separated Spacecraft Interferometer**
1.0 AU Orbit	2407 kg	2076 kg
5.2 AU Orbit	1522 kg	1008 kg

6.2 Contractor Study Overview

For the initial study of the Terrestrial Planet Finder concept, the Jet Propulsion Laboratory (JPL) extended requests to three industry leaders for technology and architecture studies [20]. Ball Aerospace and Technologies Corp., Lockheed Martin Corp., and TRW, Inc., were given 18-month

contracts to study the initial project guidelines and to develop mission designs for executing the scientific objectives behind the Terrestrial Planet Finder. Specifically, all three were asked to investigate the trade-offs in mission parameters such as instrument configuration, baseline size, mission orbit, and aperture sizes. In addition, the contractors were to identify the biggest technology drivers in designing TPF and to determine possible constraints in the mission parameters.

6.3 Contractor I: TRW

6.3.1 TRW Model Overview

TRW focused more than the other two contractors on the actual trade space in the design by examining both optical configurations, 1-3-3-1 and 1-2--2-1, signal-to-noise ratios for both 1.0 AU and 5.2 AU orbits, and a range of baselines from 60 m to 80 m. The TRW final study report [33] is also the only one to include a detailed comparison of both architectures for the Terrestrial Planet Finder. Furthermore, TRW also included potential designs for both a 1.0 AU orbit and a 5.2 AU orbit, allowing a more complete comparison between the orbit trades.

Table 6.2: TRW Planet Finder Concept

Parameter	Value
Architecture	SCI
Orbit	1.0 AU
Baseline	75 m
Lifetime	5 yr
Propulsion	Chemical[†]
Optical Configuration	1-2--2-1
Mirror Diameters	2.0 m, 4.0 m

[†] *no specific propellant specified*

Table 6.3: TRW Mass Budget

Subsystem	1.0 AU SCI Mass†	1.0 AU SSI Mass	5.2 AU SCI Mass	5.2 AU SSI Mass
Optics	588 kg	588 kg	220 kg	220 kg
Instruments	499 kg	499 kg	499 kg	499 kg
Spacecraft Bus	373 kg	296 kg	373 kg	356 kg
Sunshade	190 kg	--	190 kg	--
Truss & Deployment	240 kg	--	240 kg	--
Propellant	200 kg	250 kg	200 kg	250 kg
Total Wet Mass	**2090 kg**	**1633 kg**	**1722 kg**	**1325 kg**

†design chosen by TRW

The design which TRW selected as the most optimal is a 75 m structurally connected architecture which uses a combination of pre-tensioned guy wires and sub booms, operating in the 1.0 AU orbit. The optical configuration uses circular mirrors with diameters of 2 m and 4 m in a 1-2--2-1 layout. One major difference between the TRW truss design and the SCI reference design from Chapter 2 is the presence of a deployable sunshield, a component not included in the reference configurations. A summary of the TRW proposal is given in Table 6.2. Recognizing the fact that the architectural selection was still uncertain, in addition to their SCI design, TRW included a mass estimate for a separated spacecraft configuration. Also, designs were given for interferometers in 5.2 AU orbits as well. A first-level listing of the TRW mass budgets for all four designs is shown in Table 6.3. Further analysis of the TRW designs is limited to the 1.0 AU orbit.

6.3.2 TRW Subsystem Comparison

In order to compare the components used in the reference designs to the design presented by TRW, several groupings were made in the TRW SCI subsystem breakdown. The structures for both the inboard and the outboard collector housings were listed separately in the TRW mass bud-

Table 6.4: TRW SCI Component Comparison (1.0 AU)

Component	Reference SCI Mass Estimate	TRW Mass Estimate
Optical Combiner	150 kg	203 kg
Optical System	944 kg	588 kg
Collector	100 kg	296 kg
Spacecraft Bus	100 kg	193 kg
Truss Assembly	115 kg	430 kg†
Deployment Mechanism	998 kg	180 kg
Propellant	--	200 kg
Total Wet Mass	**2407 kg**	**2090 kg**

†*includes sunshade*

get and are taken to be the total collector mass along with the instruments for the optics, with the rest of the instrumentation in the TRW budget given over to the general combiner component, making its mass 203 kg. The structures and mechanism component was taken to be the deployment mechanism and its related hardware, so its mass was removed from the TRW bus component with the remainder of the mass assumed to be the reference spacecraft bus component. Finally, the mass for the sunshade was added to the boom assembly to constitute the mass of the truss structure itself, which includes the sub-booms and guy wires. The mass estimates for the reference and TRW SCI designs are listed in Table 6.4.

The major difference, as will be the case in the other two contractor subsystem comparisons as well, is in the mass of the deployment mechanism. Because TRW uses pre-tensioned guy wires for much of the structural rigidity of the truss, it has a much smaller cross-section than the reference truss design. In fact, the proposal by TRW lists its 'finesse' truss as having a truss diameter of 38 cm against a length of 80 m, implying an aspect ratio of more than 210, which is twice the

Table 6.5: TRW SSI Component Comparison (1.0 AU)

Component	Reference SSI Mass Estimate	TRW SSI Mass Estimate
Optical Combiner	150 kg	203 kg
Optical System	944 kg	588 kg
Collector	100 kg	296 kg
Spacecraft Bus	500 kg	296 kg
Propellant	382 kg	250 kg
Total Wet Mass	**2076 kg**	**1633 kg**

maximum aspect ratio assumed in the reference truss design. Also, the disparity in the structural mass is directly explained by the addition of the sunshade, which was not included in the reference design.

The discrepancy in the optical mass is due to the smaller mirror sizes. Although TRW places the mirrors in a 1-2--2-1 configuration, the inner mirror is only 4.0 m in diameter. The 200 kg inner mirror mass implies an areal density of around 16 kg/m^2, which is in close agreement with the reference value of 15 kg/m^2. The collector mass is much higher, though, because the housing, which provides attachment points for the sub-booms and guy wires, is included in the collector structure. TRW also includes 200 kg of propellant in their truss design, which likely includes orbital transfer maneuvers. The other two components, the combiner and the spacecraft bus, have masses which are more in agreement with the reference design.

Since TRW included an SSI design, the same subsystem comparison between the reference and the TRW models can be made. The same mass allocation process was done as for the SCI design in order to consolidate the subsystem masses, with the only difference being that the structural mass in the TRW SSI mass budget was added to the spacecraft bus component since the reference SSI design includes no explicit structural component. The SSI design comparison is

summarized in Table 6.5.

The same differences in the optics and collector masses are noted. In addition, TRW assumes a much smaller mass for the five spacecraft buses than in the reference design. The underlying reason for this discrepancy is that the propulsion system used in the TRW design is very small. Also, since the optics in the TRW design are smaller and less massive, less propellant is needed to maneuver the spacecraft around the combiner, which explains the disparity in the propellant mass.

In both subsystem comparisons, the reference TPF designs are about 400 kg more massive than the comparable TRW designs. The TRW estimates are the most detailed of the three contractors and aside from the considerable difference in the deployment mechanism, they indicate that the mass estimates in the reference designs are certainly reasonable by design standards today.

6.3.3 TRW Architecture Comparison

Since the TRW final report included a mass budget for both a structurally connected interferometer and a separated spacecraft interferometer, there is no need to extrapolate the values from one to the other. Rather, the two are listed side by side in Table 6.6, comprising the only wet mass comparison of the two architectures from the same contractor.

Here, the SCI is more massive than the SSI model, by over 450 kg, or 28%. The mass of the finesse truss which TRW utilizes, combined with the sunshade mass, has a higher mass than the additional buses and propellant for the separated spacecraft. However, the significant fact is that TRW expects the sum of the five SSI spacecraft bus masses to be much smaller than simply having five of the same bus component from the SCI design. For the SSI, TRW quadruples the power system mass of the SCI but cuts both the total propulsion and thermal system in half. A slight increase in the mass needed for guidance, navigation, & control, data management, and communi-

Table 6.6: Architectural Comparison With TRW Components (1.0 AU)

Component	TRW SCI Mass Estimate	TRW SSI Mass Estimate
Optical Combiner	203 kg	203 kg
Optical Subsystem	588 kg	588 kg
Collector	296 kg	296 kg
Spacecraft Bus	193 kg	296 kg
Truss Assembly	430 kg†	--
Deployment Mechanism	180 kg	--
Propellant	200 kg	250 kg
Total Wet Mass	**2090 kg**	**1633 kg**

†*includes sunshade*

cations accounts for the rest of the bus mass increase between the SCI and the SSI.

The propellant mass is an interesting contrast, since TRW only shows a 50 kg propellant mass difference between its structurally connected and its separated spacecraft design. Each individual spacecraft in the TRW SSI design carries 50 kg of propellant. The TPF report given by TRW does not state the actual calculations which resulted in the propellant mass estimates.

The fact that both the reference architectural comparison and the TRW designs show about the same difference between the SCI and SSI wet masses is a strong indication that the SSI is indeed likely to be less massive than the SCI.

6.4 Contractor II: Ball Aerospace

6.4.1 Ball Aerospace Model Overview

Ball Aerospace has a rich heritage in optical and cryogenic systems, and the system tasks given to them reflected that expertise by including points which focused on the optical configuration of

Table 6.7: Ball Aerospace Planet Finder Concept

Parameter	Value
Architecture	SCI
Orbit	5.2 AU
Baseline	80 m
Lifetime	15 yr
Propulsion	Xenon-Ion
Optical Configuration	1-3-3-1
Mirror Diameters	0.5 m, 1.5 m

TPF. Additionally, their final report [4] included performance studies and a technology analysis.

The final design from Ball is a structurally connected architecture using an 80 m long truss and an inflatable sunshield deployed in the 5.2 AU solar orbit. The truss is a two-segment design contributed by AEC-Able Engineering, deployed using a powered-nut system much like the reference SCI model in this study. The propulsion system is a xenon-ion thruster with an expected specific impulse of 3180 sec. The Ball design also included propellant for a 15 year mission lifetime, rather than the 5 year duration which the reference designs assume. A summary of the concept proposed by Ball Aerospace for the Terrestrial Planet Finder is given in Table 6.7, with the mass budget from their final report reproduced in Table 6.8. The total estimated mass of just over 3600 kg is the largest mass of the three contractors, with the payload element including the optics, the collector, and the combiner.

6.4.2 Ball Aerospace Subsystem Comparison

The power, command & control, communications, attitude control, and propulsion systems of the Ball design are functions included in the reference SCI and SSI spacecraft bus component. Adding together the masses for each of those subsystems gives a total bus mass of 993 kg. Only the

Table 6.8: Ball Aerospace Mass Budget

Subsystem	Mass
Structure	955 kg
Mechanisms	33 kg
Electrical Power & Distribution	345 kg
Command, Control & Data Handling	39 kg
Communications	68 kg
Thermal Control	25 kg
Attitude Control	124 kg
Propulsion System	392 kg
TPF Payload	836 kg
Propellant	791 kg
Total Wet Mass	**3608 kg**

total structural and mechanical mass is listed, so separate values for the truss and the deployment are not known. The collector and combiner elements are grouped, so the estimated mirror and collector masses from the reference designs are assumed and subtracted from the Ball payload mass, leaving the remainder of 677 kg to the combiner hardware itself. Also, since the propellant in the Ball mass budget is specifically listed as being used in the orbital transfer and not during the operational lifetime, its mass is removed to balance the comparison. The subsystem mass breakdown is shown in Table 6.9.

The components which show a major difference between the two designs are the combiner hardware and the spacecraft bus. Though not necessarily the combiner hardware *per se*, since the optics mass listing in the Ball mass budget was distributed using the reference optics and collector masses, the fact remains that Ball anticipates a much higher mass for the entire optical system needed to perform the operations of the Terrestrial Planet Finder. The difference in the bus mass

Table 6.9: Ball Aerospace SCI Component Comparison (5.2 AU)

Component	Reference SCI Mass Estimate	Ball Mass Estimate
Optical Combiner	150 kg	677 kg
Optical Subsystem	59 kg	59 kg†
Collector	100 kg	100 kg†
Spacecraft Bus	100 kg	993 kg
Truss Assembly	115 kg	988 kg
Deployment Mechanism	998 kg	
Propellant	--	--
Total Wet Mass	**1522 kg**	**2817 kg**

†*defined to equal to the reference design mass*

can be attributed to the lack of both a sunshield and a separate power component in the reference model. However, on the whole, a large divergence exists between the Ball mass projection and the reference mass values, indicating some fundamental differences in the design assumptions.

6.4.3 Ball Aerospace Architecture Comparison

Because the spacecraft bus is the largest component in the Ball design, adding four more of them drastically raises the mass of the SSI architecture in this case. The collector bus includes the solar electric propulsion (SEP) thruster which alone has a mass of 373 kg. The power and the thermal system masses in the Ball SCI mass budget are not repeated in each collector spacecraft; rather, the masses are divided by five to spread them over each of the individual spacecraft. Although the power needed by the thrusters in each collector spacecraft is likely to be one of the largest power requirements, the power given in the Ball mass budget is used for the orbital transfer maneuvers and therefore, the total power mass is unlikely to change, justifying the amortization over all five separated spacecraft. In addition, to keep the division realistic, the communication downlink is

Table 6.10: Architectural Comparison With Ball Aerospace Components (5.2 AU)

Component	Ball SCI Model	Extrapolated SSI Model
Optical Combiner	677 kg	677 kg
Optical Subsystem	59 kg	59 kg
Collector	100 kg	100 kg
Spacecraft Bus	993 kg	2598 kg
Truss Assembly	988 kg	--
Deployment Mechanism		--
Propellant	--	220 kg†
Total Wet Mass	**2817 kg**	**3654 kg**

†*only accounts for maneuvering, not orbit insertion*

kept in the combiner bus and is not added to each collector. Furthermore, since the separated spacecraft architecture does not need large momentum wheels for internal torque, the attitude control system is removed from the total SSI bus mass.

Using the predicted dry masses of the collector spacecraft, 558 kg and 534 kg for the inboard and the outboard, respectively, the propellant needed for maneuvering can be calculated. The Ball propulsion system uses a xenon-ion thruster with a specific impulse of 3180 sec which helps decrease the additional propellant needed to accelerate the larger collector spacecraft. Table 6.10 shows the architectural comparison between the baseline Ball SCI model and the SSI design extracted from the same components.

In this case, the SCI model has about a 800 kg mass savings, primarily because the spacecraft bus pushes the SSI wet mass to a much higher level. The major portion of the spacecraft bus comes from the solar electric propulsion (SEP) thrusters which have a mass of 373 kg each. The uncertainty in the SSI mass distribution from the original Ball SCI model is rather high, though,

Table 6.11: Lockheed Martin Planet Finder Concept

Parameter	Value
Architecture	SCI
Orbit	1.0 AU
Baseline	80 m (structural) 78 m (optical)
Lifetime	5 yr
Propulsion	Xenon-Ion
Optical Configuration	1-3-3-1
Mirror Diameters (oval)	0.67 x 2 m, 2 x 6 m

and realistically, the spacecraft bus is likely to be much less massive than the 2600 kg predicted in this analysis.

6.5 Contractor III: Lockheed Martin

6.5.1 Lockheed Martin Model Overview

The contract tasks given to Lockheed Martin were very similar to those for Ball Aerospace. The trade space for the two candidate TPF architectures was to be evaluated, with a recommended design to be put together. Performance and mission costs were to be evaluated and technological barriers identified. Lockheed Martin also included various launch options and a cursory study of a tethered architecture in their final report [22].

Their proposed TPF design is also a structurally connected architecture with a 80 m truss providing a 78 m optical baseline. While the optical configuration is 1-3-3-1, oval mirrors of dimensions 2 x 6 m and 0.67 x 2 m are used, rather than circular mirrors. One other difference between the Lockheed Martin and the Ball designs is the choice of mission orbit. While Ball decided that

Table 6.12: Lockheed Martin Mass Budget

Subsystem	Mass
Truss	360 kg
Spacecraft Bus	450 kg
Outboard Siderostats (2x)	250 kg
Inboard Siderostats (2x)	50 kg
Propellant	340 kg†
Total Wet Mass	**1750 kg**

†*extrapolated from total mass given*

the lower zodiacal noise at a 5.2 AU orbit justified the longer travel time, Lockheed opted for a 1.0 AU solar orbit instead. The deployment mechanism used by Lockheed is a hinged configuration which merely unfolds once in orbit, thereby avoiding large screw deployment canisters. The mass of the hinges, latches, and other mechanisms needed for the deployment is assumed to be included in the truss listing.

The mass budget given by Lockheed Martin is not as detailed as those from TRW and Ball Aerospace, but their analysis included a more in-depth look at structural damping in the truss and the financial costs of the program. A listing of the major characteristics of the design is shown in Table 6.11. The mass estimates from the Lockheed Martin candidate TPF design included a high and a low value, and the higher values are given in Table 6.12.

6.5.2 Lockheed Martin Subsystem Comparison

The components given by Lockheed are more general than those outlined in Chapter 2 for the reference models and therefore, to make a subsystem comparison, they must be subdivided. First, the Lockheed spacecraft bus component includes the combiner hardware, and so, to separate the combiner mass, the estimate used in the reference combiner component is assumed. Also, the same

Table 6.13: Lockheed Martin SCI Component Comparison (1.0 AU)

Component	Reference SCI Mass Estimate	Lockheed Martin Mass Estimate
Optical Combiner	150 kg	150 kg†
Optical Subsystem	944 kg	500 kg
Collector	100 kg	100 kg†
Spacecraft Bus	100 kg	300 kg
Truss Assembly	115 kg	360 kg
Deployment Mechanism	998 kg	
Propellant	--	340 kg
Total Wet Mass	**2407 kg**	**1750 kg**

†*defined to equal to the reference design mass*

mass for the collector hardware is assumed, making the total optics mass in the Lockheed budget approximately 500 kg. Additionally, as noted before, there is no distinct deployment mechanism listed in the Lockheed design. With these modifications, the mass budget from Lockheed is shown compared to the reference design in Table 6.13.

The disparity in the masses, with Lockheed's total mass being about three-fourths of the reference design, is almost solely due to the inclusion of the massive deployment mechanism in the reference design. Aside from that component, the masses are very close in magnitude. Because Lockheed uses oval mirrors with a smaller minor axis, their optical subsystem mass is lower. However, the provided masses imply optical areal densities of 47 kg/m^2 and 24 kg/m^2 for the outer and inner mirrors, respectively, which are both higher than the assumed value of 15 kg/m^2. The truss mass is over twice the reference mass because of thicker strut walls and larger joint masses in the Lockheed design, as well as to account for the motors and latches used in the deployment sequence. Again, the bus is more massive in the contractor model, as was the case for

the Ball Aerospace model, which is a likely indication that the reference models should have used a larger spacecraft bus mass. The propellant in the Lockheed Martin design is most likely for insertion in the 1.0 AU solar orbit, but since their report does not explicitly verify that assumption, the propellant mass is left in the comparison.

6.5.3 Lockheed Martin Architecture Comparison

The primary assumption made in extrapolating SSI mass estimates from the Lockheed Martin SCI design is that the SSI spacecraft buses are similar in size to the SCI bus. The result of this generalization is an overestimation since the bus includes functions which are not duplicated in the collector spacecraft. If the total SSI bus mass was the same multiple of the SCI bus mass as in the Ball case, a ratio of 2.6 (2598 kg to 993 kg), the Lockheed Martin SSI bus total would have a value of 786 kg, making the total wet mass 1699 kg, which is much closer to the Lockheed Martin SCI mass. The bus mass ratio is lower for the TRW design, 296 kg to 193 kg, or 1.54, but for the sake of a conservative first estimate, the Ball ratio is used.

Similar to the Ball propulsion system, Lockheed's ion propulsion has a high specific impulse which helps to reduce the propellant mass needed to maneuver the large collectors. Assuming that each individual spacecraft of the SSI uses the same size bus as the SCI is the primary reason that the Lockheed Martin SCI model is more mass efficient than an SSI design using the same components, with the mass estimates shown in Table 6.14. There is also no distinct deployment mechanism in the truss design to offset the added mass from the spacecraft bus. The propellant mass listing is skewed because the SCI design includes the propellant needed for orbital transfer, while the SSI propellant mass is only an estimation of the propellant needed for maneuvering. While the baseline architectural comparison using the Lockheed Martin components shows the SCI to be about 27% less massive than the SSI, an alternative SSI mass total using a bus mass prorated

Table 6.14: Architectural Comparison With Lockheed Martin Components (1.0 AU)

Component	Lockheed Martin SCI Model	Extrapolated SSI Model
Optical Combiner	150 kg†	150 kg†
Optical Subsystem	500 kg	500 kg
Collector	100 kg†	100 kg†
Spacecraft Bus	300 kg	1500 kg *(786 kg)‡*
Truss Assembly	360 kg	--
Deployment Mechanism		--
Propellant	340 kg	163 kg
Total Wet Mass	**1750 kg**	**2413 kg** *(1699 kg)‡*

†defined to equal to the reference design mass
‡using prorated bus mass ratio from Ball design

according to the Ball spacecraft bus mass ratio nearly equalizes the comparison, making the SSI less massive by about 50 kg.

6.6 Conclusions

6.6.1 Reference Design Assumptions

Several conclusions can be drawn from the examination of the three contractor models which pertain to the makeup of the reference SCI and SSI designs. As a top level consideration, the reference designs did not include a sunshield component, which all three contractors mentioned. Based on the contractor designs, the sunshade would have a mass of 150-200 kg, which would widen the mass difference in the reference design mass estimates.

Another contrasting point is the propulsion system and the propellant mass included in the contractor designs. Rather than pulsed plasma thrusters, ion propulsion was the type of system

used, which offers a higher specific impulse. Ion propulsion also provides the same level of impulse bit controllability, defined as the smallest discrete velocity change which can be affected by the thruster, a crucial issue in both disturbance rejection in the truss and formation flying for the separated spacecraft. The thrust levels of both a PPT system and an ion propulsion thruster are equal, as well. The major drawback to ion propulsion is the power requirement of 400 W or more, but improvements in energy efficiency could potentially offset that problem. Also, the assumption was made that the reference SCI would maintain its rotation rate through the use of reaction wheels and would reorient itself using momentum torques, requiring a negligible amount of propellant. However, while the contractors included reaction wheels, they estimated the amount of propellant needed to dump the momentum to counteract wheel saturation and added as much as 200 kg of propellant to the mass, making it a major component in the industry designs.

An important comparison is the mass of the truss deployment mechanism since it was a critical issue in the reference designs. The Ball design included an actual deployment design and specifics on the threaded canister with a deployment mass nearly equal to the calculated reference value from Chapter 2. Lockheed decided to just unfold the truss, using a hinged mechanism. TRW selected a finesse truss, depending on guy wires and sub-booms to provide the structural rigidity. Their design extends the truss using the same nut-driven mechanism, but because the truss is so much more narrow, the deployment mass is less than 200 kg. Obviously, the actual mechanism used for the SCI configuration of the Terrestrial Planet Finder will be an important design point, affecting not only the mass but the optical resolution and error as well.

6.6.2 Mass Comparison Summary

Except for the Ball aerospace model, the other two contractor models are less massive than the reference designs, which indicates that the reference mass estimates are probably reasonable and

Table 6.15: Summary of Total Mass Estimates

TPF Concept	Architecture	Orbit Radius	Total Wet Mass
Reference Model	SCI	1.0 AU	2407 kg
Lockheed Martin Model	SCI	1.0 AU	1750 kg
TRW Model	SCI	1.0 AU	2090 kg
Reference model	SCI	5.2 AU	1522 kg
Ball Aerospace Model	SCI	5.2 AU	2817 kg
TRW Model	SCI	5.2 AU	1722 kg
Reference Model	SSI	1.0 AU	2076 kg
Lockheed Martin Model†	SSI	1.0 AU	2413 kg *(1699 kg)*‡
TRW Model	SSI	1.0 AU	1633 kg
Reference Model	SSI	5.2 AU	1008 kg
Ball Aerospace Model†	SSI	5.2 AU	3654 kg
TRW Model	SSI	5.2 AU	1325 kg

†*extrapolated from component masses from contractor base SCI model*
‡*using prorated bus mass ratio from Ball design*

are certainly conservative. The three SCI models in a 1.0 AU orbit are loosely centered around a 2000 kg mass estimate, while the three 1.0 AU SSI designs have masses slightly less than that. The two additional TRW mass estimates for SCI and SSI designs in a 5.2 AU orbit are included in Table 6.15 as well, which is a summary of the mass estimates presented in this chapter. Two values are given for the 1.0 AU SSI design extrapolated from Lockheed Martin's SCI components, with the first assuming that the SSI requires five complete SCI buses and the smaller value using a prorated bus mass ratio taken from the Ball designs. The extrapolated Ball design in the 5.2 AU orbit is extremely massive due to the assumptions made in computing the total spacecraft bus mass.

With regard to the architectural comparison, there is a large variation in the total masses. TRW

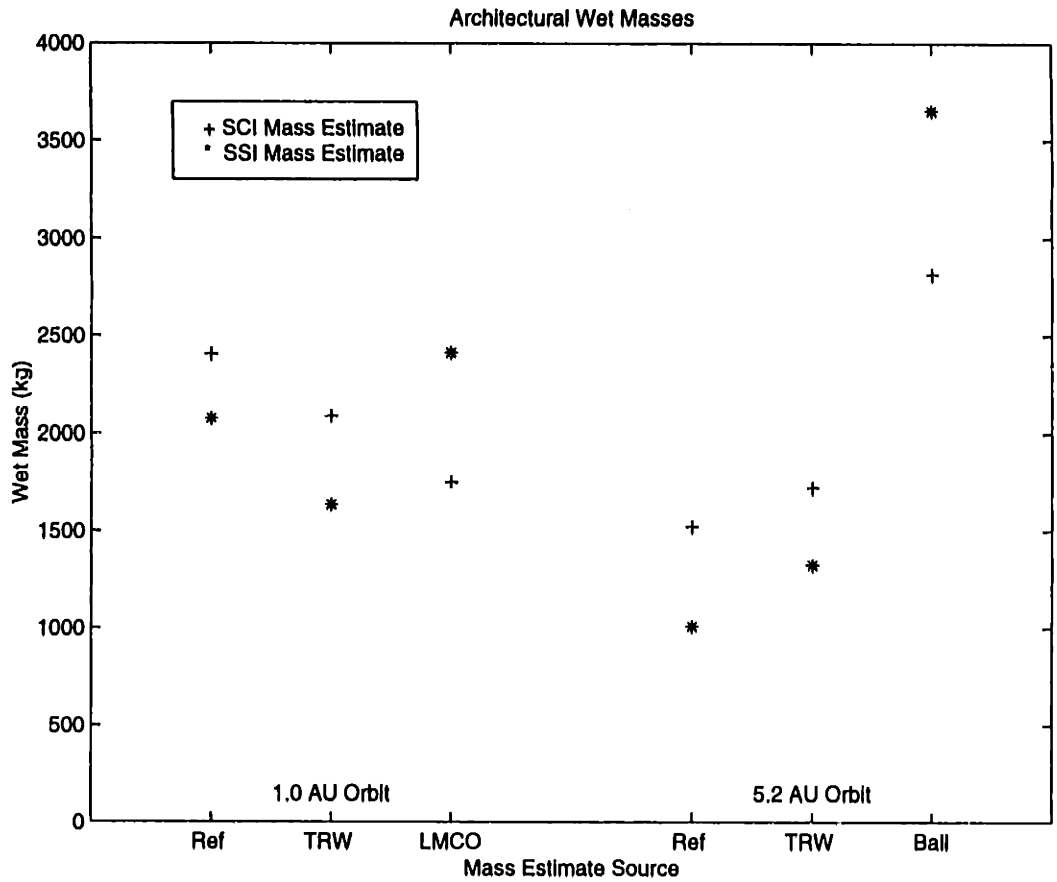

Figure 6.1: Graphical Representation of Architectural Mass Estimates

provides mass estimates for both structurally connected and separated spacecraft designs and concludes that the SSI would be smaller in both orbits, by about 450 kg. Extrapolating SSI masses from the Ball SCI mass budget results in the SSI being 800 kg more massive. The Lockheed Martin values make the mass of the SCI 660 kg less than the SSI mass, but using the same architectural ratio of the bus mass as in the Ball extrapolation nearly equalizes the two wet masses. Figure 6.1 is a graphical presentation of the architectural wet masses for both orbits, showing that the conclusion as to the more mass efficient architecture is unclear. The reference and contractor designs are divided by orbit radius and plotted along the x-axis.

Therefore, the range of variability in the architectural comparison seems to indicate that the conclusion is not clear-cut. The actual mass comparison is between the truss and deployment

mechanism of the SCI and the additional spacecraft buses and propellant needed by the SSI. The major point of uncertainty in the extrapolated SSI designs is the derivation of the collector spacecraft bus masses from the structurally connected bus mass, which attests to the need for more analysis of separated spacecraft architectures.

Chapter 7

Conclusions

7.1 Summary

This study was a comparison of two major architectures for the Terrestrial Planet Finder (TPF), a proposed space-based interferometer for detecting extra-solar planets. A structurally connected interferometer (SCI) uses a truss assembly to provide the baseline for mounting the collector optics, while a separated spacecraft interferometer (SSI) maintains the baseline with independent spacecraft flying in formation. The comparison was performed for interferometer designs in both a 1.0 AU and a 5.2 AU radius orbit. The purpose of the study was to determine which architecture would be the optimal selection for the Terrestrial Planet Finder mission.

Three metrics were applied to the comparison in order to obtain a broad and more encompassing understanding of the trade-offs between the two architectures. The primary metric was the wet mass of the two architectures as derived using reference designs for both. Secondly, the adaptability metric allowed an examination of the sensitivity of the interferometer design to changes in the functional requirements. The third metric took into account the capabilities offered by the two architectures in performing their operational roles and meeting four operational constraints: reso-

lution, rate, integrity, and availability.

7.1.1 Wet Mass Metric

Typically, the design selection for aerospace programs is made based on the lowest cost to achieve the desired objectives. But because the Terrestrial Planet Finder program is still in its earliest stages, no accurate estimates of its financial costs can be made. However, in the aerospace industry, launch costs typically scale by the amount of mass placed in orbit. So, the natural cost metric choice was a comparison of the wet mass of the system, as calculated from the beginning of its operational life in orbit, thus ignoring launch vehicle considerations and orbit transfer maneuvers. The dry mass was set by the architecture selection and the actual design, while the operational profile of the interferometer dictated the propellant mass usage.

In Chapter 2, reference designs for both architectures were developed in order to determine the projected wet mass. Each design was broken down into subsystems whose masses were separately estimated. Several of the components were identical in either configuration, so the basic comparison came down to the components unique to each architecture. The structurally connected interferometer contained the truss assembly and the mechanism needed to deploy it, while the separated spacecraft interferometer required a larger amount of propellant for maneuvering as well as additional spacecraft buses. Chapter 3 also included an examination of the mass sensitivity to modifications in the design assumptions, such as the truss and deployment mechanism design, the propulsion system, and the maneuver profiles followed by the collector spacecraft. The major conclusions which resulted from the wet mass comparison of this study were as follows.

(i) With the reference designs presented in this study, the separated spacecraft interferometer was more mass efficient than the structurally connected interferometer in both orbital

configurations. In a 5.2 AU orbit, the SSI was 340 kg, or 14%, less massive. In a 5.2 AU orbit, the SSI was over 510 kg, or 34%, less massive.

(ii) The primary mass driver for the structurally connected architecture was the deployment mechanism. Based on the empirical formula provided by AEC-Able Engineering, the estimated mass of two deployment canisters was 998 kg, or over 41% and 65% of the total wet mass in the 1.0 AU and 5.2 AU orbits, respectively. Therefore, because of the large baseline of the Terrestrial Planet Finder, the structural configuration of any monolithic interferometer concept will be critical in its efficiency.

(iii) The lower dry mass of the optical systems of an interferometer operating at the 5.2 AU orbit decreased the amount of propellant required to maneuver each spacecraft by nearly 50%, a 183 kg mass savings. The mirrors provide the same level of signal-to-noise for a much smaller diameter because of the decrease in local zodiacal noise.

(iv) Modifications in the truss and deployment mechanism are significant for the structurally connected interferometer. A 14% increase in the aspect ratio of the truss is sufficient to lower the deployment canister mass such that the SCI and SSI masses in a 1.0 AU orbit are equal. On the other hand, four deployment canisters may be required, which would effectively double the deployment mass.

(v) The propellant requirement for the separated spacecraft interferometer is also very sensitive to modified design assumptions. More efficient thrusters could significantly decrease the mass of the propulsion system, and non-circular profiles could conceivably reduce the propellant requirement at the risk of some degradation in the image quality.

Given the reference designs of Chapter 2, the SSI is the favored architecture. However, the sensitivity analysis of Chapter 3 revealed the extremely high sensitivity of the SCI wet mass to the

deployment mechanism design. Therefore, based on the results of Chapters 2 and 3, no clear and undisputable choice exists between the two architectures and other factors were then considered.

7.1.2 Adaptability Metric

The adaptability of the architecture is an important consideration in the design process because of the frequent redesigns and modifications of the functional requirements for space programs. Chapter 4 introduced the metric and considered two classes of modifications, homogenous and heterogeneous. Homogenous modifications require more of the same functions as already being provided by the instrument, while heterogeneous changes broaden the functional requirements to include other objectives. Examples of homogenous adaptations included improving the optical configuration, changing the separation baseline, extended the lifetime or the target schedule, and adjusting the rotation period. As a heterogeneous modification, the potential for synthetic imaging was discussed. The wet masses of the SCI and SSI architectures varied differently to changes in these functional characteristics and reflected contrasting sensitivities. Three primary conclusions were drawn from the adaptability analysis.

(i) While modifying the optical configuration to use a 1-2--2-1 mirror array had an equal effect on the dry mass for both architectures, the secondary affect of requiring more thrusting of larger masses by each individual spacecraft in a separated array became an issue. For the parameters used in this study, 45% more propellant, or 172 kg, was needed for an SSI in a 1.0 AU orbit and 16%, or 33 kg, more propellant was needed for a 5.2 AU orbit.

(ii) Only the structurally connected interferometer could provide protracted operations beyond the planned mission lifetime because of the additional propellant needed by the

separated spacecraft in an SSI array. A truss would be able to maintain its rotation and slew to image new targets through the use of momentum wheels, which would not require a significant amount of additional propellant. Therefore, being able to extend the operational lifetime of the instrument favored the structurally connected interferometer.

(iii) An important advantage offered by a separated spacecraft interferometer is the potential for performing synthetic imaging. Maneuvering the spacecraft array in such a way as to cover more of the Fourier plane, an SSI can provide high quality images of the entire focal plane for other astrophysical targets. Such a broadening of the mission scope by an SSI design could make the Terrestrial Planet Finder a more viable option for the astrophysical community as a whole.

The adaptability analysis pinpointed the dependence of the SSI on propellant for maneuvering as a primary drawback to larger optics or increased operations, but at the same time, the potential for synthetic imaging is a very strong contention for the SSI. But, in addition to the wet mass and the adaptability, the performance capabilities of the two architectures were compared.

7.1.3 Capability Metric

In Chapter 5, the capability metric provided a basis for comparing the performance efficiency of a system over its lifetime as measured by the ability to meet four constraints. The resolution dictated the capability of the architecture in isolating a planet apart from its parent star. The rate of the interferometer was set by the observation goals of the TPF program. The integrity constraint was placed on the control of the differential path length in the two legs of the interferometer, while the availability was an indication of the reliability of the design. The four primary observations from the chapter were that:

(i) The resolution obtained by the interferometer architecture is dependent on the effective suppression of the light from the parent star. The ability of a separated spacecraft array to adjust the optical baseline in order to tailor the angular resolution to the target system is an important one which could improve the performance of the interferometer over the wide range of stellar target characteristics.

(ii) The rate constraint is met by the optical hardware of the interferometer and therefore, it is not a distinguishing factor in the architectural comparison.

(iii) The integrity is contingent on the systems which maintain the differential path length in the interferometer. The structurally connected interferometer relies on the rigidity of the truss, along with any active structural control, for disturbance rejection, a technology which will be quite mature at the time of the TPF design, while the separated spacecraft interferometer requires precision formation flying, which has not yet been demonstrated on a large scale. However, preliminary analysis (Appendix A) indicated that the dimmer parent stars will provide insufficient fringe tracking bandwidth to meet the 0.5 nm differential pathlength stability criterion for the SCI.

(iv) The two architectures differed in their failure compensation modes in the event of a collector or spacecraft malfunction. The structurally connected interferometer would be limited to operating as a single Bracewell optical pair at a fixed baseline, while the separated spacecraft interferometer would be able to vary the baseline, thus recovering more of the operational objectives after a failure. In addition, particularly for an interferometer operating in a 1.0 AU orbit, a separated spacecraft architecture could replace a malfunctioning element through the use of a spare spacecraft, either from an on-orbit position or launched from earth.

(v) The separated spacecraft interferometer is more susceptible to optical degradation due to propellant contamination. Several different issues, including particulate deposits, transmission interference through particular cloud, and plume impingement forces, could each impact the availability of the SSI architecture.

Taken together, the three metrics provide a broad presentation of the issues which surround the architectural comparison. However, because of the uncertainties and the assumptions inherent in this study, the validity of the conclusions was verified through a comparison with other contractor models for TPF.

7.1.4 Comparison Validation

Any mass estimates and design assumptions are subject to review in light of other designs and models. In the Terrestrial Planet Finder program, three contractor models were solicited from industry leaders. Chapter 6 provided an overview of the three designs, with the assumptions and estimates made for each one. The reference designs were then compared to the contractor models to gain some measure of the certainty and accuracy of the wet mass values obtained.

Three issues were discovered which distinguished the reference SCI and SSI designs from those of the contractors. One evident difference was the omission of a sunshield in the reference components list. Another was the efficiency of the propulsion system, since the contractor models made use of ion propulsion rather than the pulsed plasma thrusters of the reference models. Finally, a large variation in the mass of the structural component and its deployment system was found, ranging from 360 kg to nearly 1000 kg. Aside from these components, the masses of the others, such as the optics, the collectors, and the combiner, were generally in agreement.

However, the certainty of the architectural conclusion from the wet mass analysis was called

into question because of the range of values in the contractor wet mass estimates. The most critical component was the spacecraft bus, since the underlying assumption in the reference designs was that each collector spacecraft contained a bus identical to the one in the SCI design. A more detailed analysis of the non-optical subsystems contained in the spacecraft bus is necessary for a more definite architectural study.

7.2 Conclusion

Based on the three metrics outlined above, a separated spacecraft architecture is certainly a viable alternative to the structurally connected interferometer. The additional mass needed for the spacecraft maneuvering was offset by the absence of a large truss and the hardware needed to deploy it, making the reference SSI design slightly more mass efficient than the reference SCI design in both a 1.0 AU and a 5.2 AU orbit. However, the tenability of that conclusion is somewhat unclear because the mass calculations are highly sensitive to the assumptions made in the reference designs.

Although an SCI is less sensitive to increased or modified operations, as discussed in Chapter 4, the potential offered by a multiple spacecraft array for performing other astrophysical objectives, such as synthetic imaging, is an attractive possibility for garnering support from the general scientific community as well as for expanding the scope of TPF's mission profile. Chapter 5 considered the inherent capabilities of an SSI for tuning the baseline to optimize the imaging resolution and for compensating in the event of collector failure, while determining that the integrity was better maintained by an SCI. The analysis coverage given in Table 1.1 is reproduced in Table 7.1 with the general conclusions from this study. Altogether, the final conclusion of this study is that a separated spacecraft interferometer merits serious consideration as the more optimal archi-

Table 7.1: Summary of Metric Results

Metric	TPF Application	Conclusion
Cost Per Function	Total mass of system architecture, including optics and propellant	The SSI is slightly more mass efficient, but conclusion is very dependent on component designs
Adaptability	Sensitivity of the design to modifications in the functional requirements	Propellent requirements hinder the SSI, but the potential for synthetic imaging is a major advantage
Capability	Ability and efficiency of system at performing its design role	
Resolution	Acquiring and isolating the planet signal from the parent star	Baseline tuning allows the SSI to maximize effective resolution
Rate	Time to construct an accurate image of the target solar system	Both architectures meet the rate requirement equally
Integrity	Image sensitivity to local and exo-zodiacal noise	Highly complex systems will be needed for the requisite DPL control in both architectures
Availability	Failure compensation modes for combiner or collector failure	The SSI allows individual spacecraft replacement, but propellant contamination must be prevented

tecture for the Terrestrial Planet Finder mission. However, due to the variability in the industry mass estimates and the high sensitivity to the SCI deployment mechanism design, rejecting either architecture at this point would be premature.

7.3 Future Issues

This study was an attempt to specifically relate the comparative trades involved in selecting an interferometer architecture to the Terrestrial Planet Finder mission. The primary objective was not to unequivocally determine which was better; rather, the intention was to study the relevant issues and to gather a more complete presentation of the comparison. The parameters for the TPF mis-

sion, as well as the model designs, are still somewhat uncertain, leaving several areas of research which may bring further light on an architectural choice.

(i) **Nulling technology** - Nulling interferometry is still a test bed technology. The hardware and software needed to suppress the central starlight to better than one part in a million has only recently begun to be implemented on ground-based telescopes, such as the Large Binocular Telescope [3]. Once more experience is gained in optical nulling, more accurate estimates as to the mass and complexity of the collector and combiner systems can be made. While their masses do not directly differentiate between the architectures, more massive collectors and combiners would require more propellant for the separated array.

(ii) **Boom deployment technology** - The deployment of a large truss assembly was a critical item in this comparison. Further development of potential structural configurations, such as the finesse truss proposed by TRW and the hinged truss proposed by Lockheed Martin, would improve the mass efficiency of the spacecraft. Such work is important in examining the trade-offs which exist between structurally connected and separated spacecraft interferometers because of its relevance both to the system mass as well as its optical resolution and operational reliability.

(iii) **Enhanced and extended bandwidth control** - While only a cursory examination of the disturbance environment and the structural response was made in this study, the stability of the collector mountings is a crucial part of the scientific operation of the interferometer. Large metered space structures such as this one have not been controlled to such a high precision before, and their behavior in the space environment is still a subject of study. Thermal responses may play a role, as well as other external and internal disturbance sources. The Shuttle Radar Topography Mission (SRTM) [27] is a key technology

demonstration mission which will utilize a 60 m truss deployed from the Space Shuttle bay, thus providing key experience and awareness of the complexities involved in space truss operations. For dimmer parent stars, fringe tracking bandwidth may be insufficient to compensate for onboard vibrations. Therefore, the application of active structural control, acceleration feedforward, and other control and metrology options may need to be developed.

(iv) **Formation flying technology** - Maintaining a formation of five independent, free-flying spacecraft to location errors of less than a centimeter magnitude requires precise relative positioning as well as global system velocity measurements. The third Deep Space mission [21] will be the first space mission to demonstrate formation flying to this level, in 2001. The spacecraft buses on each of the individual spacecraft will have to communicate with each of the other spacecraft, making it a very complex operation. Since many of the adaptability and capability advantages of the separated spacecraft interferometer lie in its ability to accurately maneuver, the formation flying is a critical area in the development and architectural decision making process.

The Terrestrial Planet Finder will seek to find terrestrial planets which may be capable of supporting life. Its design will be critical to its success, and these technological issues will play a key role in its design and eventual operation.

References

[1] Angel, J. R. P., "Use of a 16m Telescope to Detect Earthlike Planets", *Proceedings on the Workshop on The Next Generation Space Telescope*, (eds. P. Bély, C. Burrows, and G. Illingworth), Space Telescope Science Institute, Baltimore, MD, pp. 81-94, 1990.

[2] Angel, J. R. P. and N. J. Woolf, "An Imaging Nulling Interferometer To Study Extrasolar Planets," *The Astrophysical Journal*, Vol. 475, pp. 373-379, 20 January 1997.

[3] Angel, J. R. P., and N. J. Woolf, "The Large Binocular Telescope: A Unique Scientific and Technology Precursor to Planet Finder," No. 1372, Preprints of the Steward Observatory, University of Arizona, Tucson, AZ, 1996.

[4] Ball Aerospace and Technologies Corp., "Terrestrial Planet Finder," Presentation given 3 December 1997 at the Jet Propulsion Laboratory, Pasadena, CA.

[5] Barlow, M. S. and E. F. Crawley, "The Dynamics of Deployable Truss Structures in Zero-Gravity: The Mode STA Results," Tech. Rep. #1-92, Space Engineering Research Center, MIT, Cambridge, MA, January 1992.

[6] Beichman, C. A., "Exo-Zodiacal Clouds and the Terrestrial Planet Finder," Jet Propulsion Laboratory Internal Memorandum, 23 December 1996.

[7] Beichman, C. A., ed., et al. "A Road Map for the Exploration of Neighboring Planetary Systems (ExNPS)," Final Report of the ExNPS Team, Jet Propulsion Laboratory Report No. JPL 96-22, NASA, Pasadena, CA, August 1996.

[8] Bracewell, R. N., "Detecting Nonsolar Planets By Spinning Infrared Interferometer," *Nature*, Vol. 274, p 780, 24 August 1978.

[9] Burge, J. H., "Lightweight Primary Mirror for NGST Using a Thin Glass Facesheet with Active Rigid Support." Presentation given at the NGST Annual Technology Challenge Review #1, 8 July 1997.

[10] Carosso, N., "Contamination Monitoring Design Guidelines," Swales and Associates, Inc., <URL:http://www-de.ksc.nasa.gov/dedev/labs/cml_lab/CONTMON_DESIGN.html>. Accessed 15 May 1998. Contamination Monitoring Laboratory, Kennedy Space Center, NASA.

[11] Colavita, M. M., "Technology Drivers for TPF," Presentation given 24 June 1997 at the Jet Propulsion Laboratory, Pasadena, CA.

[12] Crawford, R., 16 April 1997. Telephone interview.

[13] Dettleff, G., "Plume Flow and Plume Impingement in Space Technology." *Progress in Aerospace Sciences 28*, pp.1 - 71, 1991.

[14] Griffin, M. D. and J. R. French, *Space Vehicle Design*, AIAA Education Series, American Institute of Aeronautics and Astronautics, Washington, D. C., 1991.

[15] Jet Propulsion Laboratory, *Orbiting Stellar Interferometer*, NASA Science and Technical Review, March 1996.

[16] Jilla, C. D., and D. W. Miller, "A Reliability Model for the Design and Optimization of Separated Spacecraft Interferometer Arrays," 11th AIAA/USU Conference on Small Satellites, AIAA/USU, Logan, UT, September 1997.

[17] Kong, E. M., and D. W. Miller, "Optimization of Separated Spacecraft Interferometer Trajectories in the Absence of a Gravity Well," *Astronomical Interferometry, Proceedings of the 1998 SPIE Symposium on Astronomical Telescopes and Instrumentation*, Vol. 3350, Kona, HI, March, 1998.

[18] LeDuc, J. R., et al., "Mission Planning, Hardware Development, and Ground Testing for the Pulsed Plasma Thruster (PPT) Flight Demonstration on MightySat II.1," AIAA 97-2779, 33rd Joint Propulsion Conference, Seattle, WA, July 1997.

[19] Léger, A., et al., "Could we Search for Primitive Life on Extrasolar Planets in the Near Future? The DARWIN Project," *Icarus*, Vol. 123, No. 2, pp. 249-255, October 1996.

[20] Lemmerman, L. A., "Terrestrial Planet Finder Kickoff Meeting," Presentation given 24 June 1997 at the Jet Propulsion Laboratory, Pasadena, CA.

[21] Leschly, K., "Spacecraft and Launch Vehicle Summary," *DS-3 Technology Roadmap Study Briefing*, Presentation given 30 June 1997 at the Jet Propulsion Laboratory, Pasadena, CA.

[22] Lockheed Martin Corp., "TPF Final Review," Lockheed Martin Civil Space Programs Division, Presentation given 3 December 1997 at the Jet Propulsion Laboratory, Pasadena, CA.

[23] Marzwell, N., J. Cutts, M. Colavita, and E. Mettler, "Multiple Spacecraft Interferometer Constellation (MUSIC)," Presentation given 2 May 1996 at National Aeronautics and Space Administration Headquarters.

[24] Masters, B. P., M. Ingham, Y. Kim, and D. Surka, "Project ISIS: Pointing & Dynamics," MIT Space Systems Laboratory, Presentation given 6 March 1996 at the Jet Propulsion Laboratory, Pasadena, CA.

[25] Meckel, N. J., et al., "Improved Pulsed Plasma Thruster Systems For Satellite Propulsion," AIAA 96-2735, 32nd Joint Propulsion Conference, Lake Beuna Vista, FL, July 1996.

[26] Mills, R. A., *Natural Vibrations of Beam-like Truss*, Master's thesis, Department of Aeronautics and Astronautics, MIT, Cambridge, MA, June 1985.

[27] National Aeronautics and Space Administration, "Future Topographic Radar Shuttle Mission Will Map 80% Of The Earth," NASA Press Release 96-140, Washington, D. C., 15 July 1996.

[28] Peterson, L. D., et al., "Micron Accurate Deployable Antenna and Sensor Technology For New Millennium-Era Spacecraft," A96-24101, *Proceedings of 1996 IEEE Aerospace Applications Conference*, Vol. 1, Aspen, CO, February 1996.

[29] Shao, M., and M. M. Colavita, "Long Baseline Optical and Infrared Stellar Interferometry," *Annual Review of Astronomy and Astrophysics*, Vol. 30, pp. 457-498, 1992.

[30] Shaw, G. B., G. Yashko, R. Schwarz, D. Wickert, and D. Hastings, "Analysis Tools and Architecture Issues For Distributed Satellite Systems," MIT Space Systems Laboratory, work in progress, to be published in 1998.

[31] Solomon, L. H., and M. A. Kahan, *Optical System Design for the Next Generation Space Telescope*, NASA Technical Report NASA-203490, 17 October 1996.

[32] Surka, D. M., and E. F. Crawley, "A Comparison of Structurally Connected and Multiple Spacecraft Interferometers," Tech. Rep. #9-96, Space Engineering Research Center, MIT, Cambridge, MA, June 1997.

[33] TRW, Inc., "Terrestrial Planet Finder Study," TRW Civil & International Systems Division, Presentation given 3 December 1997 at the Jet Propulsion Laboratory, Pasadena, CA.

[34] Wolff, D. M., "Orbiting Stellar Interferometer: An Overview," AIAA Aerospace Sciences Meeting, Reno, Nevada, January 9-12, 1995.

[35] Woolf, N. J., and J. R. P. Angel, "Planet Finder Options I: New Linear Nulling Array Configurations," *Planets Beyond the Solar System and the Next Generation of Space Missions*, Astronomical Society of the Pacific Conferences Series, 1997.

[36] Woolf, N. J., "Planet Finder Options II: The Development of Methods For Seeing External Planet Radiation," No. 1376, Preprints of the Steward Observatory, University of Arizona, Tucson, AZ, 1996.

[37] Woolf, N. J., J. R. P. Angel, and J. M. Burge, "Planet Finder Options III: Focal Plane Instrumentation and Adjustment," *Proceedings of the Workshop on Infrared Space Interferometry*, Toledo, Spain, March 1996.

[38] Woolf, N. J., "Planet Finder Options IV: Mechanical Aspects of a Planet Finder Mission and a Possible Precursor Mission," *Proceedings of the Brown Dwarfs and Extrasolar Planets International Workshop*, Tenerife, Spain, March 17-21, 1997.

Appendix A

Truss Control Performance Analysis

Because of the high level of precision required by the optical instruments, the differential path lengths between the collector pairs must not exceed several nanometers. In the structurally connected interferometer configuration, the truss structure must damp out vibrations to maintain the requisite displacement level. Because the truss element in this model is designed somewhat arbitrarily, a performance analysis is necessary to ensure that it meets this control requirement.

A.1 Finite Element Truss Model

First, a finite element model of the truss is made, using the geometry in Section 2.2.4. The truss is modeled as a simple Bernoulli-Euler beam using 40 beam elements. Following the analysis performed by Surka [32], the truss is restricted to planar movement, implying six degrees of freedom per element — two translations and one rotation at each boundary. The truss is subdivided equally, making each element 1.875 m long. The four collectors and the combiner are entered as point mass inputs on the truss model. A diagram of the finite element model is shown in Figure A.1. The size of the beam is calculated as to give the same stiffness characteristics as the truss itself, namely the cross-sectional area and the area moment of inertia.

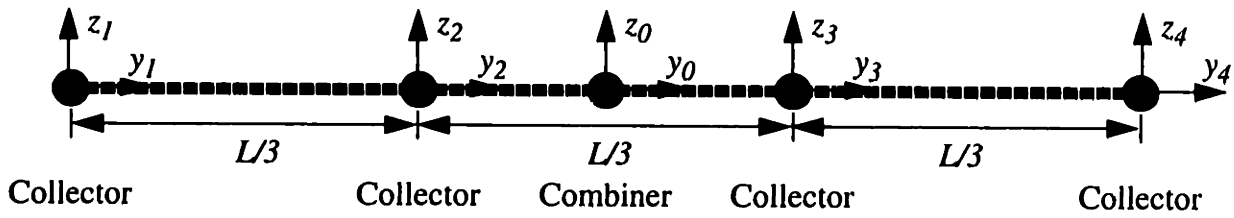

Figure A.1: Truss Finite Element Model

After generating the global mass and stiffness matrices for the truss model, the standard state space model in the form of

$$\dot{x} = Ax + B_w w \tag{A.1}$$
$$z = C_z x + D_{zw} w$$

is used, where x is the state vector, w is the disturbance input vector, and z is the performance output vector. Because the global boundary characteristics of the model are free-free, three rigid body modes, representing free translation in two directions and free rotation in the plane, are present. After the full modal model is calculated, the first 25 flexible modes are retained for numerical expediency. Furthermore, in order to examine the effect of active structural control on the performance, two values of the modal damping ratio are used. In the passive truss, the damping is assumed to be 0.1%, while to simulate active control, the damping is increased to 10%.

The two performance metrics are the path length differences between the outer pair of mirrors and the inner pair of mirrors. To have an equal coarse path length, the inner pair bounces the light twice as shown in Figure A.2. The governing equations for the differential path length (DPL) are found by calculating the error along the path as the light travels from the target to the combiner. Subtracting one path from the other, with the node displacement errors represented by y and z in

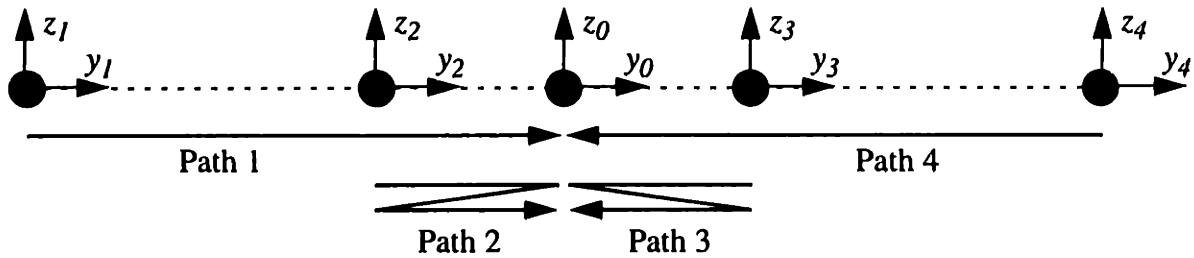

Figure A.2: Schematic of the Two Optical Paths

Figure A.2, the performance variables are given by

$$DPL_{14} = z_4 - z_1 - y_4 + 2y_0 - y_1 \tag{A.2}$$

$$DPL_{23} = z_3 - z_2 - 3y_3 + 6y_0 - 3y_2 \tag{A.3}$$

These equations constitute the C_z matrix in the performance calculation.

A.2 External Disturbance Environment

The external environment of the spacecraft is the source of several different types of disturbances. Since the focus is on the precision of the optics, only those which cause displacement errors and can be numerically modeled are included. Two such external disturbance sources are examined here, the gravity gradient from the sun's gravitational field and the solar pressure differential, both of which are modeled as torques about the center of the spacecraft.

A.2.1 Gravitational Gradient

When the Terrestrial Planet Finder is aligned such that rotational momentum vector is non-aligned with the gravitational field, a net torque is induced on the spacecraft. Since the motion is constrained to lie within the orbital plane, the torque, as given by Surka, reduces to

$$\tau_g = \frac{3\mu}{2R^3}\left|I_{zz} - I_{xx}\right| \sin(2\theta) \tag{A.4}$$

where μ is the gravitational constant of the sun, R is the radius of the orbit, I_{zz} and I_{xx} are the mass moments of inertia, and θ is the angle between the primary body axis and the gravity vector. The average torque is taken to be the integral sum of the torque magnitude over one full rotation divided by the rotation period, in which case the torque averages out and no net momentum increase is seen by the spacecraft.

A.2.2 Solar Pressure Differential

The photons impacting on the interferometer exchange momentum with the surface. A net torque results if the center of the solar pressure is offset from the spacecraft center of mass, which is calculated from Griffin and French [14] as

$$\tau_s = (1+K)\frac{P_s}{c}(\varepsilon L)\sin(\theta) \tag{A.5}$$

where K is the reflectance of the spacecraft, P_s is the solar radiation intensity at the spacecraft's orbit, c is the speed of light, εL is the center offset distance as a fraction of the total length, and θ is again the position angle. The same situation develops here as before; the sinusoidal nature of the torque caused by the constant rotation averages to zero, nullifying the net effect.

A.3 Internal Disturbance Environment

The operation of the instruments and hardware onboard the interferometer generate disturbances as well. Attitude control thrusters and reaction wheels are used to stabilize the instrument pointing and for orientation. However, since the external disturbances average out over the rotation, no momentum change is needed for normal operation; furthermore, disturbances during the reorientation do not matter since no data is being taken. One of the major internal disturbance sources is

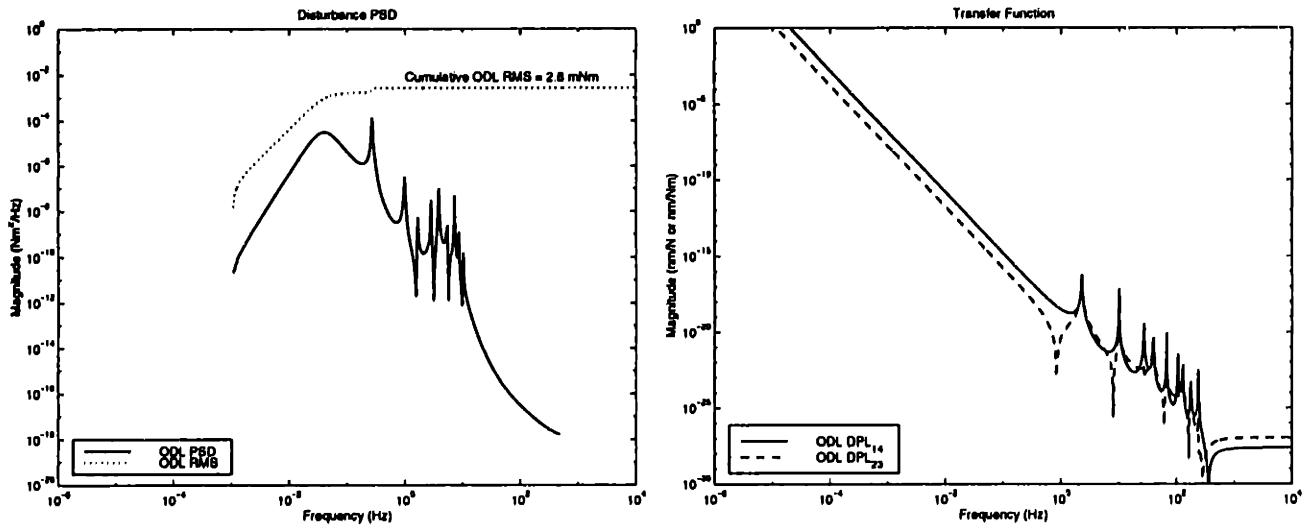

(a) (b)

Figure A.3: Optical Delay Line Disturbance Model
a) Power Spectral Density; b) DPL Transfer Function

the actuation of the optical delay lines (ODL) in compensating for the differential pathlength. Surka [32] found these to be one of the largest disturbance sources.

A.3.1 Optical Delay Line Actuation

Optical delay lines are mounted inside the combiner hardware and move to compensate for errors in the optical path length. The shifting of the ODL transmits a force to the combiner which translates into a torque on the spacecraft. Following Surka's derivation, a ODL force model from the ISIS study [24] is used as an input, with an ODL stroke length of 2 cm and a worst-case moment arm of 12.7 cm. The resulting torque is placed on the central spacecraft in the model, with the spectrum and resulting transfer function shown in Figure A.3. The root-mean-square ODL disturbance is 2.8 mNm. One drawback to this ODL model is that structural dynamics from the ISIS truss itself are contained in the power spectral density to a small degree.

A.4 Performance Results

With the state space model and the input disturbance, the predicted system performance is generated using Equations A.1. The optical delay lines only operate up to a certain frequency and the internal optical control cutoff is modeled using a high-pass filter, with both a 1 Hz and a 10 Hz cutoff value. Table A.1 summarizes the results for all eight possible configurations, while Figures A.4 - A.7 show the power spectral densities.

The values are lower for the 1.0 AU orbit because the point masses are heavier and have a higher inertia. On the whole, the values indicate that the displacement errors can be reduced to a nanometer level without active structural control, assuming adequate optical control bandwidth. Control bandwidth will depend on the brightness of the parent star and can be estimated as one-tenth of the sampling rate of a detector tracking the fringe of the parent star. Therefore, the 1 Hz and 10 Hz filters representing the low frequency DPL rejection provided by the ODLs correspond to 10 Hz and 100 Hz sampling rates on the fringe of the parent star. Results from other studies [28] support micron level performance without active structural control as well.

According to an analysis performed by Colavita [11] which made several assumptions concerning the brightness of the target star, the fringe tracking and measurement of the combiner, and the photon efficiency, the requirements placed on the structure were divided into DPL noise above and below the 1 Hz closed-loop bandwidth of the system. For frequencies above 1 Hz, the total root-mean-square of the DPL error must be less than 0.5 nm, while below 1 Hz, the noise could not exceed 0.5 nm/f^2, where f is the noise frequency. Therefore, with the simple model used in this disturbance analysis, the DPL error is too high, by about two orders of magnitude.

The 10 Hz results are close to the 0.5 nm requirement put forth by Colavita, and so if the bandwidth of the optical control system were to grow to 10 Hz, the requirement would be met.

Table A.1: Summary of Performance Results

Damping Ratio	Orbit	1 Hz Filtered DPL RMS Error	10 Hz Filtered DPL RMS Error
Open Loop (0.1%)	1.0 AU	40.0 nm	0.7 nm
Closed Loop (10%)		29.2 nm	0.3 nm
Open Loop (0.1%)	5.2 AU	72.6 nm	0.9 nm
Closed Loop (10%)		72.5 nm	0.8 nm

One solution for increasing the bandwidth might be the use of accelerometer sensors for the higher frequencies.

However, from these cursory results, the truss design used in this study is assumed to be a reasonable one, providing sufficient stiffness and damping for the collector hardware to accurately control the optical resolution. Active structural control might ensure that the required precision is available, but a more detailed finite element analysis is needed for a definitive conclusion as to its necessity.

Also, other internal disturbances should be considered. For example, if a zero angular momentum system is desired and a large reaction wheel is used to spin up the instrument, observations will be made while the reaction wheel has a high spin rate relative to the structure. Static and dynamic imbalances in the wheel, as well as bearing chatter, will cause once-per-revolution vibrations with additional super- and sub-harmonics.

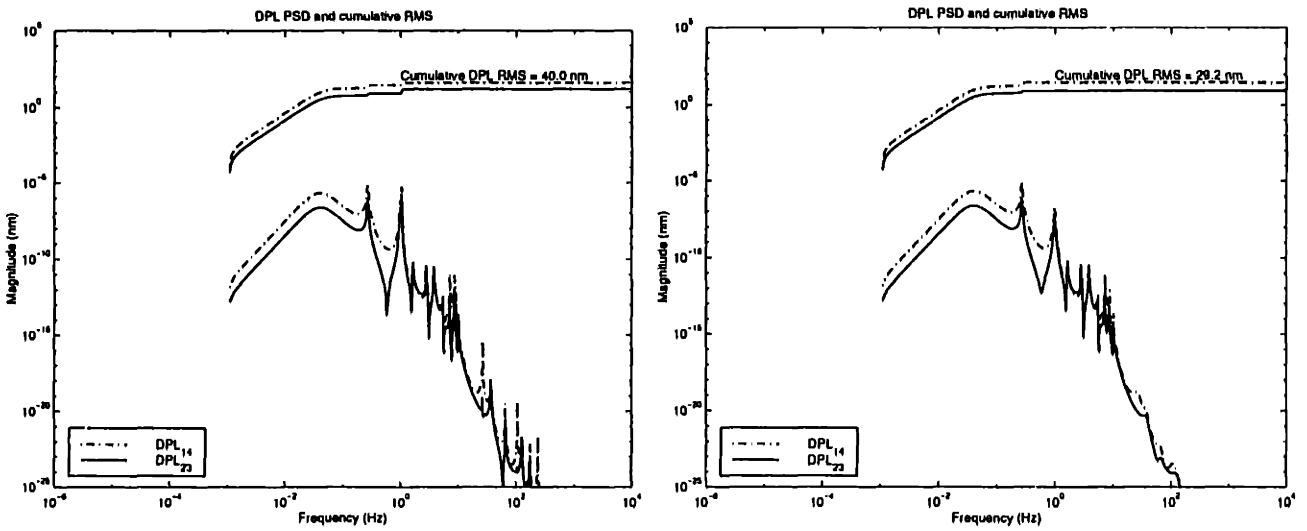

Figure A.4: Disturbance Response For 1.0 AU Orbit, 1 Hz Filter
a) Open Loop; b) Closed Loop

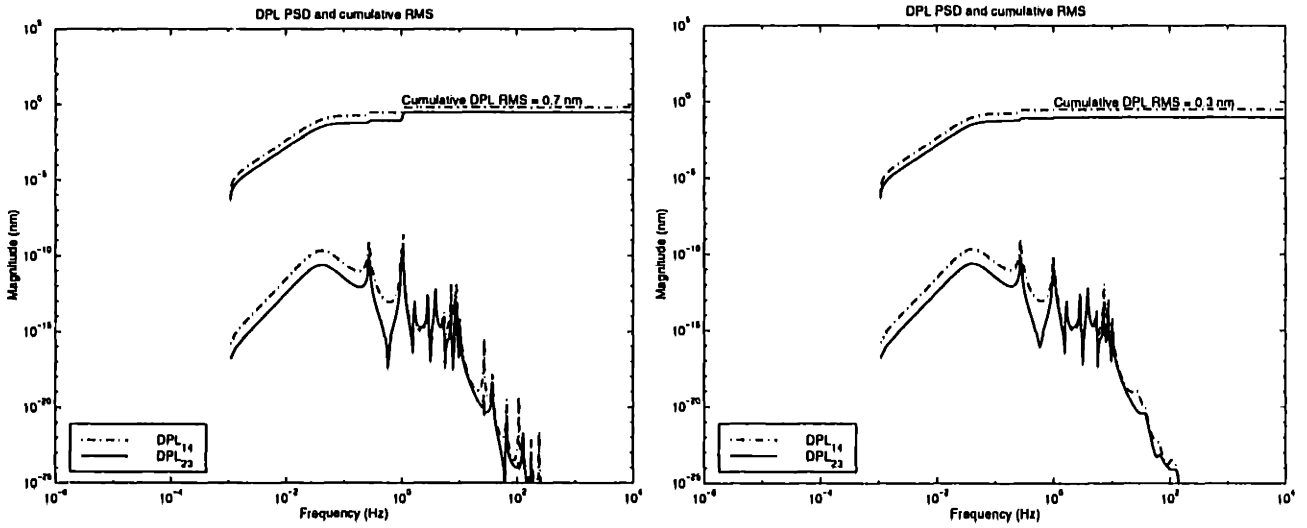

Figure A.5: Disturbance Response For 1.0 AU Orbit, 10 Hz Filter
a) Open Loop; b) Closed Loop

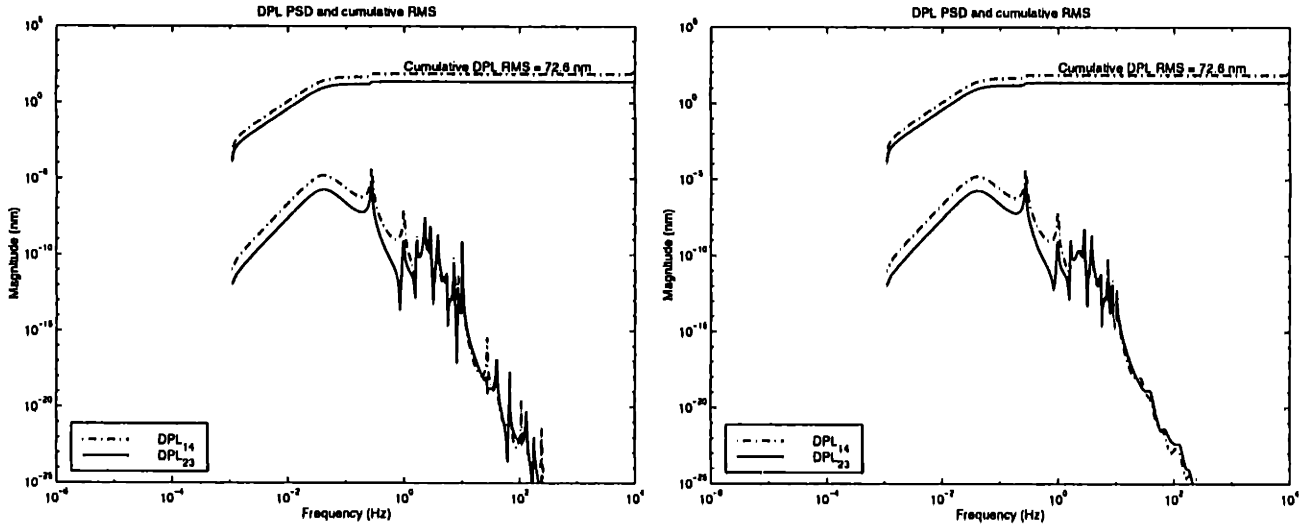

Figure A.6: Disturbance Response For 5.2 AU Orbit, 1 Hz Filter
a) Open Loop; b) Closed Loop

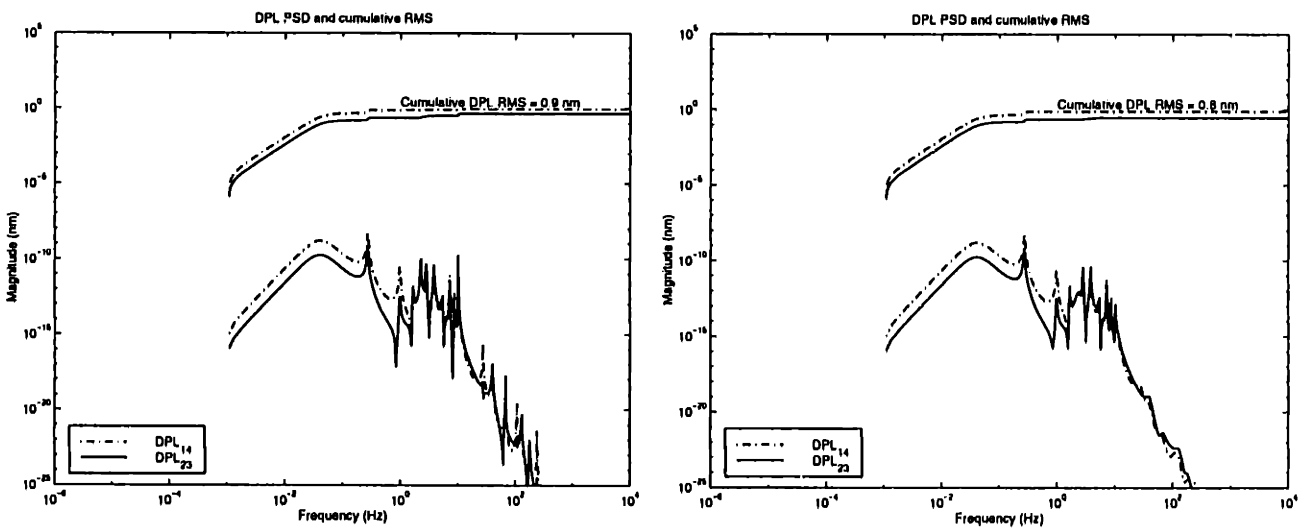

Figure A.7: Disturbance Response For 5.2 AU Orbit, 10 Hz Filter
a) Open Loop; b) Closed Loop